11-13-2014

Pseudo-Rigid-Body Models for Approximating Spatial Compliant Mechanisms of Rectangular Cross Section

Issa Ailenid Ramirez
University of South Florida, issaramirez@gmail.com

Pseudo-Rigid-Body Models for Approximating Spatial Compliant Mechanisms of Rectangular Cross Section

by

Issa A. Ramirez

A dissertation submitted in partial fulfillment
of the requirements for the degree of
Doctor of Philosophy
Department of Mechanical Engineering
College of Engineering
University of South Florida

Major Professor: Craig P. Lusk, Ph.D.
Fernando Burgos, Ph.D.
Nathan Crane, Ph.D.
Delcie Durham, Ph.D.
Jing Wang, Ph.D.

Date of Approval:
November 13, 2014

Keywords: Large-deflections, Kinematics, Cantilever beams,
Three-dimensional deflections, Axisymmetric deflections

Dedication

To my parents.

Acknowledgments

I would like to express my deep appreciation and gratitude for my advisor, Dr. Craig Lusk, for his mentorship, patience and guidance thought the completion of this degree. I would also like to thank my committee members Dr. Burgos, Dr. Crane, Dr. Durham and, Dr. Wang for their time and helping me to accomplish the doctoral program. I am grateful for the financial assistance from the McKnight Doctoral Fellowship Program, the Alfred P. Sloan Foundation Minority Ph.D. program and the National Science Foundation Grant # CMMI-1000138. I wish to express my gratitude to Mr. Batson for his support and guidance since I started my graduate studies and throughout all the years at USF. Finally, I would like to thank my mom Dinelia, my father Isaias, my sister Natasha and my husband Julio, thanks for supporting me and encouraging me to follow my dreams.

Table of Contents

List of Tables

List of Figures

Abstract

The objective of the dissertation is to develop and describe kinematic models (Pseudo-Rigid-Body Models) for approximating large-deflection of spatial (3D) cantilever beams that undergo multiple bending motions thru end-moment loading. Those models enable efficient design of compliant mechanisms, because they simply and accurately represent the bending and stiffness of compliant beams.

To accomplish this goal, the approach can be divided into three stages: development of the governing equations of a flexible cantilever beam, development of a PRBM for axisymmetric cantilever beams and the development of spatial PRBMs for rectangular cross-section beam with multiple end moments.

The governing equations of a cantilever beam that undergoes large deflection due to force and moment loading, contains the curvature, location and rotation of the beam. The results where validated with Ansys, which showed to have a Pearson's correlation factor higher than 0.91.

The resulting deflections, curvatures and angles were used to develop a spatial pseudo-rigid-body model for the cantilever beam. The spatial pseudo-rigid-body model consists of two links connected thru a spherical joint. For an axisymmetric beam, the PRB parameters are comparable with existing planar PRBMs. For the rectangular PRBM, the parameters depend on the aspect ratio of the beam (the ratio of the beam width over the height of the cross-section). Tables with the parameters as a function of the aspect ratio are included in this work.

Chapter 1

Introduction

A compliant mechanism is a device that transforms or transfers motion or energy, which gains mobility by undergoing elastic deformation on its members. Because they rely on the deflection of flexible members, they store strain energy in their flexible members. The optimal compliant mechanism is a compromise between stiffness and flexibility. Because many applications compliant mechanisms undergo large deformations, linearized beam equations are no longer valid. Current methods of designing planar compliant mechanisms include elliptic integrals and the pseudo-rigid-body model.

The pseudo-rigid-body model (PRBM) is a simple method of analyzing systems that undergo large, nonlinear deflections. It is a simplified form used to model the deflection of flexible members by using rigid-body joints, links, and springs, that have equivalent force-deflection characteristics.

1.1 Motivation

Accurate PRBMs that predict the motion of planar beams have been developed. PRBMs are often used as a first trial in the design phase of different devices and subsequent refinement can be done using a finite elements program. The PRBM has been used to design medical devices [1, 2] and MEMS [3-6]. However, spatial compliant mechanisms currently are designed by trial and error. The motivation of this work is to develop an accurate spatial PRBM to expedite the design and analysis process for three-dimensional compliant mechanisms.

1.2 Scope

Beam analysis can be separated into planar (two-dimensional) beams, axisymmetric and spatial beams. Analysis of planar PRBMs have been developed in the past with force, moment and combined loading conditions. Axisymmetric beams are a special case because they are three-dimensional beams with equal thickness and width. Accurate PRBMs for axisymmetric and rectangular cross-section spatial beams with moment-loading were developed in this dissertation.

1.3 Goals

The objective of this study is to describe kinematic models (Pseudo-Rigid-Body Models) for approximating large-deflection of spatial (3D) cantilever beams that undergo in-plane and out-of-plane bending motions thru end-moment loading. The aims of the present work are:

1. Development of large deflection, non-linear kinematic equations for a cantilever beam, consisting of curvature, location and rotation equations.
2. Development of pseudo-rigid-body models for an axisymmetric cantilever beam with in-plane and out-of-plane moment loading:
    i. Kinematic parameters: characteristic length and pseudo-rigid-body angle
    ii. Stiffness parameters: stiffness coefficients
3. Development of pseudo-rigid-body models for a rectangular cantilever beam with in-plane and out-of-plane moment loading:
    i. Kinematic parameters: characteristic length and pseudo-rigid-body angles
    ii. Stiffness parameters: stiffness coefficients

1.4 Dissertation Overview

The motivation of this work is to develop accurate spatial (3D) Pseudo-Rigid-Body Models (PRBMs) to expedite the design and analysis process of three-dimensional compliant

mechanisms. The scope of this study is to describe kinematic models, PRBMs, for approximating large-deflection of spatial cantilever beams that undergo in-plane and out-of plane bending motions thru end-moment loading. To accomplish this goal, the approach can be divided into five stages: development of the governing equations of a flexible cantilever beam, development of a PRBM for axisymmetric cantilever beams for multiple loads and multiple end-moment loading, and the development of spatial PRBMs for a rectangular cross-section beam with multiple end moments.

Chapter 2 presents an overview of the different analysis methods to study large-deflection of planar and spatial beams, and, analysis methods for compliant mechanisms. Also, an extensive review of existing pseudo-rigid-body models for cantilever beams is presented.

In Chapter 3, the governing equations of a flexible beam that undergoes large deflection are derived. The approach used is similar to that found in [7], but the reference frames and nomenclature selected here facilitates comparison with compliant mechanisms literature. These equations are validated and used to develop the spatial pseudo-rigid-body models.

Chapter 4 describes the development of a pseudo-rigid-body model for an axisymmetric multiple force loaded cantilever beam and also a PRBM for an axisymmetric beam with in-plane and out-of-plane moment loading. The effect of the direction of the loading condition is also described. The approximated PRB parameters are evaluated to find a PRBM with a relative deflection error less of 0.5%.

Chapter 5 describes the development of a pseudo-rigid-body model for a rectangular cantilever beam that undergoes in-plane and out-of-plane moment loading. The kinematic and stiffness parameters for a beam with rectangular cross-section and bending moments are described. The perturbation method is used as a measure of the magnitude of the applied out-of-

plane moment with respect to the planar moment. With this information, the exact PRBM parameters for a cantilever beam with multiple end-moments loading were developed. The PRBM parameters approximations and equations will aid the development of fast and accurate PRBM's for spatial cantilever beams.

The dissertation is concluded with a summary and accomplishments of the present work. Also, recommendations for future work are stated.

Chapter 2

Literature Review

This chapter presents an introduction to compliant mechanisms, the advantages and disadvantages and different design and analysis methods, with emphasis on the pseudo-rigid-body model.

2.1 Compliant Mechanisms

Compliant mechanisms gain mobility by undergoing elastic deformation of their members. Because they rely on their deflection of flexible members, energy is stored in form of strain energy in their flexible links. The optimal compliant mechanism is a balance between stiffness and flexibility, if too flexible, it will not transmit energy sufficient to do useful work; if too stiff, it will not deform easily.

The advantages of compliant mechanisms can be divided in two parts: cost reduction and increased performance [8]. Reduction of the part elements results in reduced assembly time and simplified manufacturing processes. Part reduction and simplified manufacture processes in compliant mechanisms are because many of them can be manufactured from an injection-moldable material or can be constructed in a single piece. Because compliant mechanisms have fewer movable joints, such as pin and sliding joints, this results in reduced wear and lubrication. Because of the aforementioned advantages of compliant mechanisms, they may be used for:

- Surgical tools and medical devices: compliant mechanisms have been used in medical devices as forceps-scissors, which is a compliant mechanism end effector that acts as

both a forceps and a scissors, and as suturing instruments. Examples of surgical devices and tools are presented in [1, 9-11].

- MEMS devices: compliant mechanisms can be miniaturized and fabricated using microfabrication techniques such as in MEMS devices. Compliant mechanisms fabricated at the micro level presents several advantages such as: can be fabricated on plane, require no assembly, are less complex, have less need for lubrication, have reduced friction and wear, integrate energy storage elements (like springs) with the other components, and have higher precision (they have less clearance due to pin joints). Examples of MEMS devices include an actuator for out-of-plane displacements [12], crash sensors [13], and compliant stroke amplification mechanisms [14].
- Applications in which the mechanism in not easily accessible or for operation in harsh environments that may adversely affect joints [8].
- Aerospace industry: in deployable wings for small unmanned aerial vehicles [15-17] and flapping wings for micro aerial vehicles [18].

Despite the aforementioned advantages of compliant mechanisms in several applications, there are disadvantages in the design of compliant mechanisms which include [19]: difficulty of analysis and design, potential for undesired energy stored in the flexible segments, design for fatigue is critical, limited rotational ability of flexible links and stress relaxation or creep.

2.1.1 Modeling

Many compliant mechanisms have been designed through trial and error in the past. These mechanisms are very simple and are not cost efficient for many applications. Knowledge and synthesis of the compliant members and the interaction with other parts needs to be properly understood in order to improve and simplify the design of such devices. Because in many

applications the flexible members undergo large deformations, linearized beam equations are no longer valid. Methods for designing planar compliant mechanisms include elliptic integrals [20], topology optimization [21] and the pseudo-rigid-body model [8].

2.1.1.1 Elliptic Integrals

Elliptic integral solutions can provide rapid feedback in early stages of design to aid the selection of an appropriate design [22]. The definition of the first and second kind elliptic integral respectively is:

$$F(\phi,k)=\int_0^{\phi}\frac{d\theta}{\sqrt{1-k^2sin^2\,\theta}} \tag{2.1}$$

$$E(\phi,k)=\int_0^{\phi}\sqrt{\sqrt{1-k^2sin^2\theta}}\,d\theta \tag{2.2}$$

where ϕ is called the magnitude and k is the modulus. Elliptic integral solutions for large deflection of a cantilever beam with a vertical load at the free end are presented in [20]. The derivation of a large-deflection solution for a cantilever beam with multiple forces at the free end is presented in [8]. In the derivation, combined forces are applied to the beam at an angle:

$$\phi_1=\text{atan}\left(\frac{1}{-n}\right) \tag{2.3}$$

The solution of the nondimensional horizontal and vertical deflection of the beams tip is [8]:

$$\frac{a}{l}=\frac{1}{\alpha\eta^{5/2}}\left\{-n\eta[F(t)-F(\gamma,t)+2(E(\gamma,t)-E(t))]+\sqrt{2\eta(\eta+\lambda)}cos\gamma\right\} \tag{2.4}$$

$$\frac{b}{l}=\frac{1}{\alpha\eta^{5/2}}\left\{\eta[F(t)-F(\gamma,t)+2(E(\gamma,t)-E(t))]+n\sqrt{2\eta(\eta+\lambda)}cos\gamma\right\} \tag{2.5}$$

where:

$$\alpha=\frac{1}{\sqrt{\eta}}(F(t)-F(\gamma,t)) \tag{2.6}$$

$$\gamma=\text{asin}\sqrt{\frac{\eta-n}{\eta+\lambda}} \tag{2.7}$$

$$t = \sqrt{\frac{\eta + \lambda}{2\eta}} \tag{2.8}$$

$$\eta = \sqrt{1 + n^2} \tag{2.9}$$

$$\lambda = \eta \cos(\theta_0 - \phi_1) \tag{2.10}$$

Elliptic integrals solutions for thin beams that undergoes large deflection with multiple inflection points are presented in [23]. Chen et.al [24] presented the solution of elliptic integrals and compared them to the PRBM to evaluate its accuracy. Disadvantages of using elliptic integrals in the design process includes: the derivations are complicated, the solutions can be found only for relatively simple geometries and loadings, and moreover, this method requires several simplifying assumptions like linear material properties and inextensible members [8].

2.1.1.2 Optimization

Optimization is the process of finding the conditions that give the maximum or minimum value of a function, to be able to find the optimum solution depending on a particular set of design variables [25]. The purpose of optimization is to choose the best design of many acceptable designs available. The general constrained optimization problem can be stated as [25]:

$$\text{Find } X = \begin{Bmatrix} x_1 \\ x_2 \\ \vdots \\ x_n \end{Bmatrix} \text{ which minimizes f}(X) \tag{2.11}$$

Subject to the constraints:

$$g_j(X) \leq 0, \quad j = 1,2,\dots,m \tag{2.12}$$

$$\mathrm{l_j}(X) = 0, \quad j = 1,2,\dots,p \tag{2.13}$$

where X is an n-dimensional vector called the design vector, f(X) is the objective function, $g_j(X)$ is known as the inequality term and $\mathrm{l_j}(X)$ is known as the equality term. The number of constraints m and p and the number of variables does not have to be related. The objective

function is the criterion with respect to which the design is optimized when expressed as a function of the design problem. It is also called the cost function or energy function. The choice of the governing function is governed by the nature of the problem.

Sizing, shape and topology optimization addresses different aspects of the design problem. The definition and design variables characterize the types of optimization such as [26]:

- Sizing: in sizing optimization, a typical size of a structure such as the thickness of a beam and shell elements and material properties such as density are optimized without changing meshes.
- Shape: in shape optimization, the shape of a structure (boundary of design domain such as the length of a beam and boundary shell) is optimized so that the meshes are varied as the design changes. The shape optimization problem may have multiple solutions, because the domain in which to look for the final design is not determined yet.
- Topology: the topology of a structure is optimized so that the shape and connectivity of design domain are altered. Topology optimization is the most general form of structural optimization.

The most popular design method is topology optimization. Sigmund et al.[27] presented an energy-based topology optimization. Lee et al.[28] presented a strain-based topology optimization method that avoids localized high strain in compliant joints of the compliant mechanism. Pedersen et al.[29] presented the design of a large displacement compliant mechanism. Compliant mechanisms design through topology optimization includes a conceptual design of a wing-flapping mechanism [30].

2.2 Pseudo-Rigid-Body Model

It was observed that in cantilever beams undergoing large deflections, the path of the beam end is nearly circular, with a center of curvature at some point on the undeflected part of the beam. This observation served as the catalyst that leads to the development of the pseudo-rigid-body model, which allows the motion of the end of the cantilever beam to be accurately predicted [8].

The pseudo-rigid-body model (PRBM) is a simple method of analyzing systems that undergo large, nonlinear deflections. It is a simplified form used to model the deflection of flexible members by using rigid-body joints that have the equivalent force-deflection characteristics. The PRBM predicts the deflection path and force-deflection relationship of flexible segments, modeling them as rigid links attached at the pin joints. Springs are added to predict the force-displacement relationship of the flexible members.

Existing PRBMs differ in the number and the location of the links and joints. Also, the pseudo-rigid-body parameters depend on the loading conditions: end-forces, end-moments and combined loading. Planar PRBMs that predict the location of the free-end of the beam for different loading conditions are presented in the following section.

2.2.1 End-Force Loading

Because the path of the free end of a cantilever beam end is nearly circular, with a center of curvature at some point on the undeflected part of the beam, it can be modeled as two links connected by a pivot. The first model of a PRBM for a cantilever beam consists of 2 rigid-body links connected through a revolute (1R) joint [31], as shown in Figure 2.1. The approximate equations for nonlinear, large deflection cantilever beams with end-forces and no moments,

assumes that the beam is linearly elastic, inextensible, rigid in shear and of constant cross-section.

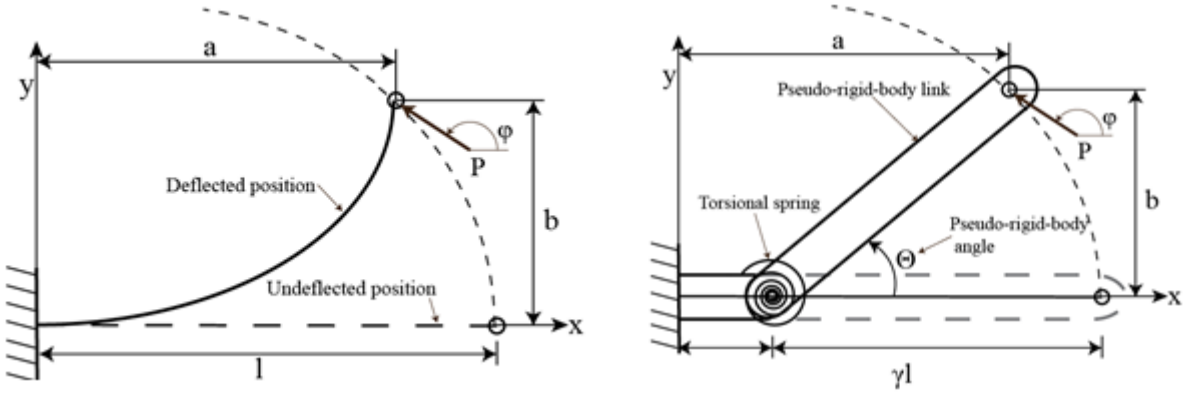

Figure 2.1. (a) Cantilever beam, and (b) One revolute joint PRBM.

The beam's resistance to the deflection is represented by a torsional spring with linear stiffness characteristics which connects the two rigid links. The distance from the spring to the end of the beam is represented by the quantity γl, where γ is the characteristic radius factor and l is the total length of the beam. The pseudo-rigid-body angle, Θ, is the angle between the pseudo-rigid-body link and the undeflected position of the beam. The end-forces were combined and treated as a single force with an angle $\phi = 1/\text{atan}(1/-n)$. From Figure 2.1, the beam's end coordinates (a, b) of the PRBM can be found using the equations:

$$a = l - \gamma l(1 - \cos\Theta) \qquad 2.14$$

$$b = \gamma l \sin\Theta \qquad 2.15$$

From the PRBM estimate of the end position, one can estimate the relative deflection error, $error/\delta_t$. This is a measure of the difference of the deflection approximation determined by the PRBM and the theoretical value determined thru numerical integration or elliptic integrals. The theoretical horizontal and vertical deflection of the beam tip are given by a_t and b_t, respectively. The relative error is calculated as [31]:

$$\frac{error}{\delta_t} = \frac{\sqrt{\left[\frac{a_t}{L}(1-\gamma(1-\cos(\Theta))\right]^2 + \left[\frac{b_t}{L} - \gamma L \sin(\Theta)\right]^2}}{\sqrt{\left(1-\frac{a_t}{L}\right)^2 + \left(\frac{b_t}{L}\right)^2}} \qquad 2.16$$

An one-dimensional optimization routine, the Golden section method, was used to find the value of the characteristic radius factor which would allow the maximum pseudo-rigid-body angle while satisfying the maximum relative deflection error of 0.5%. The inputs to the optimization routine are the relative deflection error, the length of the beam, the characteristic radius factor and the step size of the beam's end angle. The theoretical vertical and horizontal deflections were found through the use of elliptic integrals and the step size of the beams end angle is set to 0.1 degrees. The beam's end slope angle was incremented by 0.1 degrees until the maximum allowable relative deflection error exceeded 0.5%.

Using this optimization routine, the optimal value of the characteristic radius for a vertical force (*n*=0) was found to be 0.8517, and a maximum beam tip angle, θ_{0max}, of 77 degrees. Using linear and polynomial curve fitting techniques, the values of the characteristic factor as a function of the force angle, *n*, that represent a relative error of less that 0.5% are [31]:

$$\gamma_i = \begin{array}{ll} 0.841655 - .0067807n + .000438004n & 0.5 < n \leq 10.0 \\ 0.852144 - .0182867n & -1.8316 < n < 0.5 \\ 0.912364 + .0145928n & -5.0 < n < -1.8316 \end{array} \qquad 2.17$$

The tip locus of the PRBM is approximately accurate, but the estimation of the beam end angular slope had a significant error. The relationship between the pseudo-rigid-body angle and the beams end angular deflection lead to the linear relationship $\theta_0 = c_0\Theta$; where c_0 is the parametric angle coefficient.

2.2.1.1 Stiffness Coefficient

The applied force, *P*, can be separated into its components: a parallel force, F_n, normal to the path of the free-end of the beam and a perpendicular force, F_t, tangent to the path of the free-end of the beam. The tangent force generates a torque in the characteristic pivot and generates a deflection of the beam but the parallel force does not contribute to the deflection of the beam. The tangential component of the applied force, α_t , can be nondimensionalized as:

$$\alpha_t^2 = \frac{F_t l^2}{EI} \tag{2.18}$$

where $F_t = Fsin(\phi - \Theta)$, ϕ is the applied angle of the force, *E* is the modulus of elasticity, *I* is the moment of inertia and *l* is the length of the beam. The linear force-deflection relationship of the pseudo-rigid-body model is given by:

$$\alpha_t^2 = K_\Theta \Theta \tag{2.19}$$

where K_Θ is the stiffness coefficient which models the beam's resistance to deflection. The stiffness coefficient was found by a curve fitting procedure for different values of applied force angles, *n*. The stiffness coefficient and the applied angle forces are related by [32]:

$$\begin{array}{cc} K_\Theta = 3.024112 + 0.121290n + 0.003169n^2 & -5 < n \leq -2.5 \\ K_\Theta = 1.967647 - 2.616021n - 3.738166n^2 - 2.649437n^3 - 0.891906n^4 - 0.113063n^5 & -2.5 < n \leq -1 \\ K_\Theta = 2.654855 - 0.509896x10^{-1}n + 0.126749x10^{-1}n^2 - 0.142039x10^{-2}n^3 - 0.584525x10^{-4}n^4 & -1 < n \leq 10 \end{array} \tag{2.20}$$

The beam resistance to deflection is modeled using a torsional spring with a spring constant, K. The torque required to deflect the torsional spring, K, through a pseudo-rigid-body angle, Θ, is:

$$T = K \Theta \tag{2.21}$$

Knowing the displacement of the free-end of the beam, the pseudo-rigid-body angle may be found from the coordinates of the beam end and the characteristic radius factor as:

$$\Theta = \operatorname{atan}\frac{\mathrm{b}}{\mathrm{a} - \mathrm{l}(1-\gamma)} \qquad 2.22$$

The torsional spring stiffness, K, can be found as:

$$\mathrm{K} = \gamma K_{\Theta}\, {}^{\mathrm{EI}}/_{\mathrm{l}} \qquad 2.23$$

Pauly et al. [33] modified Howell's 1R PRBM optimization routine for end-loaded cantilever beams. A change in the beam's end slope, θ_0, equal to 0.1 degrees was adequate for loads in the range of $45 \leq \phi$. In order to ensure that the relative deflection error is less than 0.5%, in forces that are nearly axial, tensile end loads, were modified to have the change of the end angular deflection, $\Delta\theta_0$, equal to 1 x 10^{-5} degrees. The Golden section technique was used to solve the optimization problem with values of the change of the end angular deflection of 1 x 10^{-5} degrees and a relative deflection error of 0.5%. The pseudo-rigid-body model parameter as a function of the load parameter (*n*) was modified to accommodate the changes [33]:

$$\gamma = \begin{array}{cc} 0.855651 - .016438n & -4.0 < n \leq -1.5 \\ 0.852138 - .018615n & -1.5 < n \leq 0.5 \\ 0.851892 - 0.020805n + 0.005867n^2 - 0.000895n^3 + 0.000069n^4 - 0.000002n^5 & 0.5 < n \leq 10 \end{array} \qquad 2.24$$

Dado et al. [34] presented a variable parametric pseudo-rigid-body model for large deflection beams with end-loads based on the 1R PRBM. The model finds correlation equations that relate the stiffness and the load in terms of the characteristic radius and the pseudo-rigid-body angle through regression analysis. A disadvantage of this model is the need of an interactive procedure to find the values of the beam's end (*a* and *b*).

Feng et al. [35] presented a two revolute joint (2R) PRBM that can simulate the tip locus and the tip deflection angle, and showed that the 2R model has superior kinematics than the 1R model. The 2R PRBM consists of 3 rigid links connected thru 2 revolute joints and 2 torsion springs as shown in Figure 2.2.

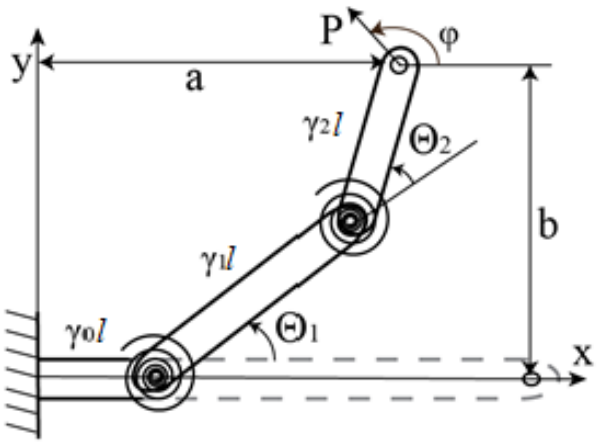

Figure 2.2. 2R PRBM.

The slope angle for the 2R PRBM is equal to $\theta_0 = \Theta = \Theta_1 + \Theta_2$, as shown in Figure 2.2. The characteristic radius factor satisfies the equation:

$$\gamma_0 + \gamma_1 + \gamma_2 = 1 \tag{2.25}$$

A two-dimensional search process is used to find the optimal characteristic radius factor. The inputs to the optimization are the length of the beam, a set of three characteristic radius factors, a step size of the beam's end angle of 0.02 and a maximum angle error of 1%. The relationship between the characteristic radius and the force angle is given by [35]:

$$\gamma_i(i = 1,2,3) = \begin{matrix} 0.08,0.52,0.40 & 0 < \phi \leq 63.4^o \\ 0.10,0.54,0.36 & 63.4^o < \phi \leq 116.6^o, \quad 153.4^o < \phi < 180^o \\ 0.12,0.56,0.32 & 116.6^o < \phi \leq 153.4^o \end{matrix} \tag{2.26}$$

Using a linear regression process, the approximated values of the spring stiffness coefficients ($K_{\Theta i}$) are found. The relation between the spring stiffness coefficients and the applied force angle is given by [35]:

$$\begin{aligned} K_{\Theta 1} &= -1.4584\phi^2 + 4.5794\phi - 0.0421 \\ K_{\Theta 2} &= -0.6133\phi^2 + 1.9403\phi - 0.0982 \end{aligned} \tag{2.27}$$

For a vertical force (n=0), the results represents an error smaller than 1% with a parametric maximum angle $\theta_{0max} = 83.5$ degrees. Because the error between the slope angle of

the 2R PRBM (Θ), and the link tip deflection (θ_0) is less than 1%, there is no need for a parametric angle coefficient (c_θ) and the link tip deflection angle can be equal to the slope of the 2R PRBM ($\theta_0 = \Theta$).

The advantages of Feng's 2R PRBM is that there is no need of a parametric coefficient because it simulates the tip locus and the tip angle, because the error between the beam's tip deflection and the slope of the 2R PRBM is less than 1%. Another advantage is that the maximum angular slope was increased from 77 degrees in the 1R PRBM to 88.5 degrees in the 2R PRBM. A disadvantage of the model is that it only takes in consideration end-beam loading and there are no cases for input moments.

2.2.2 End-Moment Loading

Compliant mechanisms undergo large deflections which introduces geometric nonlinearities. The major difference between small and large deflection analysis lies in the assumptions made to solve the Bernoulli-Euler equations [8]. The Bernoulli–Euler theory is a simplified theory for the calculation of the deflection of beams. The basic assumptions of the theory are [36]: 1) the beam is elastic and isotropic, 2) the beam deformation is dominated by bending, and, 3) the beam is long and slender with a constant cross section along the axis.

The Bernoulli-Euler equation of a cantilever beam subjected to a moment end-load states that the bending moment is proportional to the beam's curvature, such as:

$$M = EI\frac{d\theta}{ds} \tag{2.28}$$

where M is the applied moment, E is the Young's modulus, I is the moment of inertia and, $d\theta/ds$ is the rate of angular deflection along the beam, also known as curvature. For a planar beam with an applied moment at the free end, M, the internal moment is constant along the beam. The angular deflection of the beams end, θ_0, is found by separating variables,

$$\int_0^{\theta_0} d\theta = \int_0^L \frac{M}{EI} ds \tag{2.29}$$

And integrating, the angular deflection of the beam is:

$$\theta_0 = \frac{ML}{EI} \tag{2.30}$$

where the angular deflection of the beam's end, θ_0, is in radians. The rate of vertical deflection along the beam's length is $dy/ds = \sin\theta$. The vertical deflection, b, can be found by the chain rule of differentiation, and substituting, such as:

$$\frac{M}{EI} = \frac{d\theta}{ds} = \frac{d\theta}{dy}\frac{dy}{ds} = \frac{d\theta}{dy}\sin\theta \tag{2.31}$$

Separating variables,

$$\int_0^b dy = \frac{EI}{M}\int_0^{\theta_0} \sin\theta \, d\theta \tag{2.32}$$

And integrating, the vertical deflection of the beam is:

$$b = \frac{EI}{M}(1 - \cos\theta_0) \tag{2.33}$$

Substituting into Equation 2.30:

$$b = \frac{l - l\cos\theta_0}{\theta_0} \tag{2.34}$$

In the same manner, the horizontal deflection of the free end of the beam can be found. The rate of horizontal deflection along the beam's length is $dx/ds = \cos\theta$. The horizontal deflection of the free end of the beam, a, can be found by the chain rule of differentiation, substituting, and separating into variables such as:

$$\int_0^a dx = \frac{EI}{M}\int_0^{\theta_0} \cos\theta \, d\theta \tag{2.35}$$

Integrating, the horizontal deflection of the beam is:

$$a = \frac{EI}{M} \sin \theta_0 \tag{2.36}$$

Substituting in Equation 2.30:

$$a = \frac{l \sin \theta_0}{\theta_0} \tag{2.37}$$

The nondimensional large-deflection equations of a cantilever beam with a moment load can be found [8]:

$$\frac{a}{l} = \frac{\sin\left(\frac{M_0 L}{EI}\right)}{\frac{M_0 l}{EI}} \tag{2.38}$$

$$\frac{b}{l} = \frac{EI}{M_0 l} \left[1 - \cos(\theta_0)\right] \tag{2.39}$$

where a and b are the horizontal and vertical coordinates of the free-end of the beam, M_0 is the applied moment, I is the moment of inertia, l is the length of the beam and E is the modulus of elasticity.

The pseudo-rigid-body model for a beam with end-moments is similar to the 1R PRBM with applied end-load. It can be modeled as two links connected by a pivot as shown in Figure 2.3.

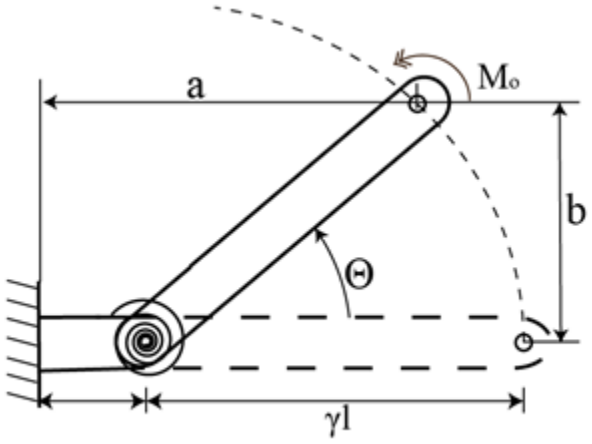

Figure 2.3. One revolute joint PRBM for end-moment loading.

The optimal value of the characteristic radius for an applied moment that gives a relative deflection error less than 0.5% was found to be 0.7346, the maximum beam tip slope angle, θ_{0max}, of 124.4 degrees and the parametric angle coefficient, c_θ, was found to be 1.5164. The spring constant for the case of an end-moment is given by [8]:

$$K = c_\theta \frac{EI}{L} \tag{2.40}$$

2.2.3 Combined Loading: End-Loads and Moments

Su et al. [37] developed a 3 revolute (3R) PRBM for a planar, initially straight beam which consists of 4 rigid links connected thru three revolute joints as shown in Figure 2.4. A three-dimensional search routine was used to find the optimal set of the characteristic radius and the spring stiffness. This model can be used to for different types of loading conditions: end-moment only, end-force and combined loading.

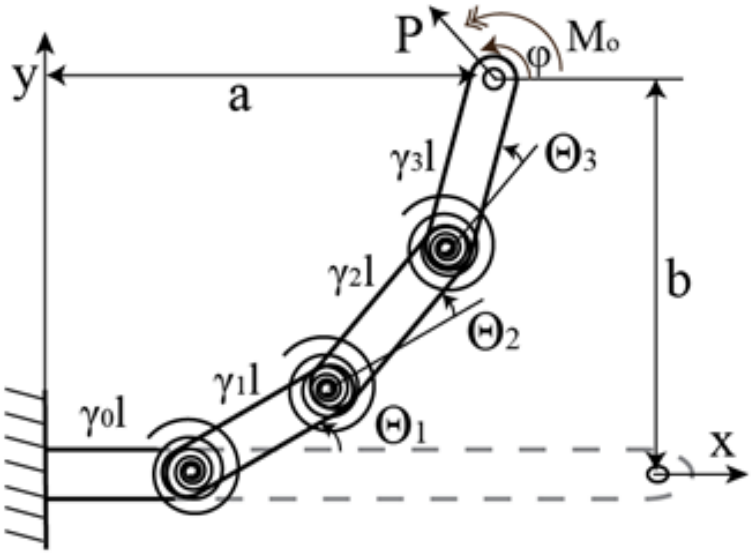

Figure 2.4. 3R PRBM.

For a pure moment load, the maximum error of the tip deflection was found to be 2.3% of the beams length for beam tip slopes less than 270 degrees. The approximated values of the spring stiffness computed are [37]:

$$k_1 = 3.51933\ {}^{EI}/_{l} \qquad k_2 = 2.78518\ {}^{EI}/_{l} \qquad k_3 = 2.79756\ {}^{EI}/_{l} \qquad 2.41$$

The effect of the force angle, ϕ, was neglected in finding the optimized PRBM because the spring stiffness was only correlated slightly to the direction of the force. The error was found to be minimized with the 3R PRBM. With a pure vertical force, $\phi = 90$ degrees, the model has an error of 1.2% when $\theta_0 = 90$ degrees compared to 3.6% for the 1R PRBM. The approximated values of the spring stiffness computed are [37]:

$$k_1 = 3.71591\ {}^{EI}/_{l} \qquad k_2 = 2.87128\ {}^{EI}/_{l} \qquad k_3 = 2.26417\ {}^{EI}/_{l} \qquad 2.42$$

For a straight cantilever beam subjected to an end-force, *P*, and an end-moment, *M*, the nondimensional force index, α, and load ratio, κ, equations are:

$$\alpha = \frac{Pl^2}{2EI} \qquad \beta = \frac{Ml}{EI} \qquad \kappa = \frac{\beta^2}{4\alpha} \qquad 2.43$$

The effect of the angle of the force is neglected because it is shown that the spring stiffness is only slightly correlated to the direction of the applied force. The maximum deflection error is 2.2% of the beam's length. The characteristic radius for combined loading with a nondimentional load ratio, κ, between 0-25 with vertical loads are:

$$\gamma_0 = 0.1 \qquad \gamma_1 = 0.35 \qquad \gamma_2 = 0.40 \qquad \gamma_3 = 0.15 \qquad 2.44$$

The spring stiffnesses for combined loading with a nondimentional load ratio, κ, between 0-25 with vertical loads are:

$$k_1 = 3.51\ {}^{EI}/_{l} \qquad k_2 = 2.99\ {}^{EI}/_{l} \qquad k_3 = 2.58\ {}^{EI}/_{l} \qquad 2.45$$

The benefits of the 3R PRBM are [25, 37, 38]: load independence, high accuracy for large deflection beams and explicit kinematic and static constraint equations. Disadvantages of the 3R PRBM include [37]: assumed no inflection point in the beam and the force angle, ϕ, is limited to $9 - 171$ degrees to have an accurate approximation.

The earlier section presented the literature review of various PRBMs for different types of loading. To develop a spatial pseudo-rigid-body model, the kinematic equations of the beam are derived. Chapter 3 presents the governing equations of a flexible beam that undergoes large deflection.

Chapter 3

Governing Equations of a Flexible Beam[1]

The governing equations of a flexible beam are derived in this chapter. The approach used is similar to the one presented in [7]. However, the reference frames and nomenclature selected for this derivation facilitates the analysis and comparison with compliant mechanisms literature. The derived equations will be validated using a finite element analysis program.

The equations that describe the large deflection of a spatial cantilever beam are derived in four steps. First, the rotation angles describing the bending and twisting of the beam are given. Next, equations for the curvature of the beam are derived. Thirdly, the stiffness properties of the beam are described. Fourthly, the internal moments due to applied forces are described. Finally, the equations are summarized in a form suitable for numerical integration.

3.1 Rotation

The equations describing the deformation of the beam from its unstressed coordinates, *xyz*, to its deformed coordinates, *x'y'z'*, may be found using three rotations matrices. The first two rotations describe the change in the orientation of a segment, *ds*, of the neutral axis. The third rotation describes the twisting of the beam about the deflected orientation of the neutral axis.

[1]Portions of this chapter were previously published in [44]. Permission is included in Appendix A.

There are 12 distinct Euler angle sets that may be chosen to describe the bending and twisting of the beam. However, they are not all equally convenient in subsequent calculations. The possible combinations are: [XYX], [XYZ], [XZX], [XZY], [YXY], [YXZ], [YZX], [YZY], [ZXY], [ZXZ], [ZYX], and [ZYZ]. In describing the unstressed beam, we have taken the neutral axis as parallel with the *x*-axis. The transformation from the unstressed *xyz* coordinate system to the deformed *x'y'z'* coordinate system is simplest when the Euler angle set has two *X* rotations, as in [XYX] and [XZX]. Much of recent literature on planar compliant mechanisms takes the *z*-axis normal to the plane in which the bending occurs. Equations of this form are easiest to obtain using the [XZX] set.

We present the deflection of a beam that is initially straight and is parallel with the *x*-axis. The *y* and *z*-axes are parallel with the principal moments of area (I_{yy} and I_{zz}) of the beam. Using the XZX Euler angle set, we find that the beam can be described using four coordinate systems. The first, ${}^{h}_{s}a$ is aligned with the beam's initial position, *x*, and the last, ${}^{a}_{s}d$ is aligned with its deformed position, *x'*. We can define the ${}^{a}_{s}d$ matrix as the rotation from the $\{s\}$-frame to the $\{a\}$-frame.

The fixed coordinates of the unstressed beam's neutral axis are given as: *x(s)*, *y(s)*, and *z(s)*, in the *xyz* coordinate system. The deflected coordinates in terms of the rotating system with respect to the beam length are *x'(s)*, *y'(s)*, and *z'(s)*. These two frames are related by the XZX sequence of rotations specified in Figure 3.1.

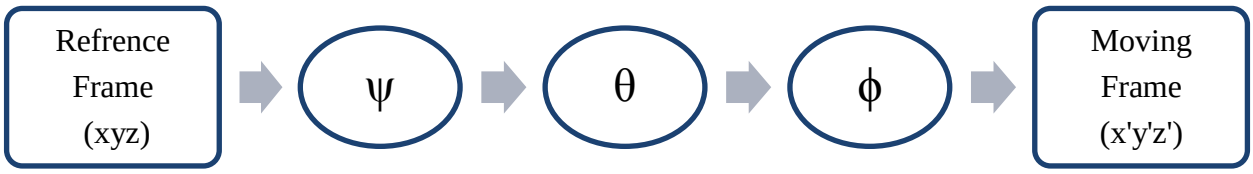

Figure 3.1. Schematic representation of an XZX Euler angle rotation.

It is also useful to define another coordinate system at the free-end of the deflected cantilever as the XYZ frame: *X(s)*, *Y(s)*, and *Z(s)* as shown in Figure 3.2.

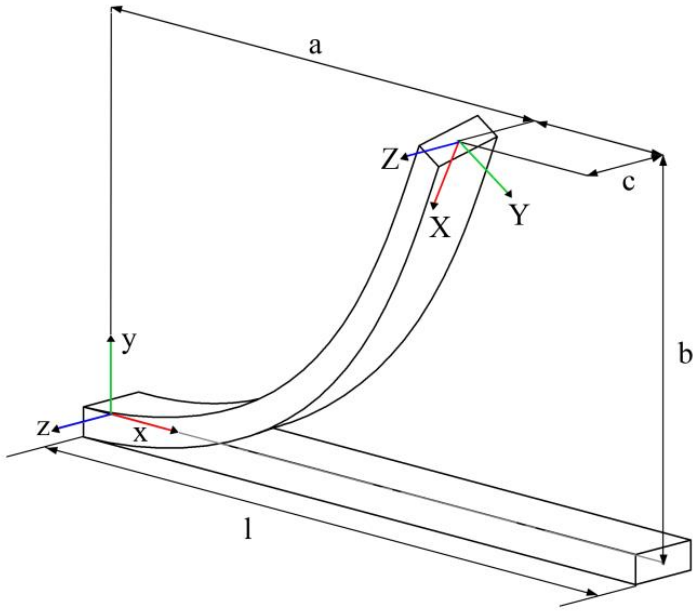

Figure 3.2. Deformed (XYZ) and undeformed (xyz) frames of the cantilever beam.

For an initially straight beam, we can choose to align the neutral axis of the unstressed beam with the *x*-axis in the *xyz* coordinate system. Thus:

$$x(s) = s \tag{3.1}$$

$$y(s) = 0 \tag{3.2}$$

$$z(s) = 0 \tag{3.3}$$

The coordinate frame ${}^{a}_{s}d$, describes the orientation of the neutral axis and the beams twist about the neutral axis. The transformation coordinates from the deformed (${}^{a}_{s}d$) to the undeformed (${}^{h}_{s}a$) frame is given by:

$${}^{a}_{s}d = {}^{a}_{p}R(\phi){}^{p}_{q}R(\theta){}^{q}_{h}R(\psi){}^{h}_{s}a = {}^{a}_{p}R(\phi){}^{p}_{q}R(\theta){}^{q}_{s}b = {}^{a}_{p}R(\phi){}^{p}_{s}c \tag{3.4}$$

where ${}^{h}_{s}a$, ${}^{q}_{s}b$, ${}^{p}_{s}c$, and ${}^{a}_{s}d$ are matrices of unit vectors, and the [XZX] Euler angle matrices are:

$$ {}^{h}_{s}a = \begin{bmatrix} 1 & 0 & 0 \\ 0 & 1 & 0 \\ 0 & 0 & 1 \end{bmatrix} \begin{bmatrix} x \\ y \\ z \end{bmatrix} \tag{3.5} $$

$$ {}^{a}_{p}R(\phi) = \begin{bmatrix} 1 & 0 & 0 \\ 0 & \cos\phi & \sin\phi \\ 0 & -\sin\phi & \cos\phi \end{bmatrix} \tag{3.6} $$

$$ {}^{p}_{q}R(\theta) = \begin{bmatrix} \cos\theta & \sin\theta & 0 \\ -\sin\theta & \cos\theta & 0 \\ 0 & 0 & 1 \end{bmatrix} \tag{3.7} $$

$$ {}^{q}_{h}R(\psi) = \begin{bmatrix} 1 & 0 & 0 \\ 0 & \cos\psi & \sin\psi \\ 0 & -\sin\psi & \cos\psi \end{bmatrix} \tag{3.8} $$

The rotation matrix, ${}^{a}_{h}d$, is:

$$ {}^{a}_{h}d = \begin{bmatrix} \cos\theta & \sin\theta\cos\psi & \sin\theta\sin\psi \\ -\sin\theta\cos\phi & \cos\theta\cos\psi\cos\phi - \sin\psi\sin\phi & \cos\theta\sin\psi\cos\phi + \cos\psi\sin\phi \\ \sin\theta\sin\phi & -\cos\theta\cos\psi\sin\phi - \sin\psi\cos\phi & -\cos\theta\sin\psi\sin\phi + \cos\psi\cos\phi \end{bmatrix} \tag{3.9} $$

3.2 Curvature

The Euler angles θ, ψ and ϕ are functions of the arclength parameter, *s*. Therefore, the curvature at a given point along the beam can be expressed as a vector quantity:

$$ {}^{h}\kappa_j = \frac{d\phi}{ds} d_{j1} + \frac{d\theta}{ds} c_{j3} + \frac{d\psi}{ds} b_{j1} \tag{3.10} $$

where *j* = 1, 2, 3. Which can be expressed in the deformed frame (${}^{a}_{s}d$) by multiplying Equation 3.10 with 3.4, resulting in:

$$ {}^{a}\kappa_i = \frac{d\phi}{ds} \delta_{i1} + \frac{d\theta}{ds} {}^{a}_{p}R_{i3} + \frac{d\psi}{ds} {}^{a}_{p}R_{ij}\ {}^{p}_{h}R_{j1} \tag{3.11} $$

where δ_{ij} is the Kronecker delta symbol. Note that δ_{ij} is equal to one (1) when *i* is equal to *j* and is zero (0) otherwise [39]. Therefore:

$$\kappa_1 = \tau_{x'} = \frac{d\phi}{ds} + \cos\theta \frac{d\psi}{ds} \quad 3.12$$

$$\kappa_2 = \kappa_{y'} = \sin\phi \frac{d\theta}{ds} - \cos\phi \sin\theta \frac{d\psi}{ds} \quad 3.13$$

$$\kappa_3 = \kappa_{z'} = \cos\phi \frac{d\theta}{ds} + \sin\phi \sin\theta \frac{d\psi}{ds} \quad 3.14$$

The inverse expressions for the rate of change of the angles ϕ, θ, and ψ in terms of the curvature components ($\tau_{x'}$, $\kappa_{y'}$, and $\kappa_{z'}$) are given by:

$$\frac{d\phi}{ds} = \tau_{x'} + \kappa_{y'} \cos\phi \frac{\cos\theta}{\sin\theta} - \kappa_{z'} \sin\phi \frac{\cos\theta}{\sin\theta} \quad 3.15$$

$$\frac{d\theta}{ds} = \kappa_{y'} \sin\phi + \kappa_{z'} \cos\phi \quad 3.16$$

$$\frac{d\psi}{ds} = -\kappa_{y'} \frac{\cos\phi}{\sin\theta} + \kappa_{z'} \frac{\sin\phi}{\sin\theta} \quad 3.17$$

A section of the deformed beam, *ds*, is parallel with the d_{i1} unit vector, the expressions for the coordinates of the beam in any coordinate system are the inner product of d_{i1} with the basis vectors of the coordinate system. Thus, in the unstressed, *xyz* coordinate frame:

$$\frac{d\,{}^{h}x_i}{ds} = {}^{h}_{a}R(\psi,\theta,\phi)\,{}^{a}d_{i1} \quad 3.18$$

Thus,

$$\frac{dX}{ds} = \cos\theta \quad 3.19$$

$$\frac{dY}{ds} = \sin\theta \cos\psi \quad 3.20$$

$$\frac{dZ}{ds} = \sin\theta \sin\psi \quad 3.21$$

3.3 Stiffness

The effect of applied loads on the beam may be calculated from the Euler beam equation, which states that the internal moment resultant is proportional to the curvature of the beam:

$$M_i = S\,\kappa_i \tag{3.22}$$

This equation takes on its simplest form when expressed in the deformed frame, which is the frame of the principal bending stiffnesses of the beam.

$$\begin{bmatrix} {}^{a}M_{x'} \\ {}^{a}M_{y'} \\ {}^{a}M_{z'} \end{bmatrix} = \begin{bmatrix} GI_{xx} & 0 & 0 \\ 0 & EI_{yy} & 0 \\ 0 & 0 & EI_{zz} \end{bmatrix} \begin{bmatrix} {}^{a}\tau_{x'} \\ {}^{a}\kappa_{y'} \\ {}^{a}\kappa_{y'} \end{bmatrix} \tag{3.23}$$

where G is the shear modulus, E is the elastic modulus and I_{xx}, I_{yy} and I_{zz} are the second moments of area with respect to the x, y and z axis, respectively. When the stiffnesses are constants, the derivative of Equation 3.23 with respect to arclength, s, expressed in the deformed frame, yields to:

$$\frac{dM_{x'}}{ds} = \mathrm{GI}_{xx}\frac{d\tau_{x'}}{ds} + \left(I_{zz} - I_{yy}\right)E\kappa_{y'}\kappa_{z'} \tag{3.24}$$

$$\frac{dM_{y'}}{ds} = \mathrm{EI}_{yy}\frac{d\kappa_{y'}}{ds} + (GI_{xx} - EI_{zz})\tau_{x'}\kappa_{z'} \tag{3.25}$$

$$\frac{dM_{z'}}{ds} = \mathrm{EI}_{zz}\frac{d\kappa_{z'}}{ds} + \left(EI_{yy} - GI_{xx}\right)\tau_{x'}\kappa_{y'} \tag{3.26}$$

3.4 Moments Due to Force

The direction of an applied load, F_k, is not a function of the arclength, s. Therefore, it is most naturally expressed in the undeformed frame, as the orientations of the other frames are functions of s. We assume that the applied load is located at a point with coordinates (a, b, c) in the XYZ coordinate system. Thus, the internal moment caused by an applied load at position, s, can be expressed as:

$$M(s)=\begin{bmatrix}X(s)-a\\Y(s)-b\\Z(s)-c\end{bmatrix}\times\begin{bmatrix}F_X\\F_Y\\F_Z\end{bmatrix}=\begin{bmatrix}(Y(s)-b)F_Z-(Z(s)-c)F_Y\\(Z(s)-c)F_X-(X(s)-a)F_Z\\(X(s)-a)F_Y-(Y(s)-b)F_X\end{bmatrix} \quad 3.27$$

Or,

$$^{h}\vec{M}=r(s)\times{}^{h}\vec{F} \quad 3.28$$

where $^{h}\vec{M}$ is the moment vector in the $\{h\}$-frame. The derivative of the moment is:

$$\begin{bmatrix}\frac{d\,^{h}M_X}{ds}\\\frac{d\,^{h}M_Y}{ds}\\\frac{d\,^{h}M_Z}{ds}\end{bmatrix}=\begin{bmatrix}\frac{dY}{ds}F_Z-\frac{dZ}{ds}F_Y\\\frac{dZ}{ds}F_X-\frac{dX}{ds}F_Z\\\frac{dX}{ds}F_Y-\frac{dY}{ds}F_X\end{bmatrix} \quad 3.29$$

When is expressed in the deformed frame, Equation 3.29 simplifies to:

$$\frac{d\,^{a}M_{i'}}{ds}={}^{a}_{h}R(\psi,\theta,\phi)\frac{d\,^{h}M_i}{ds} \quad 3.30$$

where $F_{k'}$ is the force expressed in the *x'y'z'* frame. To express the forces in the *xyz* frame, the forces are multiplied by the rotation matrix ${}^{a}_{s}d$:

$$F_{y'}=[\cos\theta\cos\psi\sin\phi+\sin\psi\cos\phi]F_y-\sin\theta\sin\phi\,F_x+[\cos\theta\sin\psi\sin\phi-\cos\psi\cos\phi]F_z \quad 3.31$$

$$F_{z'}=[\cos\theta\cos\psi\cos\phi-\sin\psi\sin\phi]F_y-\sin\theta\cos\phi\,F_x+[\cos\theta\sin\psi\cos\phi-\cos\psi\sin\phi]F_z \quad 3.32$$

Or,

$$^{a}F_{k'}={}^{a}_{h}R(\psi,\theta,\phi)\,{}^{h}F_k \quad 3.33$$

3.5 Governing Equations Summary

Thru the use of a numerical integration program (i.e. Matlab), Equations 3.34-3.42 can be used to find the Euler angles (ϕ, θ, and ψ), the curvatures (τ_x, κ_y and κ_z), and the coordinates (x, y and z) with respect to the arclength (s).

$$\frac{d\phi}{ds} = \tau_{x'} + \kappa_{y'} \cos\phi \frac{\cos\theta}{\sin\theta} - \kappa_{z'} \sin\phi \frac{\cos\theta}{\sin\theta} \tag{3.34}$$

$$\frac{d\,\theta}{ds} = \kappa_{y'} \sin\phi + \kappa_{z'} \cos\phi \tag{3.35}$$

$$\frac{d\psi}{ds} = -\kappa_{y'} \frac{\cos\phi}{\sin\theta} + \kappa_{z'} \frac{\sin\phi}{\sin\theta} \tag{3.36}$$

$$\frac{d\tau_x}{ds} = \frac{1}{\mathrm{GI}_{xx}} \left(I_{yy} - I_{zz}\right) E \kappa_{y'} \kappa_{z'} \tag{3.37}$$

$$\frac{d\kappa_y}{ds} = \frac{1}{\mathrm{EI}_{yy}} \left[\left(EI_{zz} - GI_{xx}\right) \tau_{x'} \kappa_{z'} + F_{z'}\right] \tag{3.38}$$

$$\frac{d\kappa_z}{ds} = \frac{1}{\mathrm{EI}_{zz}} \left[\left(GI_{xx} - EI_{yy}\right) \tau_{x'} \kappa_{y'} + F_{y'}\right] \tag{3.39}$$

$$\frac{d\mathrm{X}}{ds} = \cos\theta \tag{3.40}$$

$$\frac{d\mathrm{Y}}{ds} = \sin\theta \cos\psi \tag{3.41}$$

$$\frac{d\mathrm{Z}}{ds} = \sin\theta \sin\psi \tag{3.42}$$

The ODE45 command in Matlab was used to numerically integrate the above differential equations. These differential equations are derived with s=0 at the free-end of the cantilever beam, assuming no torques and no displacements or rotations in the *XYZ*-frame. The Matlab file is included in the Appendix B.

A follower force retains the same orientation to the actual configuration of the structure of motion [40]. Because the force is applied to the free-end of the beam, the applied force is a

follower load which will always be at an angle ϕ, in the *XY*-frame and an angle ζ, in the *YZ*-frame with respect to the beam tip. The force from the fixed frame of the beam, *xyz*, can be found by a rotation of π about the *z*-axis multiplied by the rotation matrix ${}^{a}_{s}d$. In a similar manner, the coordinates of the free tip end (*a*, *b*, and *c*) in the *xyz* frame are found.

3.6 Numerical Validation

A Finite Element Analysis (FEA) program was used to validate the derived equations of a spatial cantilever beam with different input loads and directions. A follower load was used in the FEA compare the approximated results to those obtained thru the numerical integration. The width (*z*-dimension) to height (*y*-dimension) ratio for this analysis was chosen to be 10. The validation consists of five case studies. These cases are when the applied force is in the *Y*-direction, in the *XY*-plane, in the *Z*-direction, in the *YZ*-plane and general *XYZ* forces.

3.6.1 Validation of Planar Force in the Y-direction

The approximated values of the normalized deflections *a/l* and *b/l*, for different loads in the *Y*-direction are plotted in Figure 3.3. As can be observed, both the deflection at the end of the beam and the tip slope increase as the forces increases.

The Pearson's correlation coefficient is a summary statistic that represents the strength and nature of linear association between two variables [41]. The Pearson's correlation coefficient for the FEA and numerical integration ranged from 0.9309-0.9915. In this case, the spatial beam behaves as a planar model with an applied force in the *Y*-direction.

3.6.2 Validation of Forces in the XY-plane

The beam deformation with an inclined load in the *XY*-plane is shown in Figure 3.4. The dots represent the results via FEA and the line represents the results via numerical integration.

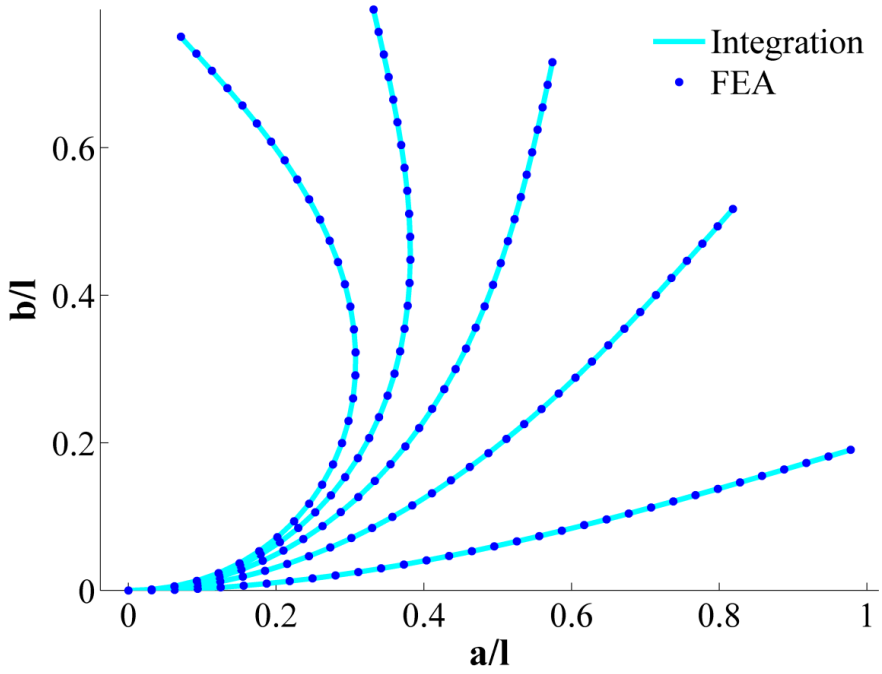

Figure 3.3. Comparison of a spatial cantilever beam results with applied vertical end load thru numerical integration and FEA.

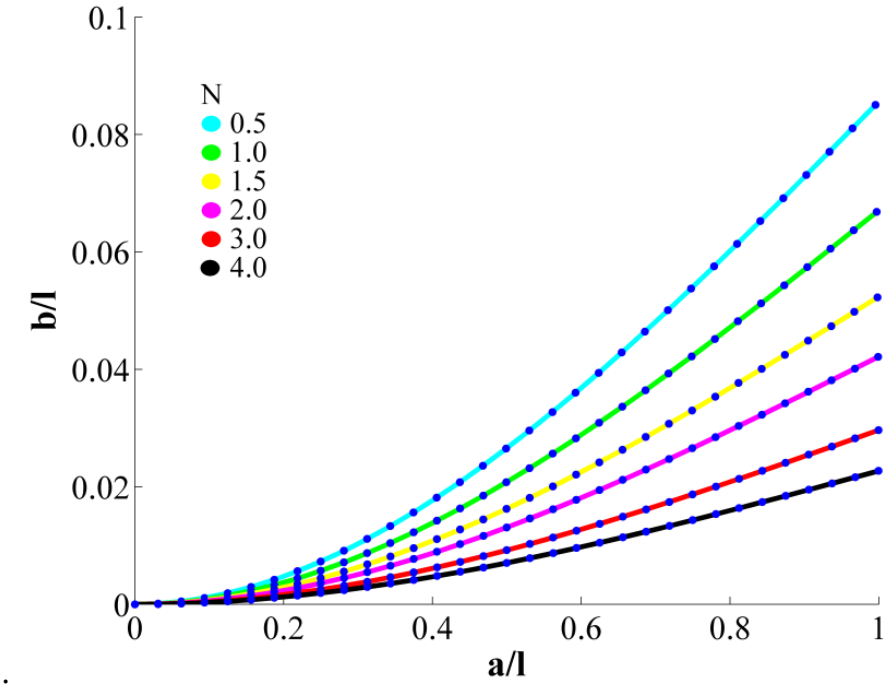

Figure 3.4. Plot of different values of N with the same force magnitude. a/l and b/l are not drawn to the same scale.

The color of the line represents the applied force angles N as shown in the legend. The legend nomenclature is similar to the one presented in [8], where N corresponds to the load angle in the XY-plane, such that:

$$N = \frac{-1}{\tan\phi} \tag{3.43}$$

The same force magnitude was applied over different angles ϕ of the force. The Pearson's correlation factor between the FEA and numerical integration is 0.9395.

3.6.3 Validation of Force in Z-direction

The approximated nondimensional values, *a/l* and *c/l*, of the deformation for a spatial cantilever beam with input forces parallel to the *Z*-direction are plotted in Figure 3.5. The Pearson's correlation coefficient for the FEA and numerical integration ranged from 0.9309-0.9914. For this case, the Pearson's correlation factor increases as a function of the magnitude of the input load.

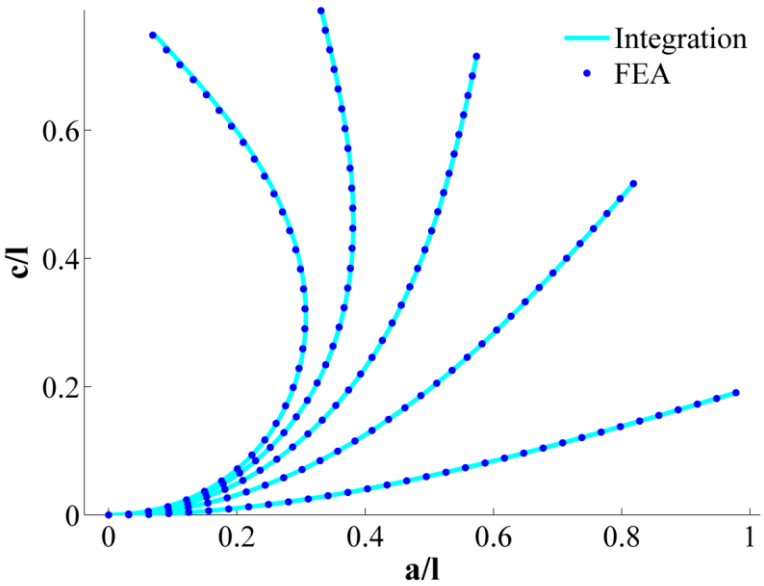

Figure 3.5. Comparison of a spatial cantilever beam results with applied axial end load thru numerical integration and FEA.

3.6.4 Validation of Force in the YZ-plane

The results *a/l* versus *b/l* and *a/l* versus *c/l* for an applied load in the *YZ*-plane at different angles are plotted in Figure 3.6a and Figure 3.6b, respectively. For both plots, the magnitude of the force remained constant as the input angles of the load varied in the *YZ*-plane. In these plots, the dots represent the results via FEA while the lines represent the results obtained by numerical integration. The color of the line represents the applied force angle. The Pearson's correlation coefficient for the FEA and numerical integration for the displacement in the *y*-direction ranged from 0.9454-0.9895 and for the *z*-direction displacement is 0.8858 - 0.9191.

3.6.5 Validation of General XYZ Forces

To validate the equations, the same force magnitude was applied to a beam at two different angles as shown in Figure 3.7a and Figure 3.7b. At N=116.6 and ζ=30 degrees, the Pearson's correlation factor is 0.7506 in the *x*-direction, 0.9556 in the *y*-direction and 0.8870 in the *z*-direction. At N=153 and ζ=60 degrees, the Pearson's correlation factor is 0.9957 in the *x*-direction, 0.9168 in the *y*-direction and 0.9149 in the *z*-direction.

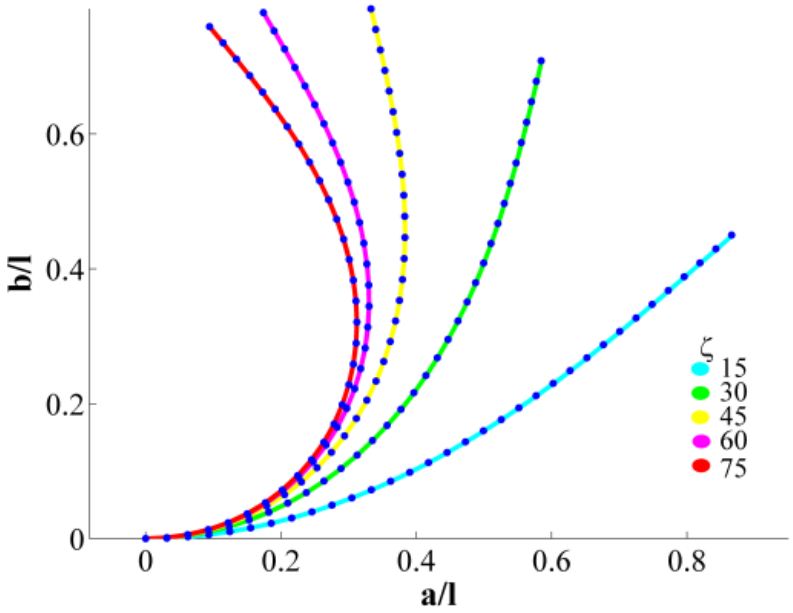

(a)

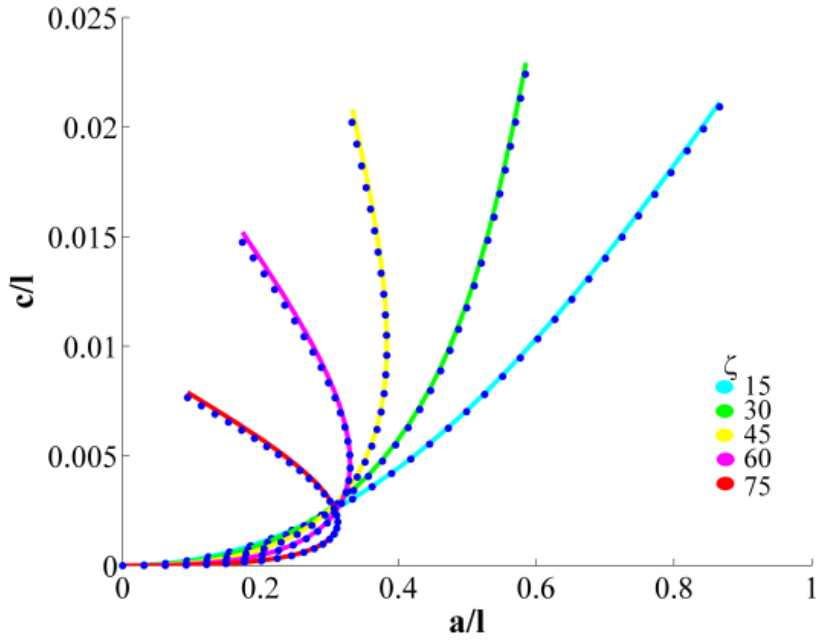

(b)

Figure 3.6. Deformation results of a beam in the (a) y-direction and (b) z-direction with inclined load via integration (line) and FEA (dots). a/l and c/l are not drawn to the same scale.

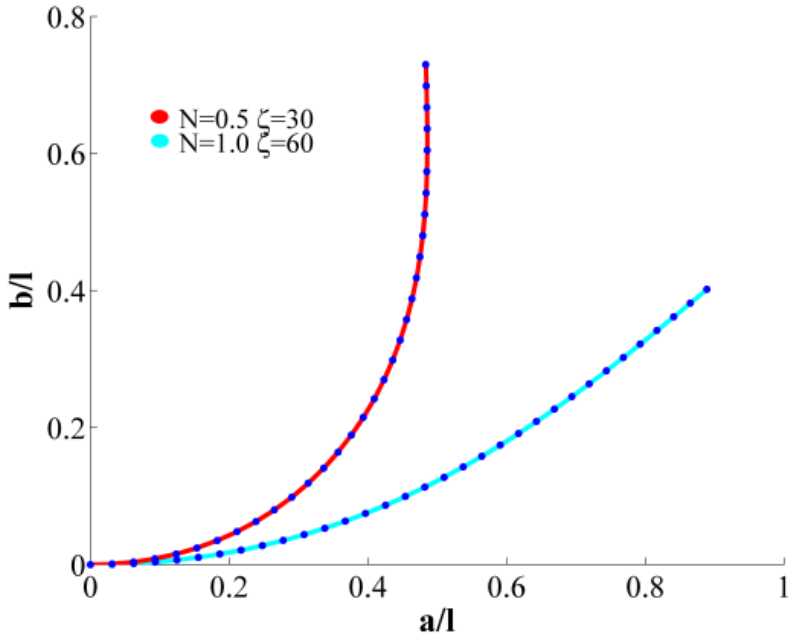

(a)

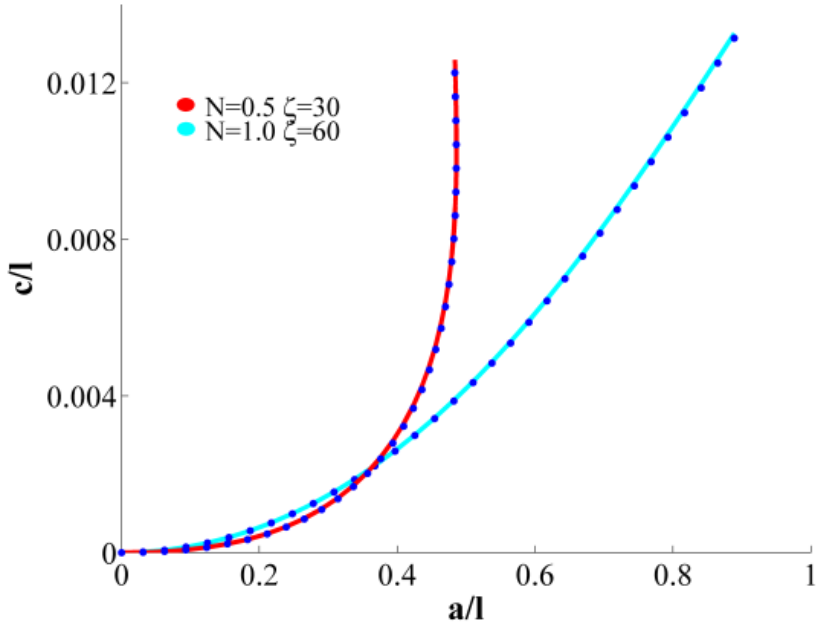

(b)

Figure 3.7. Nondimensional deformation of beam subjected to the same force at different N and ζ angles in the (a) y-direction and (b) z-direction. a/l and c/l are not drawn to the same scale.

Chapter 4

Axisymmetric Pseudo-Rigid-Body Model[2]

The objective of this chapter is to describe kinematic models, pseudo-rigid-body models (PRBMs), for approximating the spatial deflection of an elastic beam with axisymmetric cross-section. The equations that predict the rotation, curvature and location of the beam's neutral axis as function of the arclength were derived in Chapter 3. PRBMs modeling the kinematics and stiffness of an axisymmetric cantilever beam with force end-loads and with moment end-loads are presented. Also, approximations for the characteristic radius factor and the parametric coefficient for moment loading as a function of the tip angle are presented.

4.1 Axisymmetric Pseudo-Rigid-Body Model

In an axisymmetric cantilever beam, I_{zz} is equal to $I_{yy.}$ The change in the curvature of the beam can be expressed as follows:

$$\frac{d\tau_x}{ds} = \frac{1}{\mathrm{GI}_{xx}}\left(I_{yy} - I_{zz}\right)E\kappa_{y'}\kappa_{z'} \tag{4.1}$$

$$\frac{d\kappa_y}{ds} = \frac{1}{\mathrm{EI}_{yy}}\left[(EI_{zz} - GI_{xx})\tau_{x'}\kappa_{z'} + F_{z'}\right] \tag{4.2}$$

$$\frac{d\kappa_z}{ds} = \frac{1}{\mathrm{EI}_{zz}}\left[\left(GI_{xx} - EI_{yy}\right)\tau_{x'}\kappa_{y'} + F_{y'}\right] \tag{4.3}$$

[2]Portions of this chapter were previously published in [44]. Permission is included in Appendix A.

Thus, the change in torsion, dt_x/ds, is zero because the moment of inertia I_{zz} is equal to I_{yy}, Therefore, the torsion is constant throughout the beam. When there is no applied torque on the free-end ($\tau_x(s=0) = 0$), the torsion (twisting of the beam about the neutral axis) is equal to zero ($\tau_x(s) = 0$). The governing curvature equations for an axisymmetric beam with no torsion become:

$$\frac{d\tau_x}{ds} = 0 \tag{4.4}$$

$$\frac{d\kappa_y}{ds} = \frac{F_{z'}}{\mathrm{EI}_{eq}} \tag{4.5}$$

$$\frac{d\kappa_z}{ds} = \frac{F_{y'}}{\mathrm{EI}_{eq}} \tag{4.6}$$

where $I_{eq} = I_{yy} = I_{zz,}$ E is the Young's Modulus, and $F_{y'}$ and $F_{z'}$ is the force expressed in the $x'y'z'$ frame, as stated in Chapter 3, such that:

$$F_{y'} = [\cos\theta\cos\psi\sin\phi + \sin\psi\cos\phi]F_y - \sin\theta\sin\phi\,F_x + [\cos\theta\sin\psi\sin\phi - \cos\psi\cos\phi]F_z \tag{4.7}$$

$$F_{z'} = [\cos\theta\cos\psi\cos\phi - \sin\psi\sin\phi]F_y - \sin\theta\cos\phi\,F_x + [\cos\theta\sin\psi\cos\phi - \cos\psi\sin\phi]F_z \tag{4.8}$$

where ϕ, θ, and ψ are the Euler angles and F_x, F_y and, F_z are the forces applied to the beam with respect to the xyz coordinate system, as discussed in Chapter 3. Because the ϕ rotation is defined by the amount that the $\{p\}$-frame must be rotated about the neutral axis, so that I_{zz} is the smallest principal moment of area and I_{yy} is the larger principal moment of area. Because in an axisymmetric beam the moments of area are equal, ϕ becomes arbitrary and may be chosen as $\phi(s) = 0$. Thereby, Equation 3.12 requires that:

$$\frac{d\phi}{ds} = -\frac{d\psi}{ds}\cos\theta \tag{4.9}$$

Thus $\psi(s)$ is constant. This means that the beam stays in the same plane because the rotations of each beam segment are about parallel axes.

One can assume a PRBM for an axisymmetric cantilever beam similar to the one presented in [8], attaching a spherical joint instead of a revolute joint, to allow rotation about the *x*, *y* and *z*-axes. The PRBM consists of two rigid links connected by a spherical joint, as shown in Figure 4.1. The spherical joint is located at γl distance from the free-end of the cantilever beam, allowing the rotation of the pseudo-rigid-body link, and thus, the displacement of its tip.

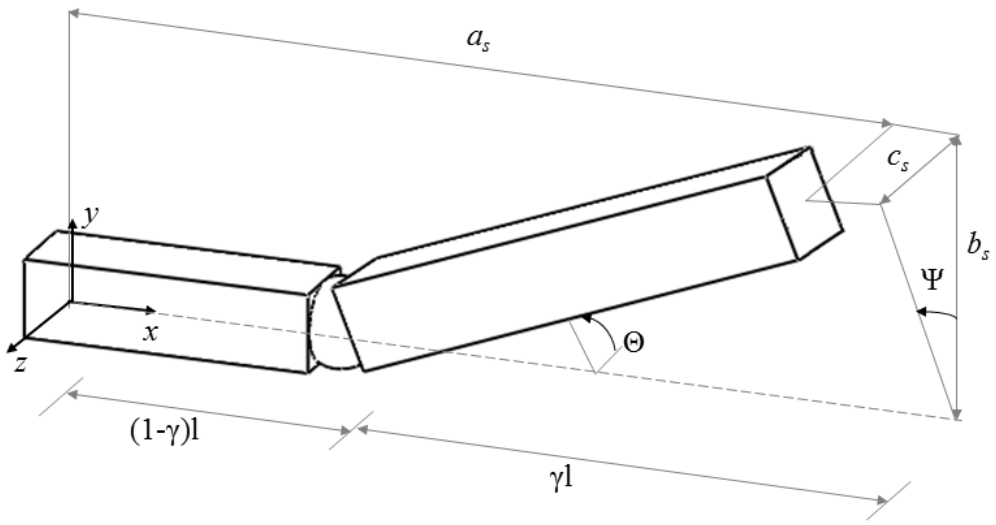

Figure 4.1. Axisymmetric PRBM of a cantilever beam.

The kinematic equations of the cantilever beam can be found by means of spherical trigonometry. The tip coordinates (a_s, b_s, c_s) of the spatial PRBM of a cantilever beam with end loads are given by:

$$a_s = l - \gamma l(1 - \cos\Theta) \tag{4.10}$$

$$b_s = \gamma l \sin\Theta \cos\Psi \tag{4.11}$$

$$c_s = \gamma l \sin\Theta \sin\Psi \tag{4.12}$$

where *l* is the length of the beam, γ is the characteristic radius factor, Θ is the rotation angle of the beam with respect to the *z*-axis, and Ψ is the rotation angle of the beam with respect to the *x*-

axis. These equations are identical to the planar PRBM found in Howell's [8], when the angle Ψ is equal to zero.

4.2 Force-Loading

We can decompose the applied force as a magnitude with two angles ζ and ϕ. Where ϕ is the angle in the XY-plane and ζ is the angle in the YZ-plane, as shown in Figure 4.2.

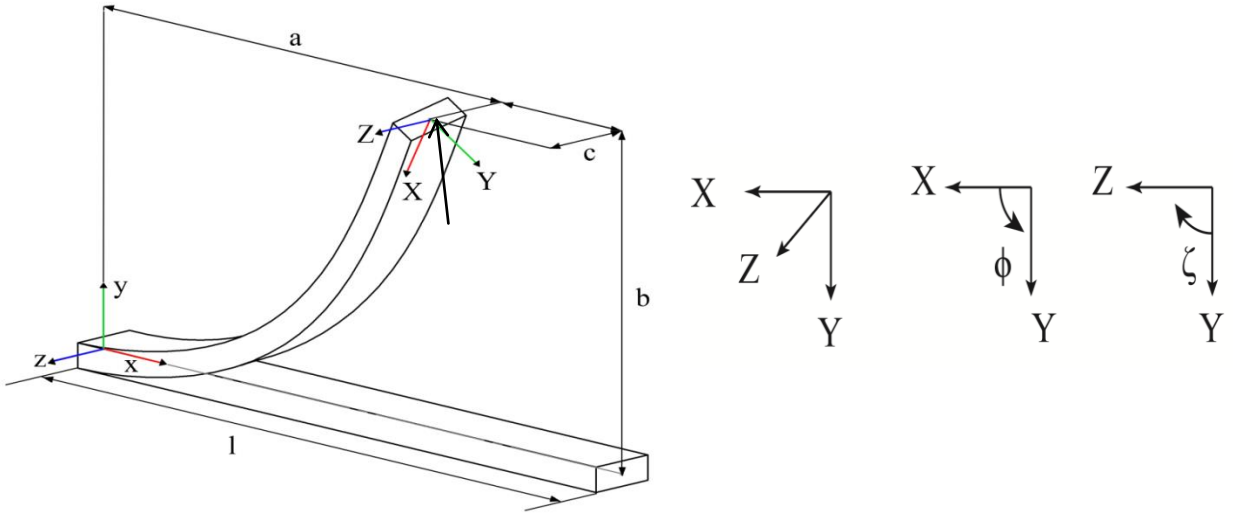

Figure 4.2. Angles of the applied force in the cantilever beam.

The ζ angle depends on the direction of the force with respect to the *XYZ* undeformed coordinate system. In the governing equations of the beam, the first rotation is about the *x*-axis of the *xyz* coordinate system. For example, an input force in the *z*-direction, ζ, equal to 90 degrees, Ψ is equal to 90 degrees. The Ψ angle is equal to the applied force input angle in the *yz*-plane:

$$\Psi = \zeta \tag{4.13}$$

In the planar case, the pseudo-rigid-body link follows the path of circle, i.e. a change in the ϕ angle changes the magnitude of the deformation of the beam, but it will always follows the same path.

The governing equations of the beam employ a follower load at the end of the beam, to acquire the deflection of the beam's tip and the non-follower forces of the beam. The governing equations are convenient to analyze beams subjected to follower loads; to obtain the non-follower loads requires to know the rotations of the Euler angles which makes the comparison with non-follower results difficult. In order to compare with non-follower based PRBM, a Finite Element Analysis (FEA) program was used to calculate the deflection of the beam instead of the governing equations. In the FEA program, the main input are the non-follower forces, whereas in the governing equation model of the beam, only follower forces yields the exact results for an applied force load, as shown in Chapter 3. Therefore, an FEA program (Ansys) was used to obtain non-follower load results.

Inclined non-follower forces in the *xy* and *yz*-plane were applied to the cantilever beam in a finite element analysis program. The non-follower forces applied to the cantilever ranged from 3.0 x10^3 N to 3.0 x10^5 N in increments of 3.0 x10^3 N, keeping a constant angle of inclination of ϕ=116.6 degrees. The force angle in the *xy*-plane was kept at ϕ=116.6 degrees, but the force angle in the *yz*-plane was changed.

With the exact values of the deflection of the beam obtained thru FEA analysis, the exact values of the pseudo-rigid-body parameters are found through an optimization routine solving Equations 4.10 - 4.12. For example, a force magnitude of 7.5 x 10^4 N was applied to the beam at an angle of ϕ=116.6 degrees in the *xy*-plane, and ζ=30 degrees in the *yz*-plane. The nondimensional deflection coordinates of the beam's tip are *a*/*l*= 0.47190, *b*/*l*= 0.67509 and, *c*/*l*= 0.38976. The PRBM parameters found via the optimization routine are γ= 0.8394, Θ= 1.1909 radians (68.2326 degrees) and, Ψ= 0.523599 radians (30.0 degrees). One can notice that the angle Ψ is equal to the input angle ζ in the *yz*-plane, as stated in Equation 4.13.

The one revolute joint (1R) PRBM parameters from Howell's [8], can be used to find the axisymmetric spatial PRBM. The 1R PRBM equations from [8] are:

$$a_p = l - \gamma l(1 - \cos\Theta) \tag{4.14}$$

$$b_p = \gamma l \sin\Theta \tag{4.15}$$

This set of equations can be used to find the horizontal and vertical coordinates of the beam (a_p, b_p) given the magnitude and the angle of inclination of the force in the *xy*-plane and the geometric parameters. These coordinates were rotated from their planar position by a rotation of the *x*-axis:

$$\begin{bmatrix} a_s \\ b_s \\ c_s \end{bmatrix} = \begin{bmatrix} 1 & 0 & 0 \\ 0 & \cos\Psi & -\sin\Psi \\ 0 & \sin\Psi & \cos\Psi \end{bmatrix} \begin{bmatrix} a_p \\ b_p \\ 0 \end{bmatrix} \tag{4.16}$$

Figure 4.3 shows the path of the spatial PRBM and the FEA when an inclined non-follower load in the *xyz* coordinate system is applied to the beam. The angle in the *xy*-plane was kept at n=0.5 (ϕ=116.6 degrees). For the PRBM calculation, the characteristic radius used was the approximation for $0.5 < n \leq 10.0$ is [8]:

$$\gamma = 0.841655 - .0067807n + .000438004n \tag{4.17}$$

Three cases were studied: when ζ=30, 45, and 60 degrees. The dots represent the PRBM results and the line represents the FEA results. The parameters are shown in Table 4.1.

Therefore, the planar PRBM parameters work for an axisymmetric beam when the planar results are multiplied by a rotation in the *x*-direction.

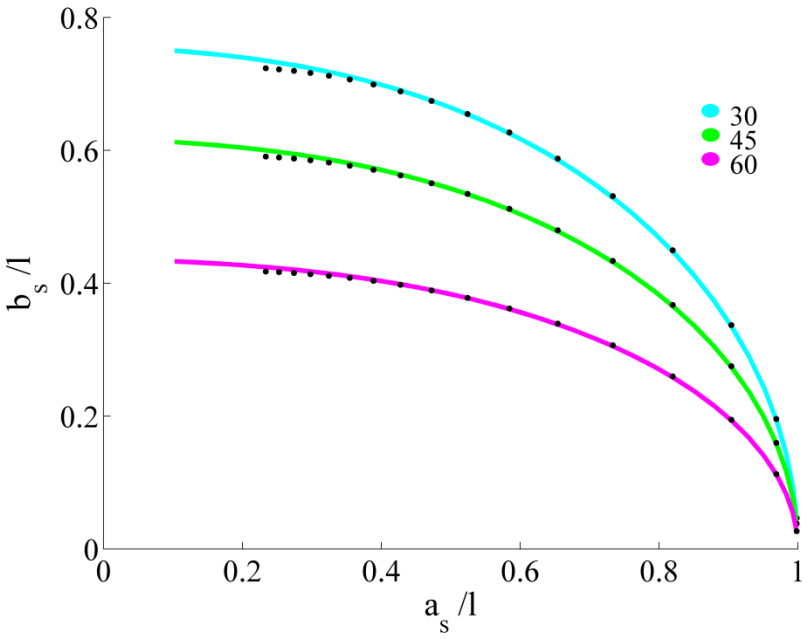

(a)

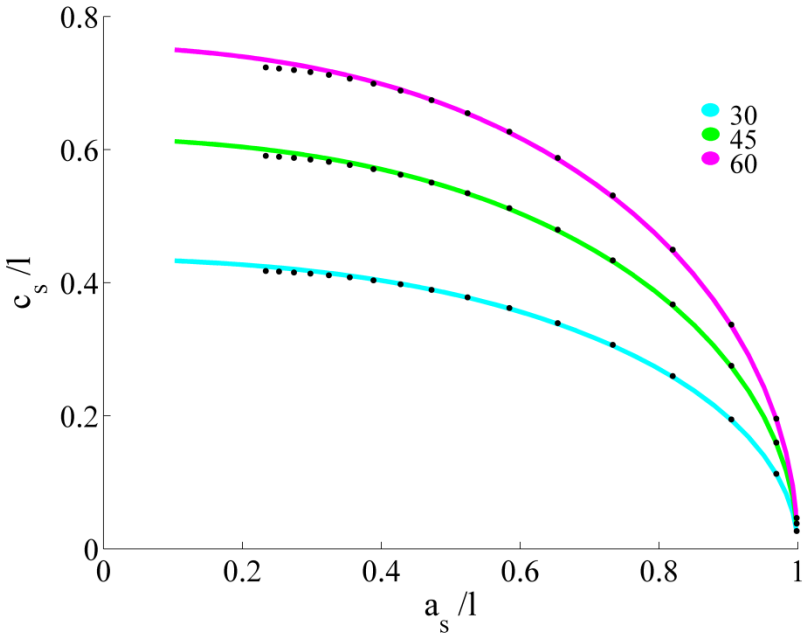

(b)

Figure 4.3. Path results for FEA and spatial PRBM in the (a) *y*-direction and (b) *z*-direction.

Table 4.1. Parameters used in the validation of the axisymmetric spatial PRBM.

Parameters	Value
w (m)	0.1
h (m)	0.1
l (m)	10
E (GPa)	207×10^9
ν	0.33
ΔF	3.0×10^3
ϕ (degrees)	116.6°

4.3 Moment Input

Non-follower in-plane moments, M_z, and out-of-plane moments, M_y, were applied in the governing equations of the axisymmetric beam. With multiple moments, the pseudo-rigid-body angle with respect to the *z*-axis is Θ, and the rotation of the *xy*-plane about the *x*-axis is the pseudo-rigid-body angle Ψ, as shown in Figure 4.1. The PRBM parameters for a planar beam with an in-plane applied moment are found as shown in [8].

4.3.1 Out-of-Plane Moment Only (M_y only)

The pseudo-rigid-body model for a planar axisymmetric beam with an out-of-plane moment, M_y, is shown in Figure 4.4. The PRBM is similar to the one found in [8], but applying an out-of-plane moment M_y, which consists of two links connected through a revolute joint.

The kinematic equations of the cantilever beam can be found by setting the value Ψ equal to 90 degrees in Equations 4.10-4.12. The end-tip coordinates of the spatial PRBM (a_s, c_s) of a cantilever beam with a M_y load are given by:

$$a_s = l - \gamma l(1 - \cos\Theta) \tag{4.18}$$

$$b_s = 0 \tag{4.19}$$

$$c_s = \gamma l \sin \Theta \tag{4.20}$$

where l is the length of the beam, γ is the characteristic radius factor and, Θ is the rotation angle of the beam with respect to the z-axis.

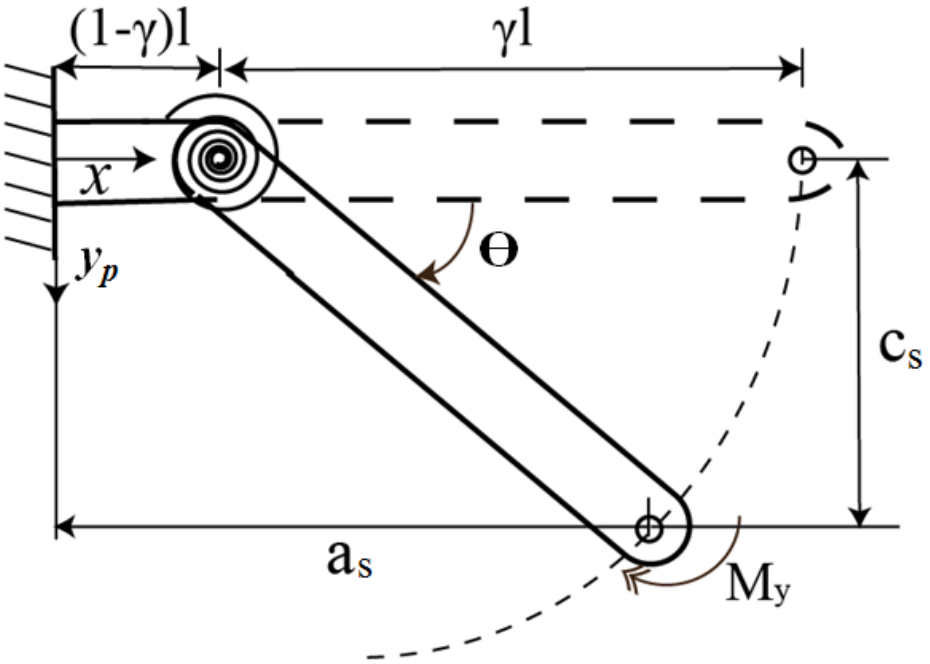

Figure 4.4. PRBM for an axisymmetric beam with an applied out-of-plane moment.

A series of out-of-plane moments were applied to a cantilever beam in order to calculate the exact deflection of the beam. Figure 4.5 presents the nondimensional path of the one revolute joint (1R) PRBM and the results of the kinematic equations, using Howell's pseudo-rigid-body parameters [8], where γ = 0.7346 and c_θ = 1.5164. With these parameters, the relative deflection error (Equation 2.16), between the results of the kinematic equations and the 1R PRBM at the tip angle of 124 degrees is 1.4070%, as shown in Figure 4.6.

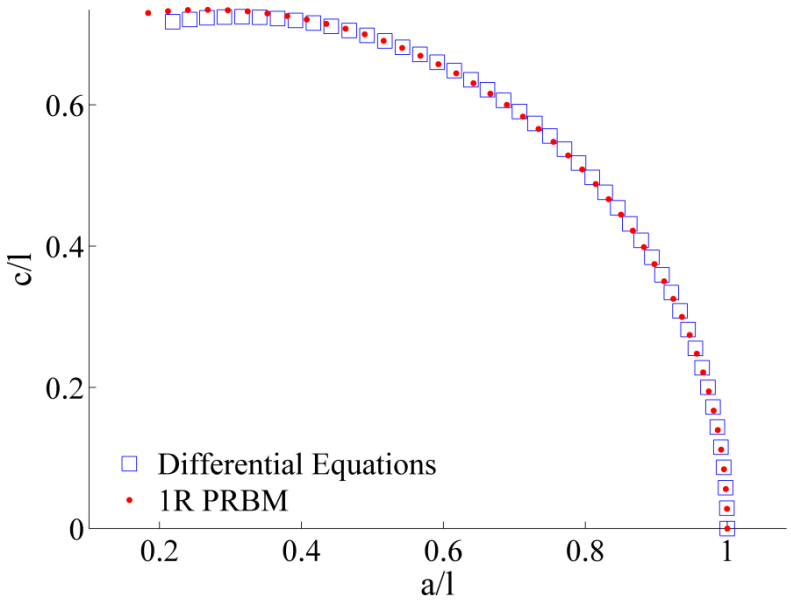

Figure 4.5. Nondimensional path results from the 1R PRBM and numerical equations for a beam with an applied moment in the *y*-direction, M_y.

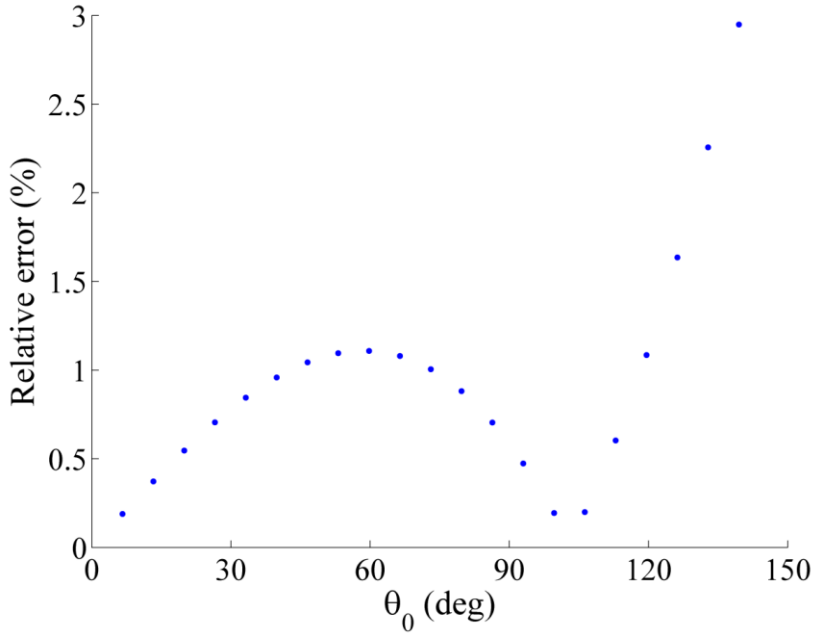

Figure 4.6. Relative deflection error of a cantilever beam versus the tip angle.

To minimize the relative deflection error, the exact values of the characteristic radius parameter and the parametric angle coefficient can be found through optimization of the coordinates. The nondimensional theoretical coordinates from the Bernoulli-Euler large-deflection equations depend only on the tip slope of the beam's end, as stated in Equations 2.34 and 2.37. Substituting tip angles from 0 to 124.4 degrees, the theoretical coordinates of the deflection of the beam can be found. Knowing the deflection of the beam's end, the exact PRB parameters can be calculated by replacing the theoretical coordinates into Equations 4.18 and 4.20. A polynomial fitting routine was implemented to find the governing equation that describes the characteristic radius factor and the parametric coefficient as a function of the tip angle as shown in Figure 4.7 and Figure 4.8, respectively.

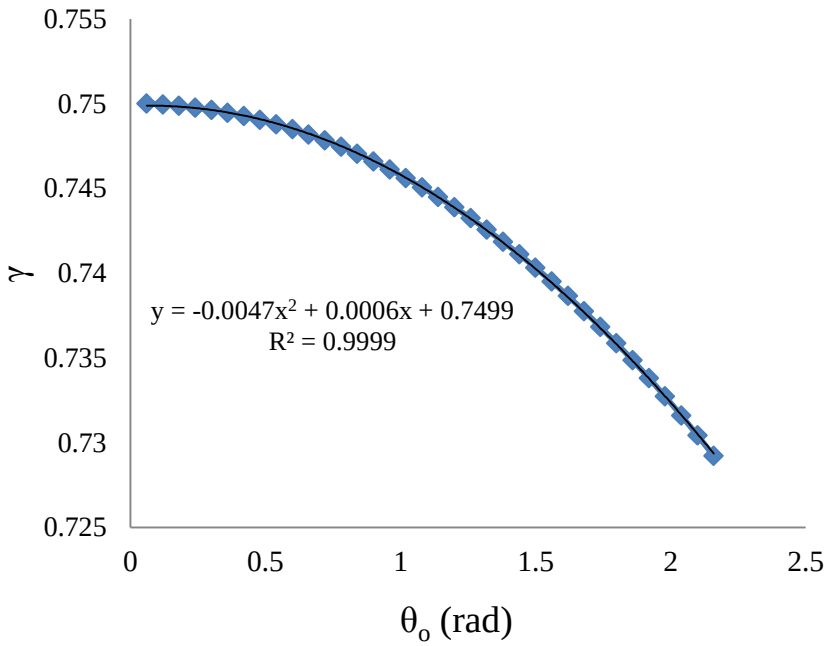

Figure 4.7. Exact value of the characteristic radius factor for different tip angles.

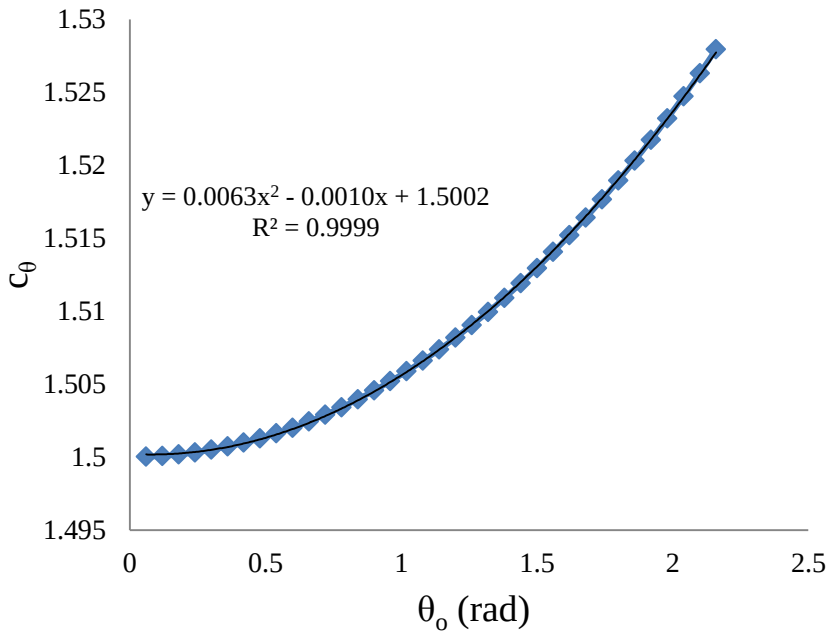

Figure 4.8. Exact value of the parametric angle coefficient for various tip angles.

From the polynomial fitting curve, the equation that relates the approximated value of the characteristic radius factor as a function of the tip angle for planar beams is given by:

$$\gamma_a = -0.0047\,\theta_0^2 + 0.0006\theta_0 + 0.7499 \tag{4.21}$$

The relation between the tip angle and the approximated parametric angle coefficient is:

$$c_{\theta a} = 0.0063\,\theta_0^2 + 0.0010\theta_0 + 1.5002 \tag{4.22}$$

where the tip angle is measured in radians. Substituting the approximated values of the characteristic radius factor and the approximated values of the parametric angle coefficient in Equations 4.18 and 4.20, the path results of the 1R PRBM are plotted in Figure 4.9. Moment loads of 0 to $5\text{x}10^5$ Nm, increased by $1\text{x}10^4$ Nm were applied to the cantilever beam. These sets of loads have tip angles ranging from 0 to 172.71 degrees. The squares in Figure 4.9 represent the results from the kinematic equations, and the dots stand for the results given by the

approximated 1R PRBM model. The Pearson's correlation factor between the 1R PRBM results and the kinematic equations is 0.99999985.

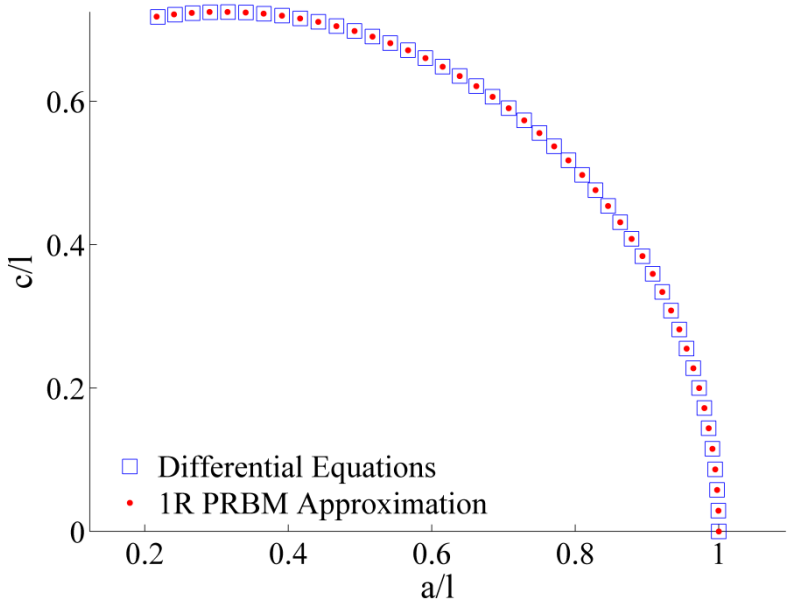

Figure 4.9. Nondimensional path results for the optimized 1R PRBM and numerical equations for a beam with an applied moment in the *y*-direction, M_y.

The relative error of the deflection between the theoretical and the kinematics equations is presented in Figure 4.10. The differential equations results were calculated applying a moment load at the free-end of the beam, ranging from 0 to $5x10^5$ Nm, increased by $1x10^4$ Nm, into the governing equations of the beam. The results from the differential equations of the beam provide tip angles that ranged from 0 to 172.71 degrees. The tip angle from the kinematic equations was substituted into the nondimensional equations to find the theoretical displacement of the beam. The theoretical displacements and the differential equations displacements were used to calculate the displacement to obtain the relative deflection error. The relative deflection error at 172.71 degrees (3.01449 radians) is 2.537×10^{-7} %, as shown in Figure 4.10.

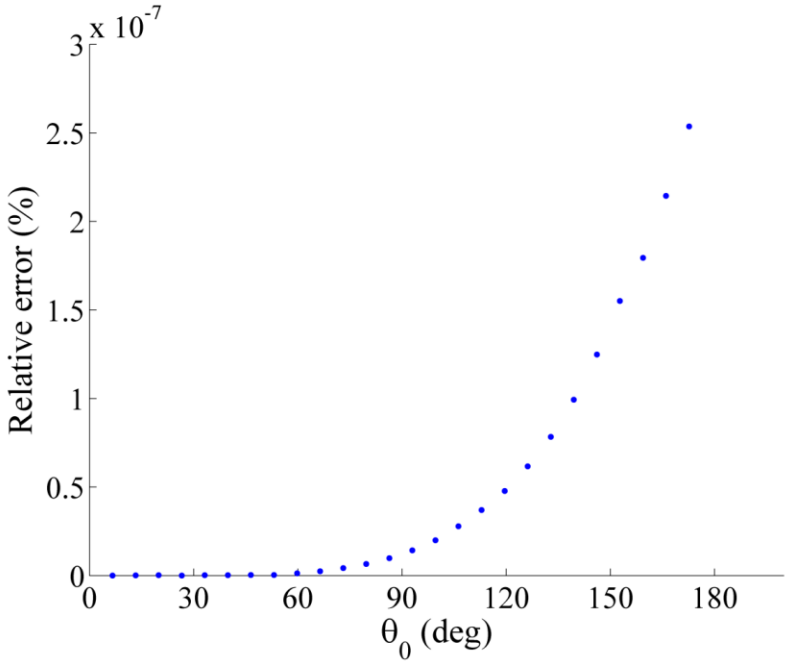

Figure 4.10. Relative deflection error between the theoretical and the governing equations of a cantilever beam.

In previous compliant mechanisms work, the maximum tip angle for a 1R PRBM to achieve a relative deflection error of 0.5% was 124.4 degrees [8]. The relative deflection error for a beam with a single moment applied at the end, using the approximated values of the characteristic radius factor and the approximated parametric coefficient, for a tip angle of 124.4 degrees, is 0.011%, as shown in Figure 4.11. This approximation provides an improvement to previous published parameters, increasing the tip angle to 169.76 degrees (2.96294 radians), where the relative error is 0.5%.

4.3.1.1 Energy Methods Using PRBMs

In force loaded pseudo-rigid-body models (PRBMs) the energy stored in the torsional spring is equal to the energy stored in the deformed beam. This is not true in moment loaded beams as shown in this section.

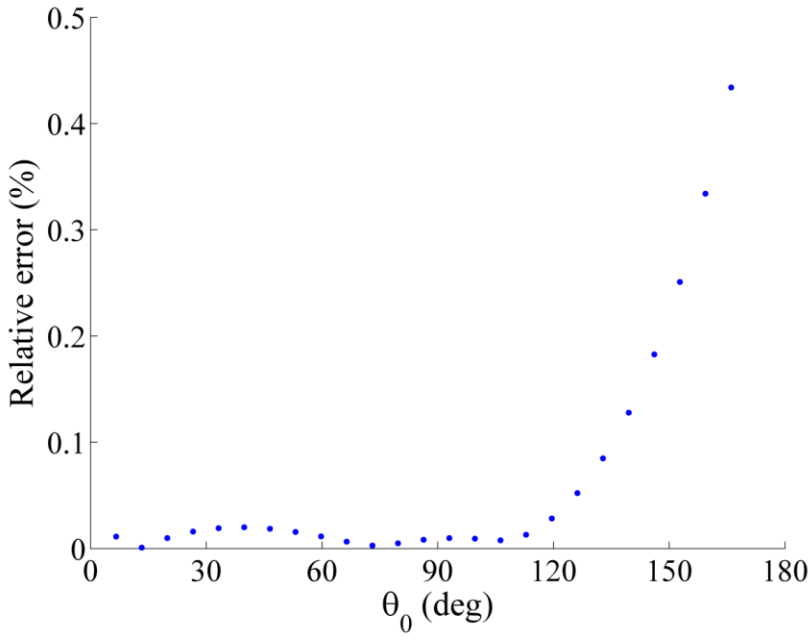

Figure 4.11. Relative deflection error of a cantilever beam versus the input angle of the applied moment load.

The PRBM with a single applied out-of-plane end-moment is shown in Figure 4.4. Assuming no energy is loss in the system, the potential energy of a spring is given by:

$$V = \frac{1}{2} K_s \Theta^2 \tag{4.23}$$

where the spring constant, K_s, and the beam end angle. The relationship between the end-slope angle and the spring constant in terms of the PRBM parameters are given by:

$$K_s = \gamma K_\theta EI/l \tag{4.24}$$

where γ is the characteristic radius factor, K_θ is the stiffness coefficient, E is the Young's Modulus, I is the moment of inertia and l is the length of the beam. For a moment end-load, the relationship can be simplified to:

$$K_s = c_\theta EI/l \tag{4.25}$$

$$\theta_0 = c_\theta \Theta \tag{4.26}$$

where c_θ is the parametric angle coefficient. In the case of a single spring, the potential energy is equal to the strain energy. After substitution of Equations 4.25 and 4.26 in the spring potential energy formula (Equation 4.23), the energy due to a spring is given by:

$$V = \frac{EI\theta_0^2}{2lc_\theta} \tag{4.27}$$

Using elastic theory, the strain energy of stored in a beam given an input moment is given by:

$$U = \int \frac{{M_0}^2 ds}{2EI} \tag{4.28}$$

where the moment at the end of the beam is given by:

$$M_0 = \frac{EI\theta_0}{l} \tag{4.29}$$

Substituting Equation 4.29 of the moment at the end of the beam in the strain energy Equation 4.28 and integrating, the potential energy of a flexible beam is found to be:

$$U = \frac{EI\theta_0^2}{2l} \tag{4.30}$$

Combining Equations 4.27 and 4.30, the potential energy of the spring, V, and the strain energy stored in the beam, U, for a beam with end-moment loading, are related as:

$$U = c_\theta V \tag{4.31}$$

The stiffness of a beam depends in the material properties and the geometry. The stiffness of a beam is the product of the moment of inertia and the Young's Modulus. The stiffness of a beam in relation with the one of the PRBM can be derived in a similar manner that the potential energy. The stiffness of a flexible beam, K_f, and stiffness of the PRBM are related by:

$$K_f = c_\theta K_s \tag{4.32}$$

Following the nomenclature of compliant mechanisms, the stiffness coefficient, K_Θ is:

$$K_\Theta = c_\theta K_s \tag{4.33}$$

The difference in the PRBM spring energy and the beams strain energy means that caution must be used in evaluating PRBMs using moment loaded segments.

4.3.2 Multiple Loading: M_y and M_z

Non-follower in-plane and out-of-plane moments, M_z and M_y, respectively, were applied to the axisymmetric beam. The torsion (twisting of the beam about the neutral axis) is constant throughout the beam. The curvature equations in the follower frame become:

$$\frac{d\tau_x}{ds} = 0 \tag{4.34}$$

$$\frac{d\kappa_y}{ds} = 0 \tag{4.35}$$

$$\frac{d\kappa_z}{ds} = 0 \tag{4.36}$$

The change of the curvature of an axisymmetric cantilever beam with applied multiple moments is zero. Thus, the curvature remains constant through the beam.

The pseudo-rigid-body angle with respect to the *z*-axis is Θ, and the pseudo-rigid-body angle with respect to the *x*-axis is Ψ, are shown in Figure 4.1. For axisymmetric beams, the Ψ angle depends on the direction of the applied moment with respect to the *xyz* undeformed coordinate system.

Figure 4.12 and Figure 4.13 shows the path of the spatial PRBM and the differential equations when an inclined non-follower load in the *xyz* coordinate system is applied to the beam. Three different paths were studied, when M_z is 4.0 x10^4 Nm (cyan), 2.0 x10^5 Nm (green) and 3.6 x10^5 Nm (magenta).

Figure 4.12 presents the horizontal deflection versus the in-plane bending. The dots represent the approximated 1R PRBM results, and the line represents the differential equations results. The Pearson's correlation factor between the differential equations and the 1R PRBM is 0.999823.

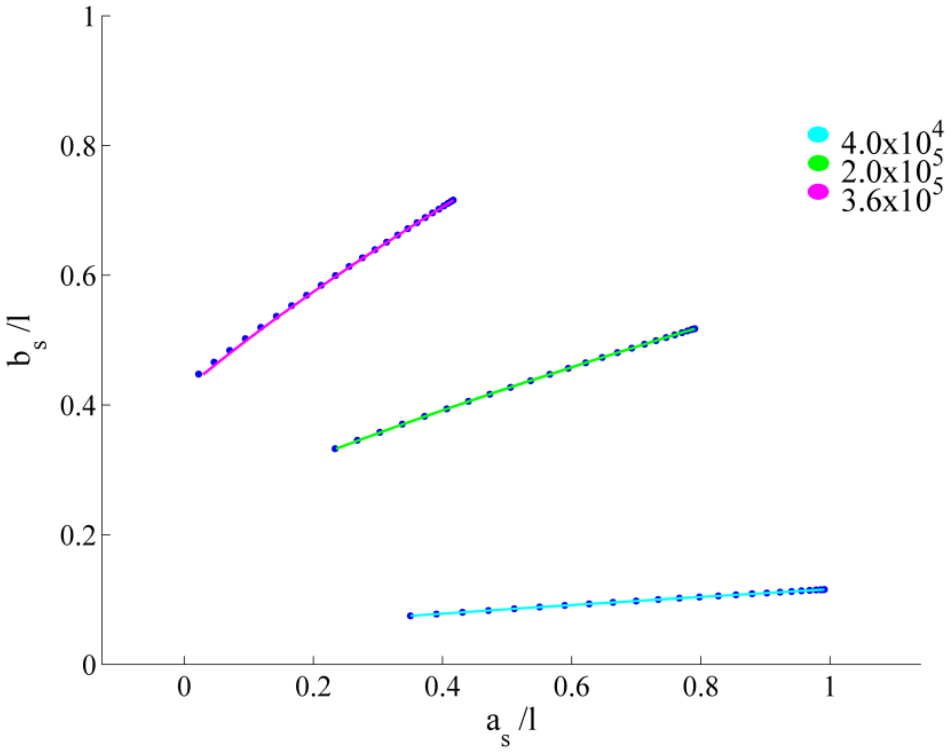

Figure 4.12. Horizontal versus in-plane deflection for various cases. Line represents the differential equations results and the dots the deflection of the 1R PRBM.

Figure 4.13 presents the horizontal deflection (a_s/l) versus the out-of-plane bending (c_s/l). The dots represent the 1R PRBM results and the line represents the differential equations results. The Pearson's correlation factor between the optimized parameters of the PRBM and the results from the spatial differential equations is 0.9997.

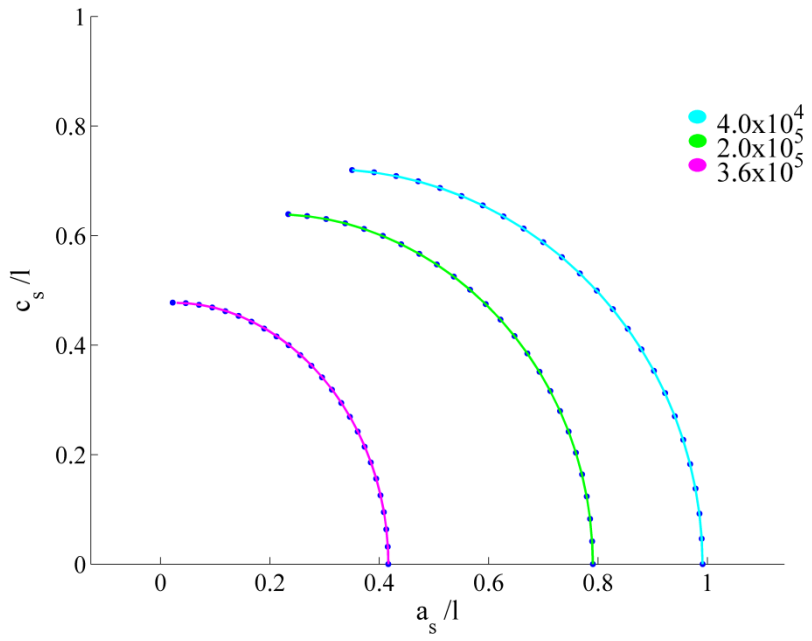

Figure 4.13. Horizontal versus out-of-plane deflection for varius cases. Line represents the differential equations results and the dots the deflection of the 1R PRBM.

4.3.2.1 Relative Deflection Error for a Spatial Beam

The relative deflection error for a spatial beam can be found in a similar manner to the relative deflection error for a planar beam. The true value of the deflection (a_t, b_t, c_t) can be found thru numerical integration of the deflection of the beam. The theoretical value of the deflection, δ_t, where a_t is the deflection with respect to the *x*-axis, b_t is the deflection with respect to the *y*-axis, c_t is the deflection with respect to the *z*-axis and *L* is the length of the beam, can be found as:

$$\delta_t = \sqrt{(L - a_t)^2 + {b_t}^2 + {c_t}^2} \tag{4.37}$$

The pseudo-rigid-body model deflection approximated value, δ_a, can be found by:

$$\delta_a = \sqrt{[\gamma L(1 - \cos\Theta]^2 + [\gamma L \sin\Theta \cos\Psi]^2 + [\gamma L \sin\Theta \sin\Psi]^2} \tag{4.38}$$

where γ is the characteristic radius factor and Θ and Ψ are the pseudo-rigid-body angles with respect to the *z*-axis and *x*-axis, respectively. The error in the deflection is:

$$\frac{error}{L} = \sqrt{\left[\frac{a_t}{L}(1-\gamma(1-\cos\Theta)\right]^2 + \left[\frac{b_t}{L} - \gamma\sin\Theta\cos\Psi\right]^2 + \left[\frac{c_t}{L} - \gamma\sin\Theta\sin\Psi\right]^2} \quad 4.39$$

And the relative deflection error of the spatial beam is expressed by:

$$\frac{error}{\delta_t} = \frac{\sqrt{\left[\frac{a_t}{L}(1-\gamma(1-\cos\Theta)\right]^2 + \left[\frac{b_t}{L} - \gamma\sin\Theta\cos\Psi\right]^2 + \left[\frac{c_t}{L} - \gamma\sin\Theta\sin\Psi\right]^2}}{\sqrt{\left(1-\frac{a_t}{L}\right)^2 + \left(\frac{b_t}{L}\right)^2 + \left(\frac{c_t}{L}\right)^2}} \quad 4.40$$

Figure 4.14 presents the relative deflections error as a function of the tip angle, θ_0. The 1R PRBM achieves a maximum relative deflection error of 0.5% at 167.3 degrees (2.919 radians) of the tip angle.

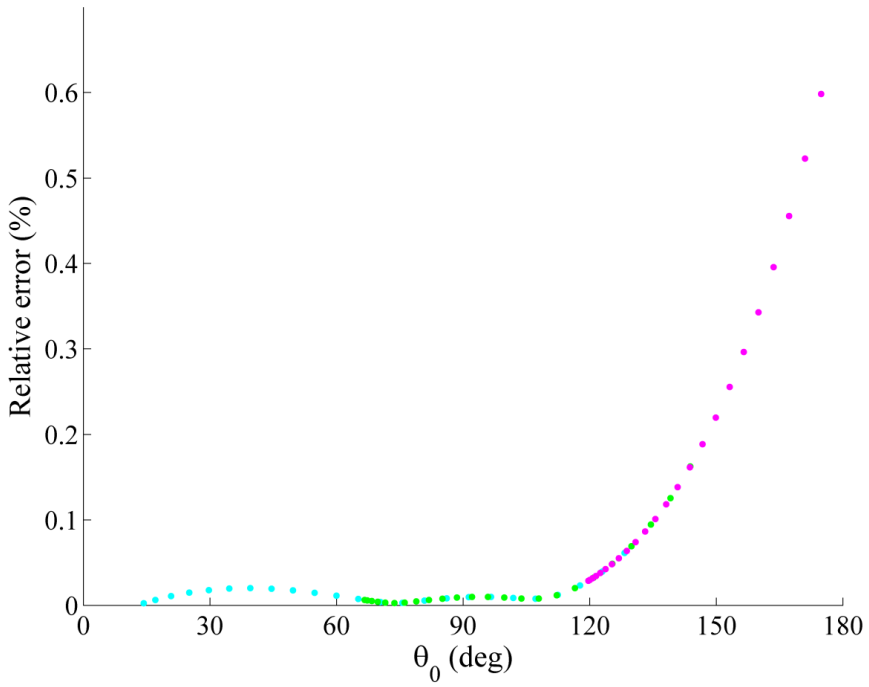

Figure 4.14. Relative deflection error of the optimized 1R PRBM versus the tip slope angle.

4.3.2.2 Stiffness for Multiple Moment Loading

Non-follower in-plane moments, M_z, and out-of-plane moments, M_y, were applied to the beam. The magnitude of the applied moment is equal to:

$$|M_0| = \sqrt{M_z^2 + M_y^2} \tag{4.41}$$

The in-plane to the out-of-plane moments can be related by means of the nondimensional factor ε, using the following relation:

$$\varepsilon = \frac{M_z}{M_y} \tag{4.42}$$

Substituting Equation 4.42 into Equation 4.43, the magnitude of the applied moment the end of the beam can be written as:

$$|M_0| = M_z\sqrt{1 + \varepsilon^2} \tag{4.43}$$

The beams resistance to deflection is modeled by the torsional spring, K_s. Because the geometric and material properties are considered in the in-plane torsional constant, K_s, in Equation 4.25, the value of the magnitude of the combined torsion spring, K_{sc}, can be defined as:

$$K_{sc} = K_s\sqrt{1 + \varepsilon^2} \tag{4.44}$$

The magnitude of the torque in the spring can be found by rotating Ψ around the *x*-axis, simplifying:

$$T_c = (\cos\Psi - \sin\Psi)\, K_{sc}\Theta \tag{4.45}$$

The magnitude of the spring torque, Equation 4.45, was compared to the magnitude of the input moment. An input in-plane moment, M_z, was applied to the end of the beam, and an out-of-plane moment M_y was increased by the nondimensional factor, ε. Three cases were studied: (1) when M_z is $0.8\text{x}10^5$ Nm, (2) when M_z is $2.0\ \text{x}10^5$ Nm and, (3) when M_z is $4.0\ \text{x}10^5$ Nm. The PRBM parameters used are specified in Table 4.2.

Table 4.2. PRBM parameters used in the stiffness study.

M_z (Nm)	θ_0 (degrees)	Θ (degrees)
0.8 x 10^5	26.57	17.70
2.0 x 10^5	66.43	44.07
4.0 x 10^5	132.86	86.74

Figure 4.15 presents the comparison of the results of the magnitude of the moment applied versus the torque applied to the spring. The squares stand for the magnitude of the input moment and the dots represent the results of the torque of the spring, T_s. The percent error between them, Equation 4.46, is shown in Figure 4.16.

$$error = \left|\frac{M_0 - T_c}{M_0}\right| * 100 \qquad 4.46$$

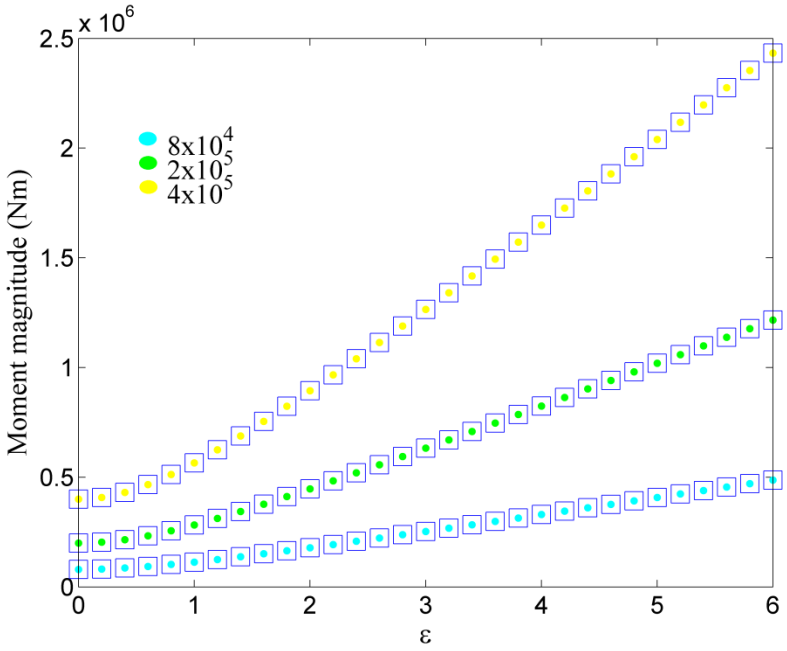

Figure 4.15. Plot of the magnitude of the moment versus the ratio of the in-plane to the out-of-plane input moment, ε. The square determine the magnitude of the input moment and the dots the torque of the spring, T_c.

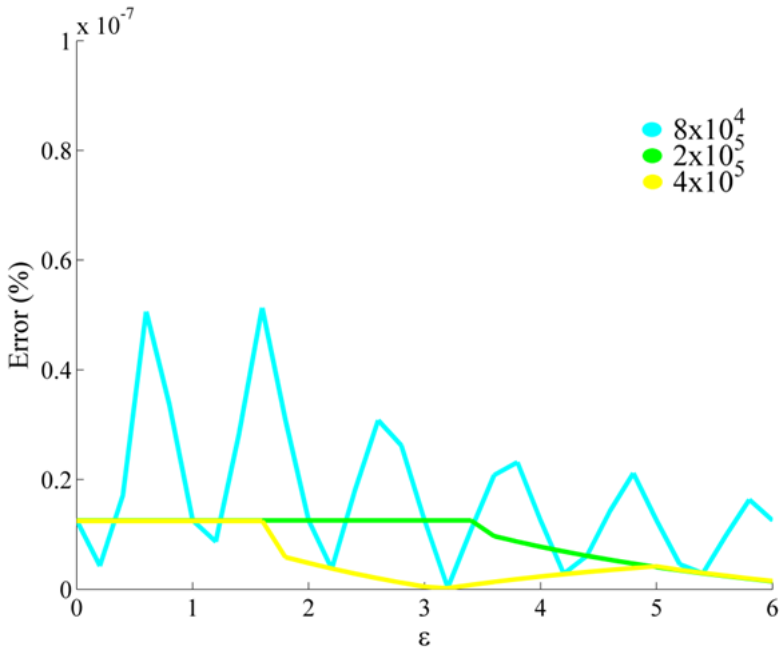

Figure 4.16. Percentage error between the applied moment at the end of the beam and the spring torque.

4.4 Conclusion

For a cantilever beam with no torques, the planar PRBM results from Howell [8], Feng [35] and Su [37] can be used to define an axisymmetric PRBM. The force vector and the moment applied at the beam tip and the axis of the beam itself are used to define a plane whose angular deviation from the *xy*-plane is described by the angle Ψ. An axisymmetric PRBM is then given when the planar results are multiplied by a rotation in the *x*-direction:

$$R_x = \begin{bmatrix} 1 & 0 & 0 \\ 0 & \cos\Psi & -\sin\Psi \\ 0 & \sin\Psi & \cos\Psi \end{bmatrix} \qquad 4.47$$

The characteristic radius factor and the PRB angle coefficient for a beam with a single moment applied at the end were optimized to minimize the error incurred using the deflection formulas of the PRBM. This approximation provides an improvement to previous published parameters, providing a relative error of 0.5% at a tip slope angle to 169.76 degrees (2.96294 radians).

In force loaded Pseudo-Rigid-Body Models (PRBMs) the energy stored in the torsional spring is equal to the energy stored in the deformed beam. In moment loaded beams, the PRBM spring energy and the beams strain energy are related by the parametric angle coefficient. This is because the parametric angle coefficient is the ratio between the tip angle and the PRB angle Θ. This means that caution must be used in evaluating PRBMs using moment loaded segments.

Chapter 5

Rectangular Pseudo-Rigid-Body Model with Bending Moment Loads

The objective of this chapter is to develop a pseudo-rigid-body model (PRBM) for a rectangular cantilever beam that undergoes planar and out-of-plane bending moments. The governing equations of the beam that were derived in Chapter 3 are used to calculate the deflection, rotation and curvature of the beam's neutral axis as a function of the arclength. A PRBM modeling the kinematics and stiffness of a spatial cantilever beam with bending moment loads is presented. With the governing equations of the beam, the PRBM and equations from virtual work, the PRBM parameters were developed.

5.1 Governing Equations of a Beam

The equations that describe deflection, rotation and curvature of a beam that experiences forces and moments were derived in Chapter 3. Because in the analysis presented in this chapter force loads are not considered, $F_{y'}$ and $F_{z'}$ are set to zero in the $\{h\}$-frame. The differential equations were derived with s=0 at the free-end of the cantilever beam, assuming no displacements or rotations in the $\{a\}$-frame. Equations 5.1-5.9 can be used to find the Euler angles (ϕ, θ, and ψ) the curvatures (τ_x, κ_y and κ_z), and the coordinates (X, Y and Z) with respect to the arclength (s) for a beam that undergoes bending moments at the free-end.

$$\frac{d\phi}{ds} = \tau_{x'} + \kappa_{y'} \cos\phi \frac{\cos\theta}{\sin\theta} - \kappa_{z'} \sin\phi \frac{\cos\theta}{\sin\theta} \qquad 5.1$$

$$\frac{d\theta}{ds} = \kappa_{y'} \sin\phi + \kappa_{z'} \cos\phi \tag{5.2}$$

$$\frac{d\psi}{ds} = -\kappa_{y'} \frac{\cos\phi}{\sin\theta} + \kappa_{z'} \frac{\sin\phi}{\sin\theta} \tag{5.3}$$

$$\frac{d\tau_x}{ds} = \frac{1}{\mathrm{GI}_{xx}} \left(I_{yy} - I_{zz}\right) E \kappa_{y'} \kappa_{z'} \tag{5.4}$$

$$\frac{d\kappa_y}{ds} = \frac{1}{\mathrm{EI}_{yy}} (EI_{zz} - GI_{xx}) \tau_{x'} \kappa_{z'} \tag{5.5}$$

$$\frac{d\kappa_z}{ds} = \frac{1}{\mathrm{EI}_{zz}} \left(GI_{xx} - EI_{yy}\right) \tau_{x'} \kappa_{y'} \tag{5.6}$$

$$\frac{d\mathrm{X}}{ds} = \cos\theta \tag{5.7}$$

$$\frac{d\mathrm{Y}}{ds} = \sin\theta \cos\psi \tag{5.8}$$

$$\frac{d\mathrm{Z}}{ds} = \sin\theta \sin\psi \tag{5.9}$$

The ODE45 command in Matlab was used to numerically integrate the differential equations, where the interval of integration from the negative of the length of the beam to zero. The planar moment (M_z) and the out-of-plane moments (M_y) are applied in the free-end of the beam as follower loads, thus both moments are at 90 degrees of each other in the $\{h\}$-frame. The non-follower moments at the fixed frame are found by rotating the follower moments by the angles ϕ, θ, and ψ:

$$^{a}\vec{M} = {}^{a}_{p}R(\,{}^{a}x, \phi\,)\,{}^{p}_{q}R(\,{}^{p}z, \theta\,)\,{}^{q}_{h}R(\,{}^{q}x, \psi\,)\,{}^{h}\vec{M} \tag{5.10}$$

where the $\{a\}$-frame is the fixed frame and the $\{h\}$-frame is the follower frame at the beams tip. Similarly, the coordinates of the beam tip (*a*,*b*,*c*) with respect to the fixed end of the beam can be found as:

$$[{}^{a}x,\ {}^{a}y,\ {}^{a}z]' = {}^{a}_{p}R({}^{a}x,\phi\ )\,{}^{p}_{q}R({}^{p}z,\theta\ )\,{}^{q}_{h}R({}^{q}x,\psi\ )[{}^{h}X,\ {}^{h}Y,\ {}^{h}Z]' \quad 5.11$$

The governing equations of the beam are valid for any magnitude of applied loads; this means that the tip can undergo more than 360 degrees rotation. Because we are only interested in solutions to the Equations 1.1-1.9 that can be reasonably approximated with a two-link pseudo-rigid-body model, the rotation of the beam tip with respect to the fixed end was restricted. The magnitude of the applied planar moment (M_z) in the follower frame was calculated as follows:

$$^{h}M_z = {}^{\theta_i EI_{zz}}/_{l} \quad 5.12$$

where θ_i is the initial tip angle, l is the length of the beam, E is the Elastic modulus and I_{zz} is the moment of inertia with respect to the z-axis. The initial tip angle was restricted to 120 degrees, which ensures that the PRBM parameters can be related to the planar PRBM parameters developed by Howell [8].

Perturbation theory can be used to apply the out-of-plane moment (M_y) such that it ensures the applied load does not produce excessive out-of-plane deflection. The perturbation method provides a simple method to find the approximate solution to a difficult problem in terms of a power series. In the perturbation method, the effect of a dimensionless small parameter, ε, is introduced in the differential equations to find a solution to the problem. Three steps are fundamental in a perturbation analysis [42]:

1. Convert the original problem into a perturbation problem by introducing a small parameter, ε.
2. Assume an expression for the answer in the form of a perturbation series and compute the coefficients of that series. In this step, the unperturbed problem is solved by obtaining the solution when ε =0 in the problem.

3. Recover the answer to the original problem by assuming the perturbation series for the appropriate value of ε.

Using the perturbation method, a follower out-of-plane end-moment load will be applied to a cantilever beam with in-plane moments.

$$ {}^{h}M_y = \varepsilon\, {}^{h}M_z \tag{5.13}$$

The small parameter, ε, will give a measure of the magnitude of the applied out-of-plane moment with respect to the in-plane moment, as shown in Figure 5.1.

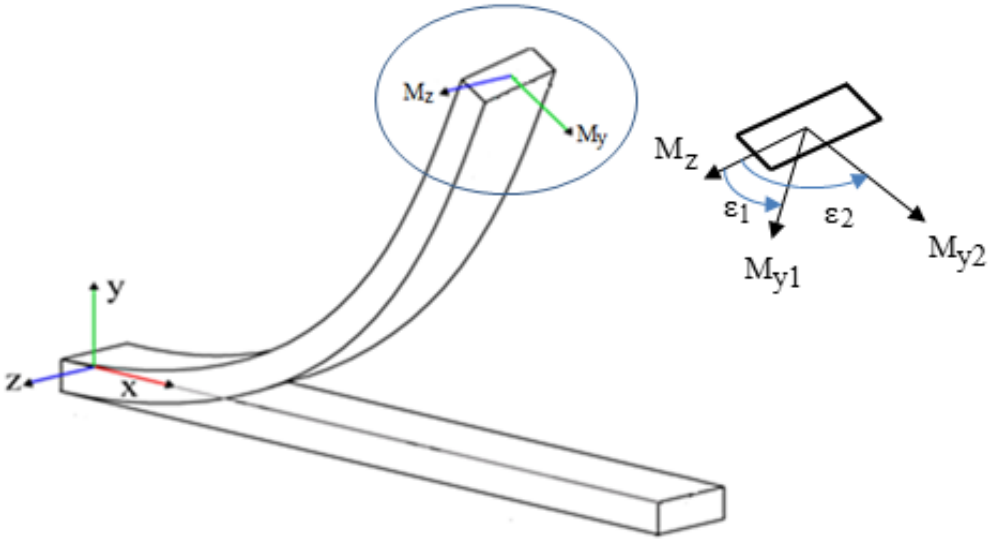

Figure 5.1. Diagram of a cantilever beam with applied moment-loading.

5.2 Rectangular Pseudo-Rigid-Body Model

One can assume a PRBM for a rectangular cantilever beam similar to the one presented in Chapter 4 for the axisymmetric beam. The PRBM consists of two rigid links connected by a spherical joint and a spherical cap, as shown in Figure 5.2. The spherical joint is located at γl distance from the free-end of the cantilever beam and allows the rotation of the pseudo-rigid-body link, and thus the displacement of its tip.

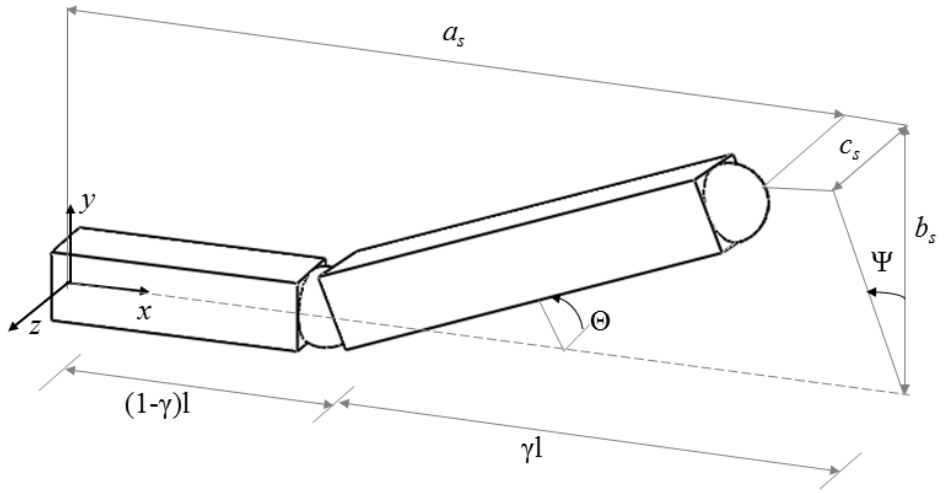

Figure 5.2. PRBM of a cantilever beam with moment loads.

The position of the tip end (a_s, b_s, c_s) of the spatial PRBM of a cantilever beam with end loads is given by:

$$a_s = l - \gamma l(1 - \cos\Theta) \tag{5.14}$$

$$b_s = \gamma l \sin\Theta \cos\Psi \tag{5.15}$$

$$c_s = \gamma l \sin\Theta \sin\Psi \tag{5.16}$$

where l is the length of the beam, γ is the characteristic radius factor, Θ is the characteristic bend angle of the beam with respect to the z-axis and, Ψ is the characteristic twist angle of the beam with respect to the x-axis.

In Chapter 4, we presented a PRBM for a beam that undergoes planar motion that allows the rotation of the pseudo-rigid-body link, and thus, the displacement of its tip. Two frames were sufficient to specify the deflection of the free-end of the beam. However, in order to describe the orientation of the beam end, a spherical cap in the tip of the beam was added to the PRBM.

To specify the orientation of the beam, we can assume another set of XZX rotations, by the angles Σ, Ω, and Φ. As shown in Figure 5.3, the $\{a\}$-frame, which is located at the fixed end

of the beam, is twisted by the characteristic twist angle Ψ. The characteristic bend angle Θ is the intersection of the plane XY-plane which contains the PRB link. The Σ angle can be viewed as the torsion in the longer PRB link. The rotation angles Ω and Φ are the rotation in the *z*-direction and the *x*-direction of the beams tip, respectively.

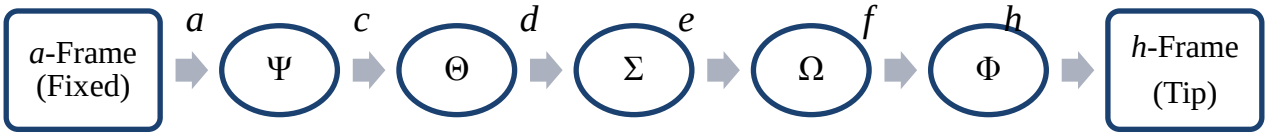

Figure 5.3. The frames and the PRBM angles from the fixed to the free-end of the beam.

The twisting components of Ψ is composed of two angles Γ and ϒ:

$$ {}^{c}_{a}R({}^{a}x, \Psi) = {}^{c}_{b}R\left({}^{b}x, \Gamma\right) * {}^{b}_{a}R({}^{a}x, \Upsilon) \tag{5.17} $$

Because Γ and ϒ have the same axis,

$$ {}^{c}_{a}\Psi = {}^{c}_{b}\Gamma + {}^{b}_{a}\Upsilon \tag{5.18} $$

where Υ is the torsion of the shorter PRB segment and Γ is the orientation of the bend direction.

Because there are five kinematic variables (Φ, Ω, Σ, Θ, and Ψ), and only three load variables (M_x, M_y, and M_z), the kinematic variables are not all independent and cannot all be used as generalized coordinates for virtual work equations. By comparison with the planar model and inspection of the data, we find that Ω is dependent on Θ, such that:

$$ \Omega = c_{\Omega}\Theta \tag{5.19} $$

where c_{Ω} is the PRB-link parametric angle coefficient. The angle Φ is also dependent, bot has a more complicated relationship to the independent variables Γ, Σ, Θ, and Ψ.

5.2.1 Virtual Work

The principle of virtual work states that "the net virtual work of all active forces is zero if and only if an ideal mechanical system is in equilibrium"[8]. The method of virtual works is a

useful tool to develop force and deflection relationships. Using the method of virtual work, the equilibrium positions of a system acted on a pure moment is given by:

$$\vec{M} \cdot d\vec{\theta} - \sum \frac{dV_{PRBM}}{dq} \delta q = 0 \tag{5.20}$$

where $\vec{M}$ is the moment, $\vec{\theta}$ is the virtual displacement, V_{PRBM} is the potential energy of the PRBM, and q is a generalized coordinate. The virtual angular displacement $d\vec{\theta}$ is given by:

$$d\vec{\theta} = d\Psi\, {}^{a}\hat{\mathrm{x}}\, d\Theta\, {}^{c}\hat{\mathrm{z}} + d\Sigma\, {}^{d}\hat{\mathrm{x}} + d\Omega\, {}^{e}\hat{\mathrm{z}} + d\Phi\, {}^{f}\hat{\mathrm{x}} \tag{5.21}$$

The virtual work due to the moment is expressed by:

$$\vec{M} \cdot d\vec{\theta} = {}^{a}M_x d\Psi + {}^{c}M_z\, d\Theta + {}^{d}M_x d\Sigma + {}^{e}M_z d\Omega + {}^{f}M_x d\Phi \tag{5.22}$$

The derivative of the angular dependencies in Equations 5.18 and 5.19 are:

$$d\Psi = d\Upsilon + d\Gamma \tag{5.23}$$

$$d\Omega = c_\Omega d\Theta \tag{5.24}$$

Substituting Equations 5.23-5.24 into 5.22, yields to:

$$\vec{M} \cdot d\vec{\theta} = {}^{a}M_x(d\Upsilon + d\Gamma) + {}^{c}M_z\, d\Theta + {}^{d}M_x d\Sigma + c_\Omega\, {}^{e}M_z d\Theta + {}^{f}M_x d\Phi \tag{5.25}$$

Applying the follower moment only on the y and the z-direction, and setting the moment in *x*-direction on the {*f*}-frame (${}^{f}M_x$) equal to zero, because there are no applied torques about the beam axis at the tip, Equation 5.25 can be expressed as:

$$\vec{M} \cdot d\vec{\theta} = {}^{a}M_x(d\Upsilon + d\Gamma) + {}^{c}M_z\, d\Theta + {}^{d}M_x d\Sigma + c_\Omega\, {}^{e}M_z d\Theta \tag{5.26}$$

We can arrange the similar terms of the Equation 5.26 as follows:

$$d\Upsilon\text{: } {}^{a}M_x \tag{5.27}$$

$$d\Gamma\text{: } = {}^{a}M_x \tag{5.28}$$

$$d\Theta\text{: } {}^{c}M_z\, d\Theta + c_\Omega\, {}^{e}M_z d\Theta \tag{5.29}$$

$$d\Sigma: {}^{d}M_x \tag{5.30}$$

5.2.2 Virtual Work of the PRBM

In the PRBM, we assume the potential energy associated with torsion in the beam is:

$$V_T = \frac{GI_{xx}\Upsilon^2}{2(1-\gamma)l}K_\Upsilon + \frac{GI_{xx}\Sigma^2}{2\gamma l}K_\Sigma \tag{5.31}$$

where G is the shear modulus, I_{xx} is the polar moment of area, l is the length of the beam, γ is the characteristic radius factor, K_Υ and K_Σ are the torsion stiffness factors for the straight part of the beam and the pseudo-rigid-body link, respectively. The equations reduce to standard torsion formulas for beams of length (1-γ)l and γl, respectively when K_Υ and K_Σ are equal to one. Thus, K_Υ and K_Σ measures how the stiffness of the curved beam differs from the straight one.

The potential energy associated with bending of the PRBM is:

$$V_B = \frac{{}^{c}I_{zz}E\gamma K_\theta \Theta^2}{2l} \tag{5.32}$$

where K_θ is the bending stiffness factor, E is the Modulus of elasticity and Θ is the characteristic bend angle. ${}^{C}I_{ZZ}$ is the second moment of area of the beam cross-section about the z-axis. Because ${}^{C}I_{ZZ}$ occurs in a rotating frame, it depends on G and the area moment invariants:

$${}^{c}I_{zz} = \bar{I} - I_R cos2\Gamma \tag{5.33}$$

where:

$$\bar{I} = \frac{I_{yy} + I_{zz}}{2} \tag{5.34}$$

$$I_R = \frac{I_{yy} - I_{zz}}{2} \tag{5.35}$$

where Γ is the angle of the bending at the end of the beam, I_{yy} and I_{zz} are the moments of inertia with respect to the y and z axis, respectively. The potential energy due to bending is a function of the angle Θ and Γ, and is given by:

$$\frac{dV_B}{dq}\delta q = \frac{E\gamma K_\theta \Theta^2 I_R sin2\Gamma}{l} d\Gamma + \frac{E\gamma\ {}^{c}I_Z K_\theta \Theta}{l} d\Theta \tag{5.36}$$

The potential energy due to torsion is a function of the angle ϒ and Σ:

$$\frac{dV_T}{dq}\delta q = \frac{GI_X \Upsilon K_\Upsilon}{(1-\gamma)l} d\Upsilon + \frac{GI_X \Sigma K_\Sigma}{\gamma l} d\Sigma \tag{5.37}$$

We can arrange the similar terms in the potential energy equations as follows:

$$d\Upsilon: \frac{K_\Upsilon GI_X \Upsilon}{(1-\gamma)l} \tag{5.38}$$

$$d\Gamma: \frac{E\ {c_\theta}^2 \Theta^2 I_R sin2\Gamma}{l} \tag{5.39}$$

$$d\Theta: \frac{{}^{c}I_Z E c_\theta \Theta}{l} \tag{5.40}$$

$$d\Sigma: \frac{K_\Sigma GI_X \Sigma}{\gamma l} \tag{5.41}$$

The rotation from the {e}-frame to the {f}-frame is about the z-direction. Thus, the moment in the z-direction in the {e}-frame and {f}-frame are the same:

$${}^{e}M_z = {}^{f}M_z \tag{5.42}$$

From the Equations 5.27-5.30, 5.38-5.41 and 5.42, the moments at the fixed frame of the beam are:

$${}^{a}M_x - \frac{K_\Upsilon GI_X \Upsilon}{(1-\gamma)l} = 0 \tag{5.43}$$

$${}^{a}M_x - \frac{E\gamma \Theta^2 I_R sin2\Gamma K_\theta}{l} = 0 \tag{5.44}$$

$${}^{c}M_z - c_\Omega\ {}^{f}M_z - \frac{{}^{c}I_Z E\Theta\gamma K_\theta}{l} = 0 \tag{5.45}$$

$${}^{d}M_x - \frac{K_\Sigma GI_X \Sigma}{\gamma l} = 0 \tag{5.46}$$

Thus, using Equations 5.43-5.46 the PRBM parameters $\gamma, K_\Upsilon, K_\theta, K_\Sigma$ and c_Ω are known. The deflection of a beam with parameters *E*, *I*, *l* subjected to a moment can be found.

5.3 Derivation of PRBM Parameters

In this section, the results from the differential equations and the virtual work are combined to obtain the equations for the parameters of the PRBM. We expect these parameters to be nearly constant across a large range of values allowing for Equations 5.43-5.46 to be used to predict the beam's motion. From the governing equations of the beam, the orientation of the beam from the free to the fixed end of the beam is given by the Euler angles $\phi, \theta, \text{and } \psi$. The rotation can also be found with thru the set of kinematic variables Φ, Ω, Σ, Θ, and Ψ. The rotation of the free-end ($\{h\}$-frame) with respect to the fixed-end ($\{a\}$-frame) can be expressed using the compliant beam data and the PRBM angles as:

$$\begin{aligned} &{}^h_qR(\,{}^qx,\psi\,)\,{}^q_pR(\,{}^pz,\theta\,)\,{}^p_aR(\,{}^ax,\phi\,) \\ &\qquad = {}^h_fR(\,{}^fx,\Phi)\,{}^f_eR(\,{}^ez,\Omega)\,{}^e_dR(\,{}^dx,\Sigma)\,{}^d_cR(\,{}^cz,\Theta)\,{}^c_aR(\,{}^ax,\Psi) \end{aligned} \tag{5.47}$$

The angles $\phi, \theta, \text{and } \psi$ are obtained from the governing equations of the beam. Thus, the rotation angles Σ, Ω, and Φ can be expressed by:

$$R_{\Sigma\Omega\Phi} = R_x(\Sigma)\,R_z(\Omega)\,R_x(\Phi) = R_z(\Theta)^{-1}\,R_x(\Psi)^{-1}R_x(\psi)\,R_z(\theta)\,R_x(\phi) \tag{5.48}$$

The exact value of the angle Ψ is calculated by solving Equations 5.15 and 5.16, and given by:

$$\Psi = \operatorname{acot}\left({}^{b_s}/_{c_s}\right) \tag{5.49}$$

The values of the characteristic bend angle Θ and the characteristic radius factors are found by solving Equations 5.14-5.16, such that the characteristic radius factor is:

$$\gamma = \frac{\left(1 - {a_s}/{l}\right)^2 + \left({b_s}/{l}\right)^2 + \left({c_s}/{l}\right)^2}{2\left(1 - {a_s}/{l}\right)^2} \tag{5.50}$$

Solving Equations 5.14 and 5.15, the characteristic bend angle is expressed by:

$$\Theta = \operatorname{atan}\left({b_s}/{a_s + l(1-\gamma)}\right) \tag{5.51}$$

where a_s, b_s, and c_s is the position of the beam tip with respect to the *x*, *y* and *z* direction, respectively. From the coefficients of the multiplication of Equation 5.48, the coefficients of Σ, Ω and Φ angles are calculated as follows:

$$\Omega = \operatorname{acos}[R_{\Sigma\Omega\Phi}(1,1)] \tag{5.52}$$

$$\Phi = \operatorname{atan}\left(\frac{R_{\Sigma\Omega\Phi}(1,3)}{sin(\Omega)} \Big/ \frac{-R_{\Sigma\Omega\Phi}(1,2)}{sin(\Omega)}\right) \tag{5.53}$$

$$\Sigma = \operatorname{atan}\left(\frac{R_{\Sigma\Omega\Phi}(3,1)}{sin(\Omega)} \Big/ \frac{R_{\Sigma\Omega\Phi}(2,1)}{sin(\Omega)}\right) \tag{5.54}$$

Equations 5.52-5.54 are sufficient to solve for the angles *Σ, Ω* and *Φ*. To solve Equations 5.43-5.46, one can assume that:

$$M_R = \frac{E\gamma I_R \Theta K_\theta}{l} \tag{5.55}$$

$$\bar{M} = \frac{E\gamma \bar{I} \Theta K_\theta}{l} \tag{5.56}$$

Equations 5.44 and 5.45 become:

$${}^{a}M_x - \Theta M_R sin2\Gamma = 0 \tag{5.57}$$

$${}^{c}M_z + c_\Omega \, {}^{f}M_z - (\bar{\mathrm{M}} - M_R \cos 2\Gamma) = 0 \tag{5.58}$$

Solving the Equations 5.57 and 5.58:

$$\sin 2\Gamma = \frac{{}^{c}M_x}{M_R\Theta} \tag{5.59}$$

$$\cos 2\Gamma = \frac{\bar{M} - \left({}^{c}M_z + c_\Omega\, {}^{f}M_z\right)}{M_R} \tag{5.60}$$

Using the trigonometric identity: $\sin^2 2\Gamma + \cos^2 2\Gamma = 1$, and because $M_R = \bar{M}\left(\frac{I_R}{\bar{I}}\right)$, Equations 5.59-5.60 can be combined into a quadratic formula of the form $A\bar{M}^2 + B\bar{M} + C = 0$, where:

$$A\colon\ 1 - \left(\frac{I_R}{\bar{I}}\right)^2 \tag{5.61}$$

$$B\colon\ -2\left({}^{c}M_z + c_\Omega\, {}^{f}M_z\right) \tag{5.62}$$

$$C\colon\ \left({}^{d}M_z + c_\Omega\, {}^{f}M_z\right)^2 + \left(\frac{{}^{a}M_x}{\Theta}\right)^2 \tag{5.63}$$

The quadratic formula can be solved using Matlab to calculate the value of $\bar{M}$. Knowing the values of $\bar{M}$, the angle Γ can be obtained by dividing Equation 5.59 over Equation 5.60:

$$\tan 2\Gamma = \frac{{}^{c}M_x}{\Theta[\bar{M} - \left({}^{c}M_z + c_\Omega\, {}^{f}M_z\right)]} \tag{5.64}$$

The bending stiffness K_θ can be calculated from Equation 5.56:

$$K_\theta = \frac{\bar{M}l}{E\gamma\bar{I}\Theta} \tag{5.65}$$

From Equation 5.46, the stiffness coefficient K_Σ:

$$K_\Sigma = \frac{\gamma l\, {}^{d}M_x}{GI_X\Sigma} \tag{5.66}$$

Because Equations 5.43 and 5.44 contain the same moment ${}^{a}M_x$, the stiffness coefficient K_Υ can be found by equating the two equations and solving for K_Υ:

$$\frac{E\gamma\Theta^2 I_R sin2\Gamma K_\theta}{l} = \frac{K_\Upsilon GI_X\Upsilon}{(1-\gamma)l} \tag{5.67}$$

$$K_\Upsilon = \frac{E\gamma\Theta^2 I_R sin2\Gamma K_\theta(1-\gamma)}{GI_X\Upsilon} \quad 5.68$$

5.4 Verification

The equations presented in the previous sections can be partially verified by showing that they reduce to the equations of a planar beam under planar loading. For planar beams, the in-plane moment (M_z) in the follower frame is equal to the moment as in the fixed frame. There is no twist of the PRB or the straight beam, which means that the rotation angles in the *x*-direction Φ, Σ and Ψ are equal to zero. The Euler angles ϕ and ψ remain at 180 and -180 degrees thru the length of the beam while the tip angle θ increases. The relationship between the beams tip angle θ and the variables Θ and Ω is equal to:

$$\theta = \Omega + \Theta \quad 5.69$$

When an out-of-plane moment (M_y) is applied in the follower frame of the beam, the straight part of the beam experiences a twist about the *x*-axis by the angle Ψ of 90 degrees, followed by an angle Θ which rotates the PRB link in the *y*-axis. There will be no twisting of the PRB link, which means that the angles Γ and Σ are equal to zero, but the angle at the beam tip Φ= -ϒ= -Ψ, rotates the tip in the negative *x*-direction to reposition direction of the beam. The relationship between the slope angle θ and the variables Θ and Ω is equal to Equation 5.69.

For a planar beam with an in-plane applied moment, the moments in the *y* and *x*-direction are equal to zero, therefore, Equations 5.43, 5.44 and 5.46 are also equal to zero. The moment in the *z*-direction remains the same through the beam, thereby, Equation 5.45 reduces to:

$$^cM_z = {}^fM_z = M_z \quad 5.70$$

Because no moments are applied in the *y* and *x*-direction, the stiffness parameter is:

$$c_\Omega = c_\theta - 1 \quad 5.71$$

Because there is no twist along the beam, Γ=0. Thus, for a planar beam:

$$^{c}I_{ZZ} = I_{ZZ} \tag{5.72}$$

And from Chapter 4, Equation 4.33:

$$K_{\theta} = c_{\theta} K_{s} \tag{5.73}$$

where K_s is the spring constant. Applying Equations 5.70-5.73 into 5.45 reduces to:

$$M_z = \frac{\gamma E I_Z K_s}{l} \Theta \tag{5.74}$$

For the axisymmetric beam, the moments of inertia with respect to the *y* and *z* directions on the $\{a\}$-frame are equal. Therefore,

$$^{c}I_Z = I_Z \tag{5.75}$$

Because there is no rotation in the pseudo-rigid-body link, Σ=0, the moments in the $\{c\}$-frame and the $\{f\}$-frame remain constant. Applying this, we have obtained the same derivation as with the planar beam, validating the equations of the rectangular pseudo-rigid-body model.

5.5 Approximations of the PRBM Constants

The flow chart in Figure 5.4 shows the procedure to find the exact values of the PRBM for a rectangular cantilever beam. The process can be divided in five parts: (1) an in-plane and out-of-plane moment were applied in the follower frame (2) using the governing equations of the beam, we obtain the displacement coordinates, curvature and the rotation of the beam for a given aspect ratio with Equations 5.1-5.9 (3) find the rotation angles Σ, Ω and Φ from Equations 5.52-5.54, (4) calculate the parametric angle coefficients c_{θ}, c_{Ω} from Equation 5.19 and the moment vector at the different frames ($^{c}\vec{M}$, $^{d}\vec{M}$, $^{e}\vec{M}$, $^{f}\vec{M}$) with the rotations obtained in step 3, (5) calculate $\bar{M}$ with Equations 5.61-5.63, (6) calculate the twist angles Γ and ϒ with Equations 5.33 and 5.18, respectively and the stiffness parameters K_{θ}, K_{Υ} and K_{Σ} from Equations 5.65, 5.66 and 5.68, respectively.

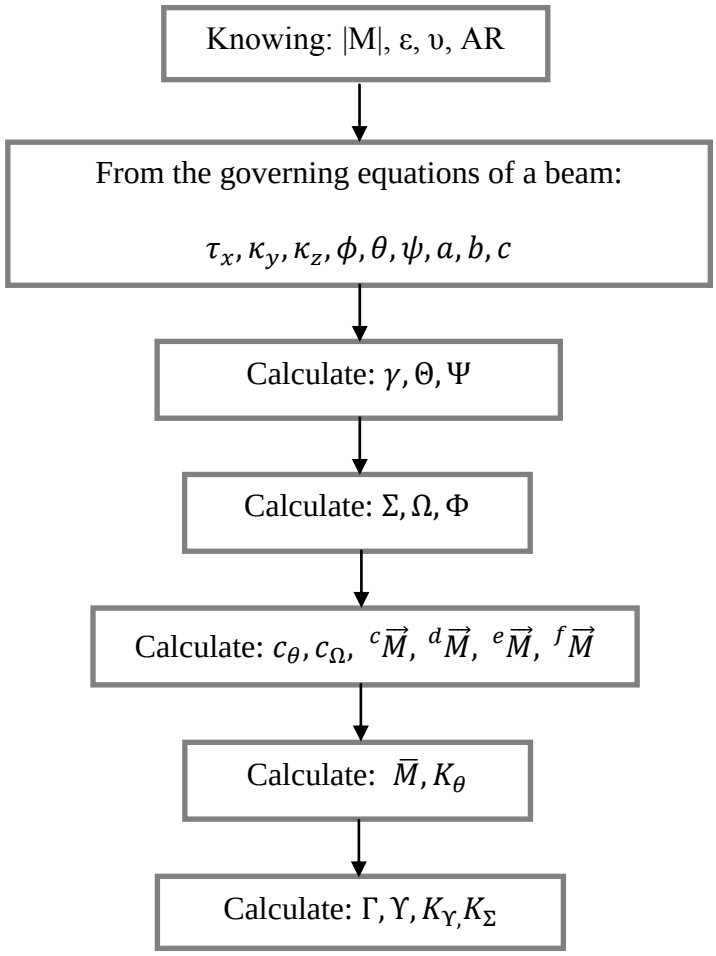

Figure 5.4. Flow chart with the process to derive the PRBM parameters.

With the exact values of the PRBM, this section presents the approximations of the characteristic radius factor γ, the parametric angle coefficients c_θ and c_Ω, the stiffness coefficients K_θ, K_Υ, K_Σ and the rotation angles Ψ, Θ, Σ, Ω, Φ, Γ and ϒ as a function of the aspect ratio of the beam.

When the perturbation ratio is less than one, the angle between the in-plane and the out-of-plane moment is less than 45 degrees. The process to obtain the PRBM parameters is similar to the one in the preceding section, with the difference that the perturbation ratio was limited to values ranging from 0.1 to 1.0.

The moments in the fixed frame from rectangular (${}^{a}M_x$, ${}^{a}M_y$, ${}^{a}M_z$) can be expressed in spherical coordinates as [43]:

$$ {}^{a}M_x = |M| \sin\eta \sin\xi \tag{5.76}$$

$$ {}^{a}M_y = |M| \cos\eta \tag{5.77}$$

$$ {}^{a}M_z = |M| \sin\eta \cos\xi \tag{5.78}$$

where |M| is the magnitude of the non-follower moment, ξ is the azimuth angle (the angle of the moment in the *xz*-plane) and, η is the angle inclination angle (angle of the moment in the *xy*-plane), as shown in Figure 5.5.

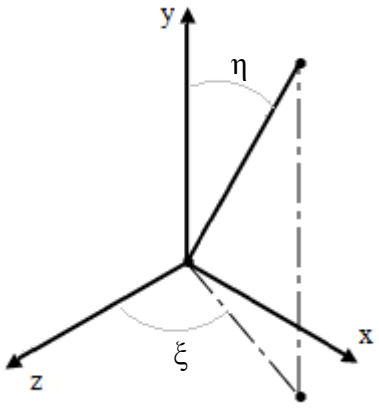

Figure 5.5. Angles of the applied moment in the fixed frame.

Because the angle of the moment changes with the perturbation ratio, we can obtain the radius and the angle and find the location where the maximum coordinates are valid. The angle of the moment in the non-follower frame ξ and η can be used to obtain the limits where the PRBM parameters are valid.

For example, a moment in the follower frame ${}^{h}M_z$ and a perturbed moment of ${}^{h}M_y = \varepsilon\, {}^{h}M_z$ was applied to the beam with a cross section of 2.5. Using the governing equations of the beam, the Euler angles ϕ, θ and ψ are found. The moments in the fixed frame (${}^{a}\vec{M}$) is found by

multiplying the moment in the follower frame (${}^{h}M_z$) by the XZX matrix of Euler rotations ${}^{a}_{h}R$ such as:

$$ {}^{a}\vec{M} = {}^{a}_{p}R({}^{a}x, \phi){}^{p}_{q}R({}^{p}z, \theta){}^{q}_{h}R({}^{q}x, \psi)\ {}^{h}\vec{M} \tag{5.79} $$

From Equations 5.76-5.78, the inclination and azimuth angle (η and ξ, respectively) of the moment in the fixed frame are:

$$ \xi = \text{atan}\left(\frac{{}^{a}M_x}{{}^{a}M_z}\right) \tag{5.80} $$

$$ \eta = \text{acos}\left(\frac{{}^{a}M_y}{|M|}\right) \tag{5.81} $$

As shown in Figure 5.6, the simplified parameters are not valid in the entire area of the quadrant. We can approximate the area that covers the applied moments with a radius (ρ) and an angle (Λ). Figure 5.6 shows the area where the perturbation factor is less than one for the 2.5 aspect ratio as a function of the angles at the fixed frame ξ and η. For this case, the radius would be the distance between point A and point B in the figure and the angle Λ is the angle between the horizontal and the point A. With this information, we can obtain the maximum inclination and azimuth angle (η and ξ, respectively) where the model is valid.

Table 5.1 contains the limit area of the simplified PRBM parameters for different aspect ratios when non-follower moments are applied to the cantilever beam. When the aspect ratio is higher than 2.75, the simplification is valid for the entire quadrant.

The maximum inclination and azimuth angle (η and ξ, respectively) for the aspect ratios presented in Table 5.1 are calculated as:

$$ \xi_{max} = \rho \sin\Lambda + \pi/2 \tag{5.82} $$

$$ \eta_{max} = \rho \cos\Lambda \tag{5.83} $$

The approximation of the PRBM parameters for perturbation ratios less than 1 is below. The maximum tip slope angle for the approximation is 120 degrees.

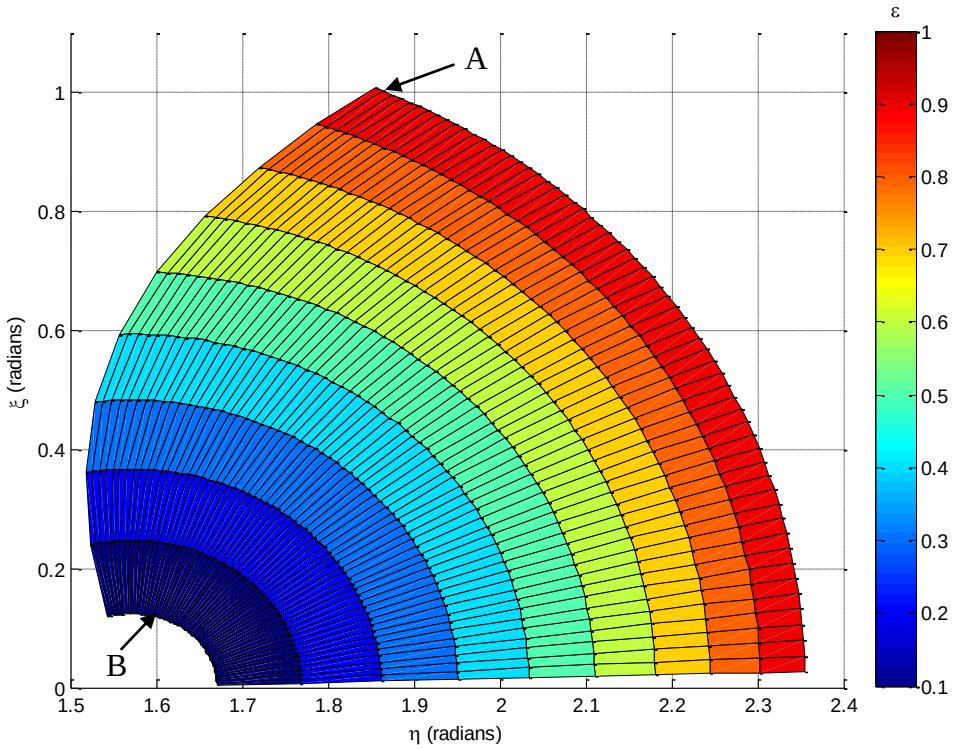

Figure 5.6. Perturbation ratio as a function of the angles of the applied moment ξ and η for the 2.5 aspect ratio.

Table 5.1. Limits of the PRBM parameters for different aspect ratios.

AR	ρ	Λ (radians)
1.25	0.97	0.79
1.50	1.02	1.02
1.75	0.99	1.16
2.00	0.92	1.29
2.25	0.87	1.39
2.50	0.83	1.52
2.75	0.80	1.57

5.5.1 Approximation of the Characteristic Radius Factor

The characteristic radius factor gives the location of the pseudo-rigid-body model joint. The exact values of the angles Ψ and Θ where calculated from Equations 5.49 and 5.51, respectively with the theoretical coordinates of the beam. The exact value of the characteristic radius was calculated from Equation 5.50.

Figure 5.7 shows the relationship between the exact characteristic radius, as a function of the angle θ, ϕ and the beam aspect ratio ranging from 1.25 to 4. The plot shows the exact characteristic radius factor for the different aspect ratios. As shown in the plot, the relationship between the characteristic radius and the aspect ratio depend on the tip angle θ.

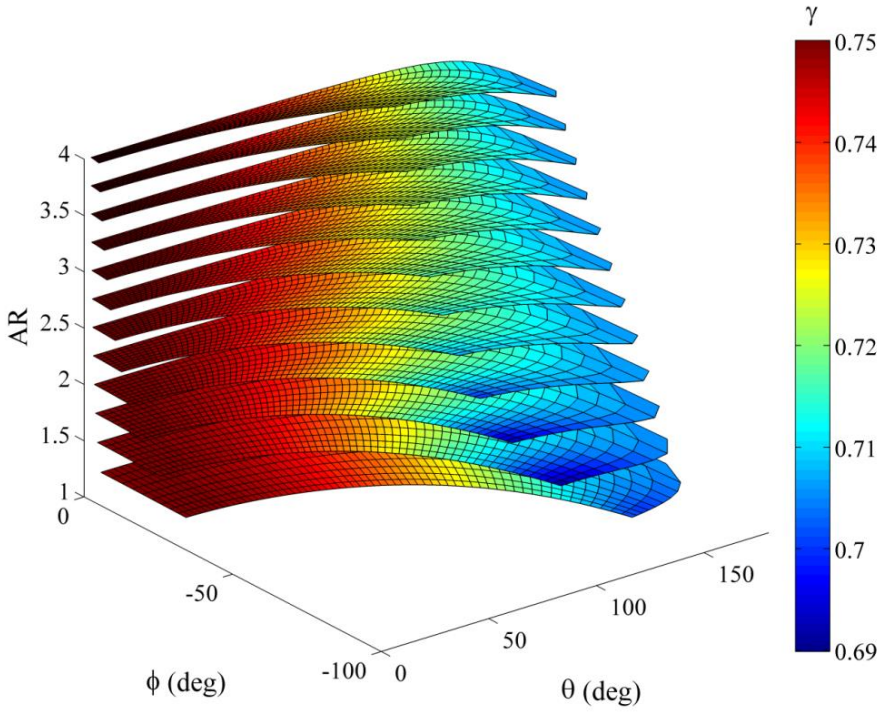

Figure 5.7. Exact values of the characteristic radius factor, γ, as a function of the tip angles ϕ and θ and the beam aspect ratio.

Table 5.2 contains the approximated values of the characteristic radius factor. The average of the characteristic radius factor was calculated with the exact values of the PRB angles Θ and Ψ. With the theoretical values of the tip location (a_t, b_t and c_t), we are able to calculate the

relative deflection error. The relative deflection error estimates the difference between the theoretical and the approximated tip location, where the maximum relative deflection error is 6%. The maximum error of the approximated characteristic radius factor is along the horizontal axis (*x*-direction) of the beam.

Table 5.2. Approximated values of the characteristic radius factor as a function of the aspect ratio of the beam.

AR	γ	Std. Dev. γ	Relative error (%)	Max. error a (%)	Max. error b (%)	Max. error c (%)
1.00	0.7432	0.0056	1.617	2.119	0.898	0.898
1.25	0.7401	0.0086	3.499	4.479	1.294	1.294
1.50	0.7358	0.0137	6.653	7.967	1.870	1.870
1.75	0.7354	0.0140	6.590	7.835	1.921	1.921
2.00	0.7365	0.0124	5.664	6.448	1.772	1.772
2.25	0.7378	0.0107	4.676	5.291	1.600	1.600
2.50	0.7389	0.0094	3.898	4.913	1.460	1.460
2.75	0.7398	0.0085	3.351	4.280	1.345	1.345
3.00	0.7404	0.0078	2.968	3.757	1.266	1.266
3.25	0.7409	0.0073	2.715	3.431	1.192	1.192
3.50	0.7413	0.0070	2.527	3.333	1.146	1.146
3.75	0.7415	0.0068	2.389	3.262	1.114	1.114
4.00	0.7417	0.0066	2.208	2.928	1.084	1.084

In the approximation of the characteristic radius factor, the maximum error comes from the horizontal deflection (a). The approximated characteristic radius factor over estimates the horizontal deflection. Figure 5.8 presents the difference between the theoretical and approximated horizontal deflection for a beam with aspect ratio equal to 2. The red points represent the theoretical deflection and the blue squares the approximated deflections. The error occurs at tip angles over 100 degrees. The cause of the discrepancy in the theoretical and

approximated values is because for the horizontal deflection we are only taking in consideration the PRB angle Θ and not the out of plane angle Ψ. The vertical and out-of-plane deflection maximum error are the same, which are less than 2%, where the maximum error occurs at lower aspect ratios.

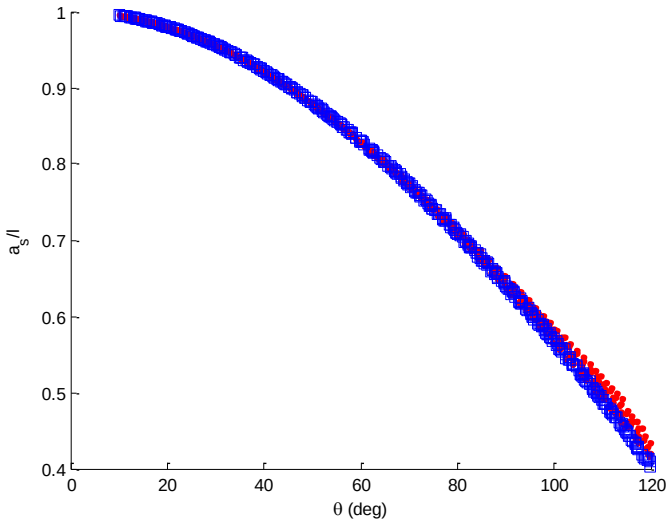

Figure 5.8. Theoretical and approximated horizontal deflections versus tip angles for aspect ratio equal to 2.

5.5.2 Approximation of the Parametric Angle Coefficients

The bending parametric angle coefficient is the ratio of the tip angle to the bending PRB angle Θ.

$$c_\theta = \theta/\Theta \tag{5.84}$$

Figure 5.9 presents the exact values of the bending parametric angle coefficient (c_θ), as a function of the tip angle θ for aspect ratios ranging from 1.25 to 5.0. The parametric angle ranges from 1.47 to 1.56, as shown in the figure. A linear regression routine was used to obtain the approximated bending parametric angle coefficient given the exact values of the tip angle θ and

the PRB link angle Θ for tip slope angles less than 120 degrees. Table 5.3 presents the approximated bending parametric angle coefficients for different aspect ratios.

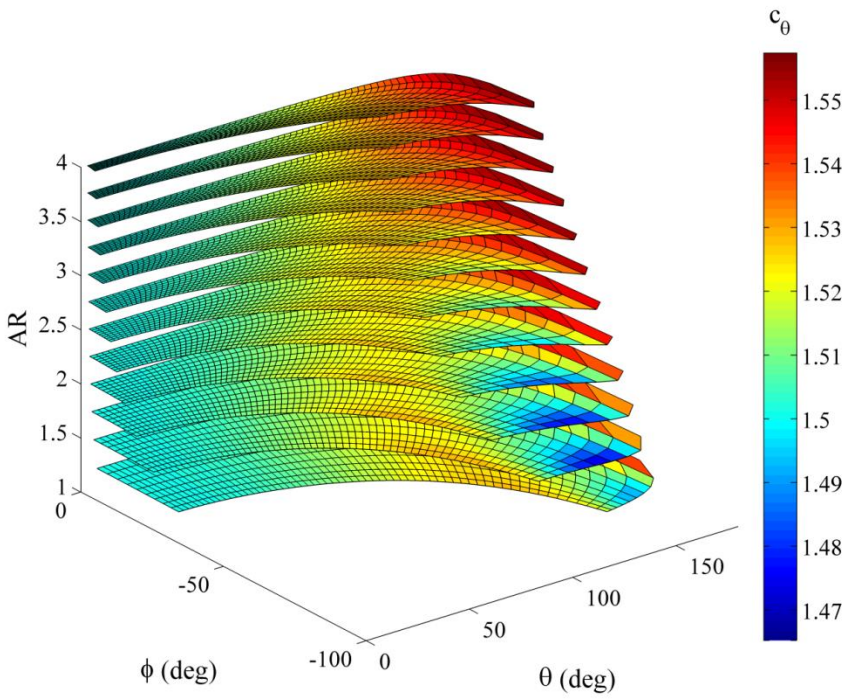

Figure 5.9. Exact values of the parametric angle coefficient, c_θ, as a function of the tip angles θ for aspect ratios ranging from 1.25 to 4.

The function of the approximated bending parametric angle coefficient ($c_{\theta a}$) in the PRBM is to calculate the PRB angle Θ. The error between the exact and approximated angle Θ is defined as:

$$error\ (\Theta) = \frac{\Theta - \Theta_a}{\Theta} * 100 \qquad 5.85$$

where $\Theta_a = \theta_0 / c_{\theta a}$. Table 5.3 presents the approximated bending parametric angle coefficients and the percentage error the PRB angle Θ as a function of the aspect ratio. The maximum error found between the approximated and exact PRB angle Θ is 1.24%.

From Equation 5.19, the PRB-link parametric angle coefficient is the ratio of the tip angle to the bending PRB angle Θ and the rotation angle Ω:

$$c_{\Omega} = \Omega/\Theta \tag{5.86}$$

Table 5.3. Approximated values of the bending parametric angle coefficient (c_{θ}) as a function of the aspect ratio of the beam.

AR	$c_{\theta a}$	R^2 $c_{\theta a}$	Max. error Θ_a(%)
1.00	1.5150	0.9999	0.978
1.25	1.5178	0.9999	1.160
1.50	1.5191	0.9999	1.240
1.75	1.5184	0.9999	1.197
2.00	1.5182	0.9999	1.181
2.25	1.5183	0.9999	1.187
2.50	1.5183	0.9999	1.188
2.75	1.5183	0.9999	1.189
3.00	1.5182	0.9999	1.185
3.25	1.5180	0.9999	1.169
3.50	1.5178	0.9999	1.161
3.75	1.5178	0.9999	1.156
4.00	1.5176	0.9999	1.146

Figure 5.9 presents the exact values of the PRB-link parametric angle coefficient c_{Ω}, as a function of the tip angles ϕ and θ for aspect ratios ranging from 1.25 to 4.0. The exact values of c_{Ω} ranges from 0.5 to 0.56 for tip angles ranging from 0-120 degrees, and increases to 0.59 for higher tip angles. A linear regression routine was used to find the approximated relationship between the tip angle and the PRB-link angle for tip slope angles less than 120 degrees. Table 5.4 presents the approximated values of the PRB link parametric angle coefficient c_{Ω} for different aspect ratios.

The error associated with the Ω angle can be found thru:

$$error\ (\Omega) = \frac{\Omega - \Omega_a}{\Omega} * 100 \tag{5.87}$$

where $\Omega_a = c_\Omega \Theta_a$. As shown in Table 5.4, the error of the approximated Ω can be 10% for low aspect ratios. The error in the approximated angle Ω is higher because Ω_a depends on the values of the approximated angle Θ_a. The error is also higher at low aspect ratios because there is an increase in the torsion of the PRB link given by the angle Σ.

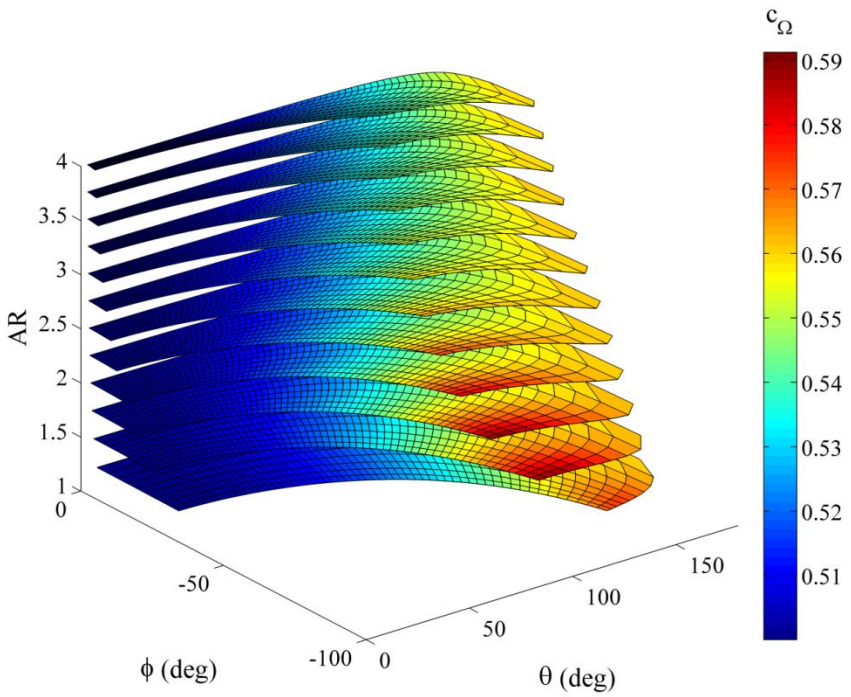

Figure 5.10. Exact values of the PRB-link parametric angle coefficient, c_Ω, as a function of the tip angles ϕ and θ.

Because the angles Ω and Θ depend on c_θ, the rotation angle Ω can be calculated as:

$$\Omega = (c_{\theta a} - 1)\Theta \tag{5.88}$$

We can also assume that the angles Ψ and Φ are linearly related as:

$$\Psi = c_\Psi \Phi \tag{5.89}$$

Figure 5.11 presents the exact value of the parametric angle coefficient c_Ψ as a function of the aspect ratio of the beams cross-section and the tip angles ϕ and θ.

Table 5.4. Approximated values of $c_{\Omega a}$ as a function of the aspect ratio of the beam.

AR	$c_{\Omega a}$	R^2 $c_{\Omega a}$	Max. error Ω_a (%)
1.00	0.5150	0.9991	1.25
1.25	0.5226	0.9975	4.31
1.50	0.5335	0.9918	9.72
1.75	0.5349	0.9910	10.40
2.00	0.5326	0.9925	9.15
2.25	0.5296	0.9943	8.08
2.50	0.5271	0.9956	6.94
2.75	0.5248	0.9966	5.84
3.00	0.5232	0.9973	5.05
3.25	0.5217	0.9978	4.44
3.50	0.5207	0.9981	3.93
3.75	0.5201	0.9983	3.51
4.00	0.5194	0.9985	3.01

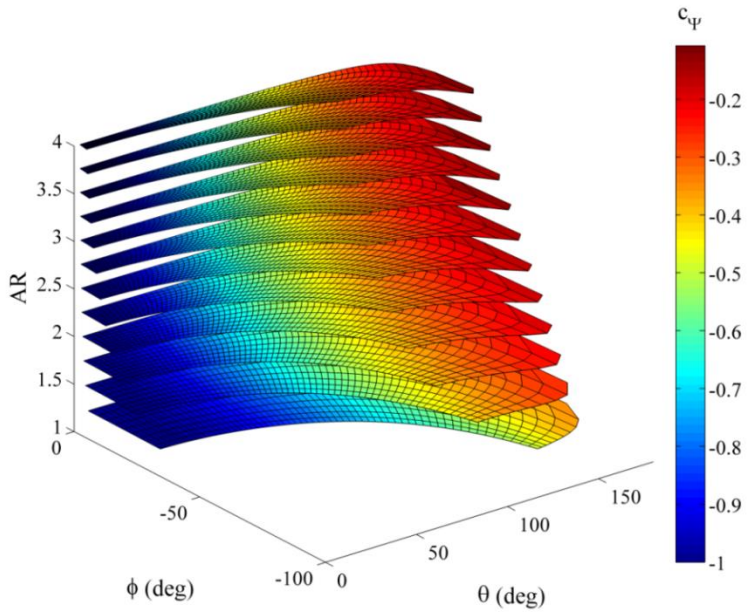

Figure 5.11. Exact values of the parametric angle coefficient, c_Ψ, as a function of the tip angles ϕ and θ.

An approximated value of the parametric angle coefficient c_Ψ can be found as a function of the tip angles θ and ϕ as shown in Figure 5.11. For tip angles θ less than 120 degrees, c_Ψ varies from -1.0 to -0.4.

5.5.3 Approximation of the Stiffness Coefficients

For the approximation of stiffness coefficients, a series of loads where applied to the free-end of the beam ($\{h\}$-frame), which caused a maximum tip slope which ranged from 0 to 120°. To this loads, a perturbed out-of-plane moment in the Y-direction was applied at the end for different aspect ratios. The moments at the different frames were calculated using the coordinate transformations.

The bending stiffness coefficient K_θ was calculated from Equation 5.65. Figure 5.12 presents the bending stiffness coefficient K_θ as a function of the tip angles θ and ϕ. The bending stiffness coefficient ranges from 2.03 to 2.3. Table 5.5 presents the approximate the bending stiffness coefficient for each aspect ratio. The mean and the standard deviation for each aspect ratio was calculated to approximate K_θ.

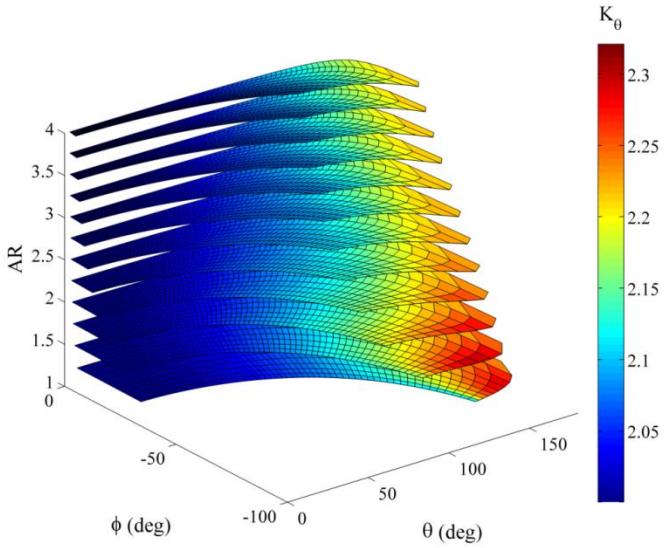

Figure 5.12. Bending stiffness coefficient K_θ as a function of the tip angles ϕ and θ.

Table 5.5. Approximated values of the bending stiffness coefficient K_θ and the standard deviation as a function of the aspect ratio of the beam.

AR	$K_{\theta a}$	Std. Dev. K_θ
1.00	2.0306	0.0254
1.25	2.0415	0.0343
1.50	2.0553	0.0476
1.75	2.0570	0.0497
2.00	2.0518	0.0428
2.25	2.0460	0.0358
2.50	2.0415	0.0310
2.75	2.0383	0.0278
3.00	2.0362	0.0261
3.25	2.0344	0.0248
3.50	2.0334	0.0243
3.75	2.0329	0.0240
4.00	2.0324	0.0239

The torsion of the beam is a function of the Υ and Σ angles. Where Υ is the deformation at the fixed end of the beam and Σ is the rotation of the pseudo-rigid link. From Equation 5.68, the stiffness coefficient K_Υ:

$$K_\Upsilon = \frac{\gamma\,(1-\gamma)K_\theta \Theta^2 \sin(2\Gamma)(1+\upsilon)(AR^2-1)}{\Upsilon(AR^2+1)} \qquad 5.90$$

Figure 5.13 shows the stiffness coefficient K_Υ as a function of the tip angles ϕ and θ. From the fixed frame {a}, the first rotation is about the Υ-angle. ${}^{a}M_x$ is the first rotation about the *x*-frame, the moment in the *x*-frame is the same. The stiffness coefficient K_Υ is a measure of resistance to deformation on the straight part of the beam.

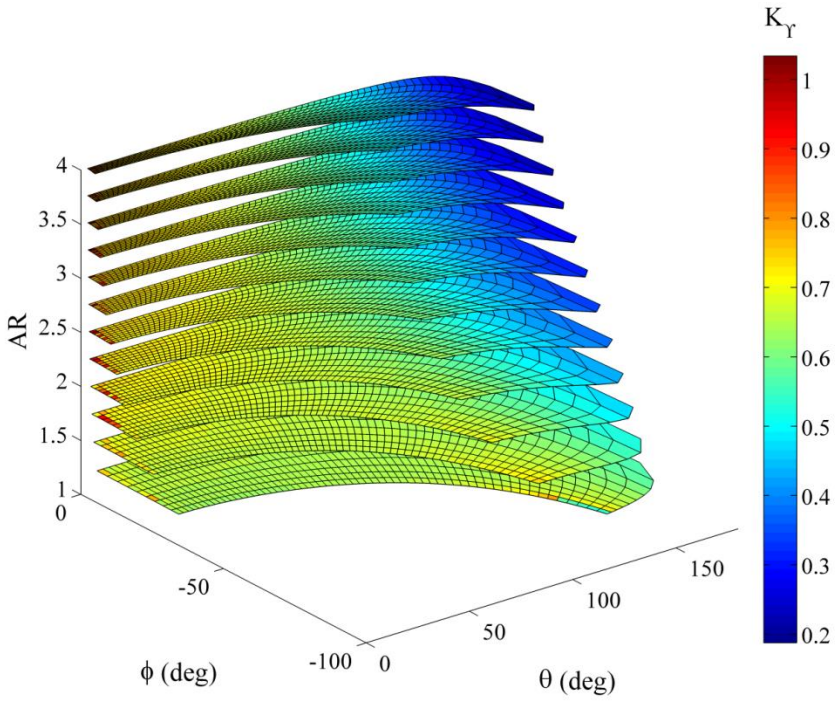

Figure 5.13. Stiffness parameter K_Υ as a function of the tip angles ϕ and θ.

The mean and the standard deviation for each aspect ratio were calculated to approximate K_Υ. Table 5.6 presents the approximate the bending stiffness coefficient for each aspect ratio.

The stiffness coefficient K_Σ can be calculated from Equation 5.66, such as:

$$K_\Sigma = \frac{\gamma l \, {}^{d}M_x}{G I_X \Sigma} \tag{5.91}$$

The rotation of the angle Σ, there is a rotation about the Ψ-angle around the *x*-axis and a *Θ*-rotation about the *z*-axis. We can find the stiffness coefficient is a function of the aspect ratio of the beam and the tip angles θ and ϕ, as shown in Figure 5.14.

As shown in Figure 5.14, for aspect ratios higher than 3.0, K_Σ is approximately 0.75. For lower aspect ratios, the torsion stiffness coefficient is a function of the aspect ratio and the tip angles θ and ϕ. The mean and the standard deviation of the torsion stiffness coefficient are presented in Table 5.7.

Table 5.6. Approximated values of the bending stiffness coefficient K_{Υ} and the standard deviation as a function of the aspect ratio of the beam.

AR	$K_{\Upsilon a}$	Std. Dev. $K_{\Upsilon a}$
1.00	0.0000	0.0000
1.25	0.6450	0.0160
1.50	0.6641	0.0206
1.75	0.6709	0.0217
2.00	0.6724	0.0295
2.25	0.6720	0.0382
2.50	0.6710	0.0456
2.75	0.6701	0.0517
3.00	0.6688	0.0569
3.25	0.6687	0.0603
3.50	0.6677	0.0639
3.75	0.6665	0.0670
4.00	0.6659	0.0694

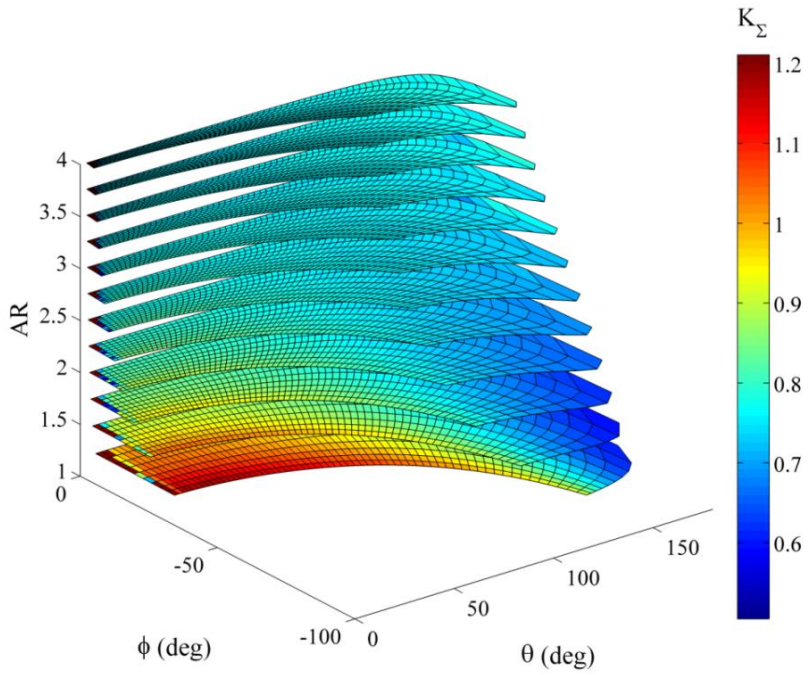

Figure 5.14. Stiffness parameter K_{Σ} as a function of the tip angles ϕ and θ and the beam aspect ratio.

Table 5.7. Approximated values of the torsion stiffness coefficient K_Σ as a function of the aspect ratio of the beam.

AR	$K_{\Sigma a}$	Std. Dev. $K_\Sigma a$
1.00	0.0000	0.0000
1.25	1.0174	0.0887
1.50	0.9079	0.0742
1.75	0.8466	0.0560
2.00	0.8134	0.0407
2.25	0.7940	0.0294
2.50	0.7820	0.0211
2.75	0.7741	0.0150
3.00	0.7685	0.0107
3.25	0.7645	0.0079
3.50	0.7615	0.0064
3.75	0.7592	0.0062
4.00	0.7574	0.0068

5.6 Summary of PRBM Equations

The following equations are sufficient to find the rotation, displacement and stiffness of a rectangular beam subjected to end-moment loading:

$$a_s = l - \gamma l(1 - \cos\Theta) \tag{5.92}$$

$$b_s = \gamma l \sin\Theta \cos\Psi \tag{5.93}$$

$$c_s = \gamma l \sin\Theta \sin\Psi \tag{5.94}$$

$$\theta = c_\theta \Theta \tag{5.95}$$

$$\Omega = c_\Omega \Theta \tag{5.96}$$

$$\Psi = c_\Psi \Phi \tag{5.97}$$

$${}^c_a\Psi = {}^c_b\Gamma + {}^b_a\Upsilon \tag{5.98}$$

$$ {}^{a}M_x - \frac{K_\Upsilon G I_X \Upsilon}{(1-\gamma)l} = 0 \tag{5.99} $$

$$ {}^{a}M_x - \frac{E\gamma\Theta^2 I_R sin2\Gamma K_\theta}{l} = 0 \tag{5.100} $$

$$ {}^{c}M_z - c_\Omega \, {}^{f}M_z - \frac{{}^{c}I_Z E\Theta\gamma K_\theta}{l} = 0 \tag{5.101} $$

$$ {}^{d}M_x - \frac{K_\Sigma G I_X \Sigma}{\gamma l} = 0 \tag{5.102} $$

Knowing the aspect ratio of the beams cross section (the ratio of the width of the beam over the height of the beam) we can obtain the approximation of the PRBM parameters $\gamma, c_\Omega, c_\theta, c_\Psi, K_\Upsilon, K_\theta$ and K_Σ from section 5.5. Equations 5.92- 5.102 can be added into Matlab to solve for the other parameters.

5.7 Conclusion

The pseudo-rigid-body model for a beam of rectangular cross-section consists of two rigid links connected by a spherical joint and a spherical cap. The spherical cap was added to describe the orientation of the beams tip. The deflection of the beam's tip is found by substituting the PRB parameters in Equations 5.14-5.16.

Perturbation theory was used to apply the out-of-plane moment (M_y) in the follower frame such that it ensures the applied load does not produce excessive out-of-plane deflection. The limits of the PRBM parameters which contain a relative deflection error of 6.0% for selected aspect ratios and perturbation factors less than one were described. The PRBM parameters $\gamma, c_\Omega, c_\theta, c_\Psi, K_\Upsilon, K_\theta$ and K_Σ depend on the aspect ratio of the beam. Tables with the approximations of the PRBM parameters as a function of the aspect ratio are included in this Chapter.

Chapter 6

Conclusions and Recommendations

The objective of this study was to describe kinematic models (Pseudo-Rigid-Body Models) for approximating large-deflection of spatial cantilever beams that undergo multiple bending motions thru end-moment loading. PRBMs for axisymmetric and rectangular cross-section spatial beams with moment-loading were developed in this dissertation.

The governing equations of a cantilever beam that undergoes large deflection due to force and moment loading where developed and validated. These non-linear kinematic equations for a cantilever beam contains the curvature, location and rotation of the beam. The resulting deflections, curvatures and angles where used to developed a spatial Pseudo-Rigid-Body Model.

The pseudo-rigid-body model for an axisymmetric beam consists of two links connected thru a spherical joint. It was found that the coordinates of the deflection of an axisymmetric beam can be found by using the planar PRBM multiplied by a rotation in the *x*-direction. The characteristic radius factor and the PRB angle coefficient for a beam with a single moment applied at the end were optimized to minimize the error incurred using the deflection formulas of the PRBM. This approximation provides an improvement to previous published parameters, providing a relative error of 0.5% at a tip slope angle to 169.76 degrees.

The pseudo-rigid-body model for a beam of rectangular cross-section consists of two rigid links connected by a spherical joint and a spherical cap. The spherical cap was added to describe the orientation of the beam. The PRB parameters $\gamma, c_\Omega, c_\theta, c_\Psi, K_\Upsilon, K_\theta$ and K_Σ depend on

the aspect ratio (the ratio of the beams width over the height) of the beam. Tables with approximations of the PRBM parameters as a function of the aspect ratio are included in Chapter 5.

6.1 Recommendations for Future Work

1. It was found that for a rectangular cantilever beam with multiple loading moments, the PRB-link undergoes torsion. Another approach to model this torsion would be to develop a PRBM consisting of 3 links connected thru 2 revolute joints to model the torsion of the longer PRB-link.
2. Most of the error of the characteristic radius factor is from the horizontal deflection of the beam. This error may be minimized by assuming that the total length of the PRBM is less than the length of the straight beam.
3. A spatial PRBM with combined forces and moments will be the next step of this work.

References

[1] Frecker MI, Powell KM, Haluck R. Design of a Multifunctional Compliant Instrument for Minimally Invasive Surgery. J.Biomech.Eng. 2005; 127: 990-993

[2] Gu D, Zhou Y. An approach to the capsule endoscopic robot with active drive motion. Journal of Zhejiang University. 2011; 12: 223-231

[3] Yung-Lien W. Modular design process for a micro motion actuator. Mechatronics. 2005; 15: 793-806

[4] Bandopadhya D. Quasi-Static Tip Positioning of Multi-Segmented IPMC for Micro-Manipulation following Euler-Bernoulli and Pseudo-Rigid Body Model. Journal of Reinforced Plastics and Composites: 743

[5] Zubir MNM, Shirinzadeh B, Tian Y. A new design of piezoelectric driven compliant-based microgripper for micromanipulation. Mechanism and Machine Theory. 2009; 44: 2248-2264

[6] Kennedy JA, Howell LL, Greenwood W. Compliant high-precision E-quintet ratcheting (CHEQR) mechanism for safety and arming devices. Precision Engineering. 2007; 31: 13-21

[7] Frisch-Fay R. Flexible bars. Washington, D.C.: Butterworths. 1962

[8] Howell LL. Compliant mechanisms. New York: Wiley. 2001

[9] Aguirre ME, Frecker M. Design Innovation Size and Shape Optimization of a 1.0 mm Multifunctional Forceps-Scissors Surgical Instrument. Journal of Medical Devices March, 2008; 2: 015001

[10] Cronin JA, Frecker IMI, Mathew A. Design of a Compliant Endoscopic Suturing Instrument. J.Med.Devices. 2008; 2: 025002

[11] Zoppi M, Sieklicki W, Molfino R. Design of a Microrobotic Wrist for Needle Laparoscopic Surgery. J.Mech.Des. 2008; 130: 102306

[12] Vitellaro G, L'Episcopo G, Trigona C, Ando B, Baglio S. A Compliant MEMS Device for Out-of-Plane Displacements with Thermo-Electric Actuation. Journal of Microelectromechanical Systems. 2014; 23: 661-671

[13] Sonmez U. Compliant MEMS Crash Sensor Designs: The Preliminary Simulation Results. Intelligent Vehicles Symposium. IEEE 2007: 303-308

[14] Kota S, Joo J, Li Z, Rodgers S. M, Sniegowksi, J. Design of Compliant Mechanisms: Applications to MEMS. Analog Integrated Circuits and Signal Processing. 2001; 29: 7-16

[15] Landon S. Development of Deployable Wings for Small Unmanned Aerial Vehicles Using Compliant Mechanisms. 2007

[16] Kota S, Hetrick JA, Osborn R, Paul D, Pendleton E, Flick P, Tilmann C. Design and application of compliant mechanisms for morphing aircraft structures. 2003: 24-33

[17] Khataita JP, Mukherjeeb S, Sethc B. Compliant design for flapping mechanism: A minimum torque approach. Mechanism and Machine Theory: 3

[18] Yao-Wei Chin, Gih-Keong Lau. "Clicking" compliant mechanism for flapping-wing micro aerial vehicle. Intelligent Robots and Systems (IROS), 2012 IEEE/RSJ International Conference on 2012: 126-131

[19] Allred TM. Compliant mechanism suspensions. 2003

[20] Bisshopp KE, Drucker DC. Large Deflection of Cantilever Beams. Quarterly of applied Math. 1945; 3: 272-275

[21] Sigmund O. On the design of compliant mechanisms using topology optimization. Mechanics of structures and machines. 1997; 25: 493

[22] Howell LL, Magleby SP, Olsen BM. Handbook of compliant mechanisms. Chichester, West Sussex, United Kingdom: John Wiley & Sons, Ltd, 2013

[23] Zhang A, Chen G. A Comprehensive Elliptic Integral Solution to the Large Deflection Problems of Thin Beams in Compliant Mechanisms. Journal of Mechanisms and Robotics. 2013; 5: 021006

[24] Chen, G., and Zhang, A. Accuracy Evaluation of PRBM for Predicting Kinetostatic Behavior of Flexible Segments in Compliant Mechanisms. Proceedings of the ASME 2011 International Design Engineering Technical Conferences and Computers and Information in Engineering Conference. 2011

[25] Rao SS. Engineering Optimization: Theory and Practice, Fourth Edition. Hoboken, NJ, USA: John Wiley & Sons, Inc. 2009

[26] Arora JS. Optimization of structural and mechanical systems. Hackensack, NJ: World Scientific. 2007

[27] Sigmund O. On the Design of Compliant Mechanisms using Topology Optimization. Mechanics of Structures and Machines. 1997; 25: 493

[28] Lee E, Gea HC. A strain based topology optimization method for compliant mechanism design. Structural and Multidisciplinary Optimization. 2014; 49: 199-207

[29] Pedersen CBW, Buhl T, Sigmund O. Topology synthesis of large-displacement compliant mechanisms. International Journal for Numerical Methods in Engineering. 2001; 50: 2683-2705

[30] Stanford B, Beran P. Conceptual Design of Compliant Mechanisms for Flapping Wings with Topology Optimization. AIAA Journal. 2011; 49: 855-867

[31] Howell LL, Midha A. Parametric Deflection Approximations for End-Loaded, Large-Deflection Beams in Compliant Mechanisms. Journal of Mechanical Design. 1995; 117: 156-165

[32] Howell LL, Midha A, Norton TW. Evaluation of Equivalent Spring Stiffness for Use in a Pseudo-Rigid-Body Model of Large-Deflection Compliant Mechanisms. Journal of Mechanical Design. 1996; 118: 126-131

[33] Pauly J, Midha A. Improved Pseudo-Rigid-Body Model Parameter Values for End-Force-Loaded Compliant Beams. ASME Conference Proceedings 2004; 2004: 1513-1517

[34] M.H. D. Variable parametric pseudo-rigid-body model for large-deflection beams with end loads. International Journal of Non-Linear Mechanics. 2001; 36: 1123-1133

[35] Feng Z, Yu Y, Wang W. Modeling of large-deflection links for compliant mechanisms. Frontiers of Mechanical Engineering in China. 2010; 5: 294-301

[36] Yang XS. Applied Engineering Mathematics

[37] Su H. A Pseudo-Rigid-Body 3R Model for Determining Large Deflection of Cantilever Beams Subject to Tip Loads. Journal of Mechanisms and Robotics. 2009; 1: 021008

[38] Wittwer JW. Robust Design and Model Validation of Nonlinear Compliant Micromechanisms. Journal of microelectromechanical systems. 2006; 15: 33

[39] Chorlton F. Vector & tensor methods. Chichester, Eng.; New York: E. Horwood Ltd; Halsted Press. 1976

[40] Axisa F, Trompette P. Modelling of Mechanical Systems [electronic resource]: Structural Elements: Oxford: Elsevier Science & Technology, 2005. 2005

[41] LeBlanc DC. Statistics: concepts and applications for science / David C. LeBlanc: Sudbury, MA : Jones and Bartlett. 2004

[42] Bender CM, Orszag SA. Advanced mathematical methods for scientists and engineers. 1, Asymptotic methods and perturbation theory. Carl M. Bender, Steven A. Orszag. New York: Springer. 1999

[43] Spiegel MR, Lipschutz S, Liu J. Mathematical Handbook of Formulas and Tables. New York: McGraw-Hill. 2009

[44] Ramirez IA, Lusk CP. Spatial-Beam Large-Deflection Equations and Pseudo-Rigid-Body Model for Axisymmetric Cantilever Beams. Proceedings of the ASME International Design Engineering Technical Conferences, August 28-31, 2011

Appendices

Appendix A. Copyright Clearance

The following permission is for use of material in Chapter 3 and Chapter 4.

On Fri, Nov 21, 2014 at 12:24 PM, Philip DiVietro <DiVietroP@asme.org> wrote:
Dear Ms. Ramirez,

To confirm our conversation, you indeed have permission as stated in your request. There is no charge to you for this permission.

Regarding, IDETC 2011 Conference Paper 47389, Spatial-Beam Large-Deflection Equations and Pseudo-Rigid-Body Model for Axisymmetric Cantilever Beams, by Issa A. Ramirez and Craig P. Lusk, pages 43-49, as published by ASME, 2011.

Thank you for your support of ASME.

Sincerely,

Philip DiVietro

Philip V. DiVietro
Managing Director, Publishing
ASME
2 Park Avenue, 6th Floor
New York, NY 10016-5990
Tel 1.212.591.7696
Mobile 1.631.553.1088
divietrop@asme.org

From: Issa Ramirez Rivera [mailto:iramire3@mail.usf.edu]
Sent: Friday, November 21, 2014 12:17 PM
To: Philip DiVietro
Subject: Fwd: Permission request for dissertation

---------- Forwarded message ----------
From: **Issa Ramirez Rivera** <iramire3@mail.usf.edu>
Date: Mon, Nov 17, 2014 at 8:44 AM
Subject: Permission request for dissertation
To: permissions@asme.org
Cc: Issa Ramirez <issaramirez@gmail.com>
Good morning,

I am one of the authors of the IDETC 2011 Conference Paper 47389. In the attachment is the filled permissions request form to add parts of the conference paper as part of my dissertation.

If you have any questions, please let me know.

Thank you,

Issa A Ramirez

Appendix B. Matlab M-file

This Matlab code contains the main algorithm to obtain the curvatures, displacements and rotations of a beam with moment-loading.

```
function moment_only_master

clc;clear all;close all

b=.04;e_p=1;

lb=10;h=.0100; AR=b/h;

Iy=(h*b^3)/12; Iz=(b*h^3)/12; Ix=Iy+Iz; ae=1;
s=[0:lb]; x=s; y=0; z=0; %initial coordinates of the undeformed free end
E=2.00000000E+11;   %Young's Modulus
v_p=.300; G=E/(2*(1+v_p));
AI=G*Ix; BI=E*Iy; CI=E*Iz;

%% Moments at the free-end
theta_input=120*pi/180;
MZ=(theta_input*E*Iz)/(lb);MX=0;MY=-e_p*MZ;

%% initial conditions at the deformed frame (X Y Z) at the end of the beam
psi=0; theta=.0000000001; phi=0; dX=0; dY=0; dZ=0;
kx_0=MX/(G*Ix); ky_0=MY/(E*Iy); kz_0=MZ/(E*Iz);
K_input=[kx_0;ky_0;kz_0]
y0=[psi theta phi kx_0 ky_0 kz_0 dX dY dZ] ;
length_scale=[0:-lb/21:-lb];

[s_lenght,r]=ode45(@straight2,length_scale,y0);

function ds_out=straight2(s,y0);

si=y0(1); theta=y0(2); phi=y0(3);tx=y0(4); ky=y0(5); kz=y0(6);

dpsi=-ky*(cos(phi)/sin(theta))+kz*(sin(phi)/sin(theta));
dtheta=ky*sin(phi)+kz*cos(phi);
dphi=tx+ky*cos(phi)*(cos(theta)/sin(theta))-
kz*sin(phi)*(cos(theta)/sin(theta));

F_dky=0;F_dkz=0;

dtx=(1/AI)*(((BI-CI)*ky*kz)+ 0);
dky=(1/BI)*(((CI-AI)*kz*tx)+F_dky);
dkz=(1/CI)*(((AI-BI)*tx*ky)+F_dkz);

dx_ds=cos(theta);
dy_ds=cos(si)*sin(theta);
```

```
dz_ds=sin(si)*sin(theta);

ds_out=[dpsi dtheta dphi dtx dky dkz dx_ds dy_ds dz_ds]';
end

%% seen from the H-frame to the fixed frame A
r(end,:);

AA=r(:,7); BB=r(:,8);CC=r(:,9);psi=r(:,1);theta=r(:,2);phi=r(:,3);

si=r(:,1)-r(1,1); theta=r(:,2)-r(1,2); phi=r(:,3)-r(1,3);
kx=r(end,4);ky=r(end,5);kz=r(end,6);

kxyz_d=[r(end,4);r(end,5);r(end,6)]
end_angles_XYZ=[si(end),theta(end),phi(end)]

%%  change of frames: seen from the fixed (A) to the moving frame (H)
for ii=1:1:length(theta);

R_qh= [1 0 0; 0 cos(phi(ii)) sin(phi(ii)); 0 -sin(phi(ii)) cos(phi(ii))];
R_pq=[cos(theta(ii)) sin(theta(ii)) 0;-sin(theta(ii)) cos(theta(ii)) 0; 0 0
1];
R_ap= [1 0 0; 0 cos(si(ii)) sin(si(ii)); 0 -sin(si(ii)) cos(si(ii))];
rot_ha=R_qh*R_pq*R_ap;

xyz=-rot_ha*[AA(ii);BB(ii);CC(ii)];
a_v(ii)=xyz(1);
b_v(ii)=xyz(2);
c_v(ii)=xyz(3);

Mxyz=rot_ha*[MX;MY;MZ];
Mx_v(ii)=Mxyz(1);
My_v(ii)=Mxyz(2);
Mz_v(ii)=Mxyz(3);

end
%% Transformations to the A-frame (fixed)

Mx=Mxyz(1);My=Mxyz(2);Mz=Mxyz(3);Mxyz_a=[Mx,My,Mz]
a=a_v(end);b=b_v(end);c=c_v(end); abc_xyz=[a,b,c]

%% PRBM parameters gamma Theta Psi

Psi = atan(c_v./b_v);
lb_v=abs(length_scale);
gamma = ((b_v./lb_v).^2+(c_v./lb_v).^2+(1-a_v./lb_v).^2)./(2*(1-a_v./lb_v));
Theta=atan2((b_v./(lb_v.*cos(Psi))) , ((a_v./lb_v-1)+gamma));

gamma_capTheta_capPsi_pro=[gamma',Theta'*180/pi,Psi'*180/pi]

 % loop for Omega, Sigma, Phi
for ii= 1:1:length(theta)
```

```
R_dc=[cos(Theta(ii)) -sin(Theta(ii)) 0; sin(Theta(ii)) cos(Theta(ii)) 0; 0 0
1];
R_ca=[1 0 0; 0 cos(Psi(ii)) -sin(Psi(ii)); 0 sin(Psi(ii)) cos(Psi(ii))];

RZ_hq=[1 0 0;0 cos(phi(ii)) sin(phi(ii));0 -sin(phi(ii)) cos(phi(ii))];
RX_qp=[cos(theta(ii)) sin(theta(ii)) 0;-sin(theta(ii)) cos(theta(ii)) 0;0 0
1];
RZ_pa=[1 0 0;0 cos(psi(ii)) sin(psi(ii));0 -sin(psi(ii)) cos(psi(ii))];
Rxzx_hd=R_dc^-1*R_ca^-1*RZ_hq*RX_qp*RZ_pa;

% from the Rxzx_hd rotation: Psi, Omega, Sigma
 Omega=acos(Rxzx_hd(1,1));
 Sigma=atan2(Rxzx_hd(3,1)/sin(Omega) , Rxzx_hd(2,1)/sin(Omega));
 Phi = atan2(Rxzx_hd(1,3)/sin(Omega) , -Rxzx_hd(1,2)/sin(Omega));

SigOmePhi(ii,1:3)=[Sigma, Omega, Phi];
end

Sigma_Ome_Phideg=SigOmePhi*180/pi;

end
```